UNCLASSIFIED

CENTRAL RESEARCH LIBRARY
DOCUMENT COLLECTION

MARTIN MARIETTA ENERGY SYSTEMS LIBRARIES
3 4456 0350494 6

ORNL-2320 cy. 4
Physics and Mathematics

FISSION FRAGMENT STUDIES BY MAGNETIC ANALYSIS

C. B. Fulmer

CENTRAL RESEARCH LIBRARY
DOCUMENT COLLECTION
LIBRARY LOAN COPY
DO NOT TRANSFER TO ANOTHER PERSON
If you wish someone else to see this document, send in name with document and the library will arrange a loan.

OAK RIDGE NATIONAL LABORATORY
OPERATED BY
UNION CARBIDE NUCLEAR COMPANY
A Division of Union Carbide and Carbon Corporation
UCC
POST OFFICE BOX X · OAK RIDGE, TENNESSEE

UNCLASSIFIED

Printed in USA. Price 50 cents. Available from the

Office of Technical Services
U. S. Department of Commerce
Washington 25, D. C.

LEGAL NOTICE

This report was prepared as an account of Government sponsored work. Neither the United States, nor the Commission, nor any person acting on behalf of the Commission:

A. Makes any warranty or representation, express or implied, with respect to the accuracy, completeness, or usefulness of the information contained in this report, or that the use of any information, apparatus, method, or process disclosed in this report may not infringe privately owned rights; or

B. Assumes any liabilities with respect to the use of, or for damages resulting from the use of any information, apparatus, method, or process disclosed in this report.

As used in the above, "person acting on behalf of the Commission" includes any employee or contractor of the Commission to the extent that such employee or contractor prepares, handles or distributes, or provides access to, any information pursuant to his employment or contract with the Commission.

UNCLASSIFIED

ORNL 2320

Contract No. W-7405-eng-26

ELECTRONUCLEAR RESEARCH DIVISION

FISSION FRAGMENT STUDIES BY MAGNETIC ANALYSIS

by

Clyde Benson Fulmer

DATE ISSUED

AUG 5 1957

OAK RIDGE NATIONAL LABORATORY
Operated by
UNION CARBIDE NUCLEAR COMPANY
A Division of Union Carbide and Carbon Corporation
Post Office Box X
Oak Ridge, Tennessee

UNCLASSIFIED

MARTIN MARIETTA ENERGY SYSTEMS LIBRARIES

3 4456 0350494 6

INTERNAL DISTRIBUTION

1. C. E. Center
2. Biology Library
3. Health Physics Library
4-5. Central Research Library
6. Reactor Experimental Engineering Library
7-56. Laboratory Records Department
57. Laboratory Records, ORNL R.C.
58. A. M. Weinberg
59. L. B. Emlet (K-25)
60. J. P. Murray (Y-12)
61. J. A. Swartout
62. E. H. Taylor
63. E. D. Shipley
64. S. C. Lind
65. M. L. Nelson
66. W. H. Jordan
67. R. R. Dickison
68. C. P. Keim
69. R. S. Livingston
70. F. L. Culler
71. A. H. Snell
72. A. Hollaender
73. M. T. Kelley
74. G. E. Boyd
75. K. Z. Morgan
76. T. A. Lincoln
77. C. S. Harrill
78. A. S. Householder
79. C. E. Winters
80. D. W. Cardwell
81. E. M. King
82. D. D. Cowen
83. G. C. Williams
84. R. J. Jones
85. A. L. Boch
86. B. L. Cohen
87. F. T. Howard
88. J. S. Luce
89. J. A. Martin
90. A. M. Perry
91. A. Zucker
92. J. A. Lane
93. M. J. Skinner
94. S. J. Cromer
95. R. A. Charpie
96-105. C. B. Fulmer
106. ORNL - Y-12 Technical Library, Document Reference Section

EXTERNAL DISTRIBUTION

107. R. F. Bacher, California Institute of Technology
108. Division of Research and Development, AEC, ORO
109-683. Given distribution as shown in TID-4500 (13th ed.) under Physics and Mathematics category (100 copies - OTS)

ABSTRACT

Various properties of U^{235} fission fragments were studied with a high resolution magnetic spectrograph. The equilibrium charge of fragments in gas were studied as a function of fragment velocity, gas pressure, and type of gas. The mean radioactive lifetime of excited ionized fission fragments was determined. A thin CsI(Tl) crystal was successfully used to detect the fragments in a high background of gamma and beta radiation; the scintillation response of the crystal to fission fragments was studied. No saturation was observed. Energy vs range curves were obtained for median light and heavy fission fragments in H_2, He, air, A, Al, Ni, and Au. The long range particles from fission of U^{235} were verified to be alpha particles; the energy distribution of the particles was determined with high resolution, and no fine structure was found. The capabilities of a magnetic fission-fragment mass separator were studied. This study yielded a measure of the nuclear charge distribution of fission fragments of a given mass.

TABLE OF CONTENTS

	Page
Introduction	1
Chapter 1: Description of Apparatus and Experimental Procedures	3
1.1 Magnetic Wedge Spectrograph	3
1.2 Mass Identification Studies	7
1.3 Studies by Scintillation Detection	7
Chapter 2: Equilibrium Charges of Fission Fragments in Gases as Functions of Velocity, Gas Pressure, and Type of Gas	9
2.1 Introduction	9
2.2 Approximate Description of Heavy Ion Constitution	10
2.3 Experimental	13
2.4 Presentation of Data and Discussion of Results	16
2.5 Mean Radiative Lifetime of Fission Fragments	32
Chapter 3: Response of Cesium-Iodide Crystals to Fission Fragments	40
3.1 Introduction	40
3.2 Experimental	40
3.3 Presentation and Discussion of Data	41
Chapter 4: Energy of Fission Fragments as a Function of Range in Various Materials	48
4.1 Introduction	48
4.2 Survey of Previous Measurements	48
4.3 Experimental	50
4.4 Presentation and Discussion of Results	50
Chapter 5: Magnetic Analysis of the Long Range Particles from Nuclear Fission	63
5.1 Existence of Long Range Particles from Nuclear Fission	63
5.2 Survey of Previous Studies of Long Range Particles from Fission	63
5.3 Advantages of Studying the Long Range Particles by Magnetic Analysis	65
5.4 Experimental	65
5.5 Presentation of Data and Discussion of Results	68

TABLE OF CONTENTS (Continued) Page

Chapter 6: A Fission Fragment Mass Separator and the Nuclear Charge Distribution of Single Mass Fission Fragments 73

6.1 Introduction and Operating Principles 73
6.2 Experimental 75
6.3 Factors Affecting Resolution 79
A. Charge Changing Statistics 79
B. Multiple Scattering 79
C. Velocity Dependence of the Quantity $\bar{e}/v$ 79
D. Source and Detector Size 80
E. Nuclear Charge Distribution 80
6.4 Nuclear Charge Distribution of Single Mass Fission Fragments 81
6.5 Performance of the Fission Fragment Mass Separator 82

Conclusions 84

Bibliography 86

LIST OF TABLES

Table		Page
I	Maximum Pressure Effect on Equilibrium Charges of Light and Heavy Fission Fragments	25
II	Mean Radiative Lifetime as Determined from H_ℓ Data in Various Gases	39
III	Rate of Occurrence of Long Range Alpha Particles in Fission of U^{235}	72
IV	Empirical Determination of $\underline{n}$	83

LIST OF FIGURES

Figure		Page
1	Magnetic Fission-Fragment Spectrograph	4
2	Theoretical Electron Capture and Loss Cross Sections for Median Light Fission Fragments in Argon Gas at Low Pressure	12
3	$H\rho$ Distribution of Fission Fragments in Air at Pressure of 100 Microns	15
4	$H\rho$ Values of Median Light and Heavy Fission Fragments in Hydrogen as Functions of Pressure	17
5	$H\rho$ Values of Median Light and Heavy Fission Fragments in Helium as Functions of Pressure	18
6	$H\rho$ Values of Median Light and Heavy Fission Fragments in Air as Functions of Pressure	19
7	$H\rho$ Values of Median Light and Heavy Fission Fragments in Argon as Functions of Pressure	20
8	$H\rho$ Values of Median Light and Heavy Fission Fragments in Hydrogen as Functions of (Pressure x Velocity)	21
9	$H\rho$ Values of Median Light and Heavy Fission Fragments in Helium as Functions of (Pressure x Velocity)	22
10	$H\rho$ Values of Median Light and Heavy Fission Fragments in Air as Functions of (Pressure x Velocity)	23
11	$H\rho$ Values of Median Light and Heavy Fission Fragments in Argon as Functions of (Pressure x Velocity)	24
12	Equilibrium Charges of Median Light and Heavy Fission Fragments as Functions of Velocity in Various Gases	26
13	Equilibrium Charge of Mass-97 Fission Fragments as a Function of Velocity in Helium	27
14	Equilibrium Charges of Fission Fragments with Initial Energies as Functions of Atomic Number of Stopping Gas	28
15	Comparison of Theoretical and Experimental Values of Equilibrium Charge of Median Light Fission Fragments as a Function of Velocity	30

LIST OF FIGURES (Continued)

Figure		Page
16	Comparison of Theoretical and Experimental Values of Equilibrium Charge of Median Heavy Fission Fragment as a Function of Velocity	31
17	Fraction of Excitation Energy Retained by Median Light Fragment as a Function of Time Between Collisions--Hydrogen Data for Velocity Independent Cross Section	34
18	Fraction of Excitation Energy Retained by Median Light Fragment as a Function of Time Between Collisions --Hydrogen Data for (1/v) Cross Section	35
19	Graph of Fraction of Excitation Energy Retained by Median Light Fragment as a Function of Time Between Collisions for Velocity Independent Cross Section--Helium Data	36
20	Fraction of Excitation Energy Retained by Median Light Fragment as a Function of Time Between Collisions for (1/v) Cross Section--Helium Data	37
21	Scintillation Pulse Height Distributions of 5.3-Mev Alpha Particles and Median Light and Heavy Fission Fragments in Cesium-Iodide (Thallium) Crystals	42
22	Scintillation Pulse Heights of Median Light and Heavy Fission Fragments in Cesium-Iodide (Thallium) Crystals as Functions of Range in Argon	44
23	Scintillation Pulse Height of Fission Fragments in Cedium-Iodide (Thallium) Crystals as a Function of Residual Range in Argon Gas at Standard Pressure	45
24	Specific Fluorescence as a Function of Specific Energy Loss of Fission Fragments in Cesium-Iodide (Thallium)	46
25	Scintillation Pulse Heights of Median Light and Heavy Fission Fragments as Functions of Range in Aluminum	51
26	Energy of Median Light and Heavy Fission Fragments as Functions of Range in Aluminum	52
27	Energy Calibration of Scintillation Detector for Fission Fragments	53
28	Energy of Median Light and Heavy Fission Fragments as Functions of Range in Hydrogen Gas at Standard Pressure	54

LIST OF FIGURES (Continued)

Figure		Page
29	Energy of Median Light and Heavy Fission Fragments as Functions of Range in Helium at Standard Pressure	55
30	Energy of Median Light and Heavy Fission Fragments as Functions of Range in Air at Standard Pressure	56
31	Energy of Median Light and Heavy Fission Fragments as Functions of Range in Argon at Standard Pressure	57
32	Energy of Median Light and Heavy Fission Fragments as Functions of Range in Nickel	58
33	Energy of Median Light and Heavy Fission Fragments as Functions of Range in Gold	59
34	Energy of Median Light Fission Fragment as a Function of Range on Various Materials	61
35	Energy of Median Heavy Fission Fragment as a Function of Range in Various Materials	62
36	Scintillation Pulse Heights of Long Range Alpha Particles from Fission of Uranium-235 as a Function of Energy	66
37	Energy Distribution of the Long Range Alpha Particles from Pile Neutron Fission of Uranium-235	69
38	Coulomb Barrier Penetration Factors for Emission of Alpha Particles from a Compound Nucleus as Functions of Particle Energy	71
39	$H\rho$ Distributions of Mass-97 Fission Fragments in Helium at Various Pressures	76
40	Width of $H\rho$ Distribution of Mass-97 Fission Fragments as a Function of $(1/P)^{1/2}$	77
41	Width of $H\rho$ Distribution of Mass-97 Fission Fragments Due to Various Contributions and Graph of Experimentally Determined Widths	78

INTRODUCTION

Since the discovery of the phenomenon of nuclear fission by Hahn and Strassman in 1938 the properties of fission fragments have been the subject of many investigations. In his review article on nuclear fission, Turner (1940) showed that fission products played an important role in the experiments which led to the discovery of fission. In addition to serving as a source of information about the process, the fission fragments are a unique source of high speed ions of large charge and mass. The phenomena connected with the penetration of these particles through matter are an important source of information about atomic processes.

The term "fission" implies a number of associated processes. The most common of these is binary fission in which the nucleus divides into two fragments of comparable size. These fragments have mass numbers ranging from about 70 to 170, nuclear charges ranging from 30 to 60, and initial velocities of the order of magnitude of 10^9 cm/sec. In a minority of cases, nuclei of low atomic weight are emitted at the instant of fission in addition to the main fragments. Very rare processes have been reported in which the nucleus divides into three or more fragments of comparable size (Whitehouse, 1952).

Due to the high initial velocities, nuclei of the primary fission fragments are unable to carry a sufficient number of electrons to form neutral atoms. The fragments are thus ions with charges determined by their velocities and the medium in which they are moving. Initially the fragments have charges ranging from about 15 to 25 electron charges and are thus well suited to study by magnetic analysis.

Magnetic analysis of fission fragments was employed by Lassen at the Institute of Theoretical Physics, University of Copenhagen, Denmark. In the experimental arrangement used by Lassen, fission was achieved by bombarding a uranium foil with neutrons emitted from a beryllium target which in turn was bombarded with deuterons in a cyclotron. Some of the fission fragments would move through the

magnetic field of the cyclotron and enter an ionization chamber, located about 20 cm away, which detected them. Analysis of the fragments was achieved by moving a narrow slit across the paths of the fragments so as to vary the curvature of the allowed path from the source to the window of the ionization chamber.

Measurements were made by Lassen (1945[a,b], 1950) to determine the charges of fission fragments in gases and in vacuum after the fragments passed through thin metallic foils. Estimates of electron-capture cross sections of fission fragments in gases were made from data that were obtained.

Under the direction of Dr. Bernard L. Cohen a high resolution system for magnetic analysis of fission fragments from pile neutron fission of uranium-235 was build and installed in the Oak Ridge National Laboratory Graphite Reactor. The energy distribution of fission fragments of mass 97 was determined by Cohen, Cohen, and Coley (1956) from data obtained with this apparatus.

The purpose of this thesis is to report the results of some fission fragment studies by the author. The studies include the following items:

1. Equilibrium charges of light and heavy fission fragments as functions of fragment velocity, gas pressure, and type of gas.
2. Response of CsI(Tl) crystals to fission fragments.
3. Energy vs range in various materials for fission fragments.
4. Magnetic analysis of long range particles from fission of U^{235}.
5. A fission fragment mass separator and the nuclear charge distribution of single mass fission fragments.

The fission fragment spectrograph developed by Cohen at Oak Ridge National Laboratory was used for these studies.

CHAPTER 1

DESCRIPTION OF APPARATUS AND EXPERIMENTAL PROCEDURES

1.1 Magnetic Wedge Spectrograph

A photograph of the magnetic wedge spectrograph used for these studies is shown in Fig. 1. It consists of a 40-degree single focusing wedge magnet, entrance arm, and exit arm. The magnet is installed just outside the shield wall of the Oak Ridge National Laboratory Graphite Reactor. The entrance arm is a 16-ft aluminum tube 3 1/2 in. in diameter situated in a reactor hole with its far end near the center of the reactor core. A 150-$\mu g/cm^2$ plating of uranium-235 on a nickel surface 1 in. wide and 2 1/2 in. high is mounted in the end of the tube. A flux of 5×10^{11} neutrons/cm^2-sec is available at the end for irradiation of the uranium. Fission fragments are thus produced at a rate of approximately 10^9 per second of which about one in 10^5 is emitted in the right direction to travel down the tube and enter the deflection chamber. The fragments whose radii of curvature in the magnetic field is between 96.2 and 104.3 cm are focused at the focal plane which is six ft beyond the magnet. The path length of the fragments through the magnetic field is about 69 cm.

The fragments enter and leave the deflection chamber at normal incidence to the magnet edge and thus are not focused in the vertical direction. The beam is defined by 1-in. high slits at the entrance and exit of the deflection chamber. At the focal plane the beam is about 2 1/4 in. high.

Protection against scattering from the wall of the 16-ft entrance arm is achieved by four approximately equally spaced diaphrams of 2 1/4 in. inside diameter. The diaphrams are of 0.001-in. aluminum foil which is opaque to fission fragments and thin enough to avoid edge scattering problems.

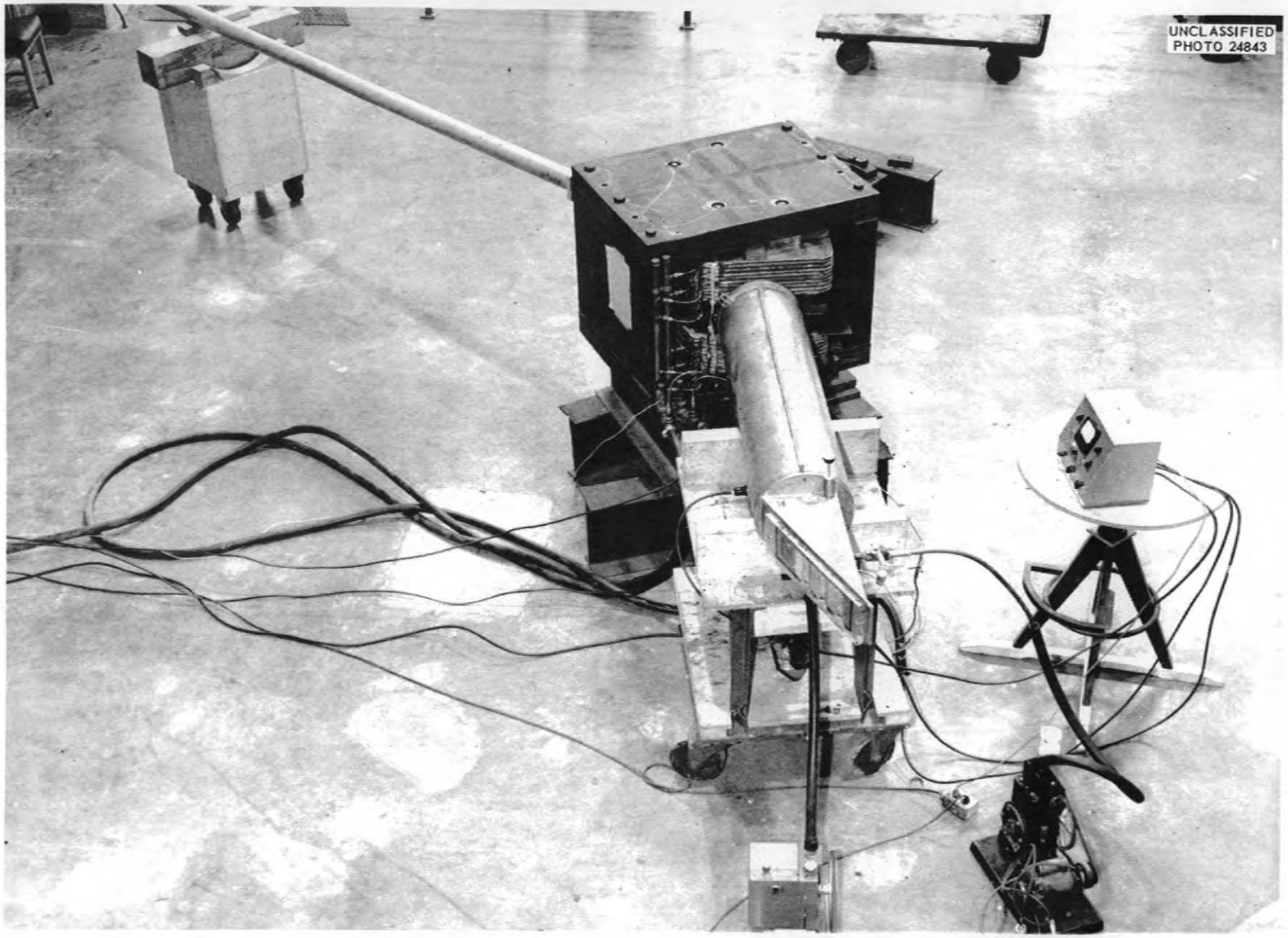

Fig. 1. Magnetic Fission-Fragment Spectrograph.

A 0.1-millicurie plating of Po^{210} on Pt, 1-in. high and 1/16-in. wide is installed beside the U^{235} source. The Po alphas were used for alignment purposes when the system was installed at the reactor and for numerous energy calibrations during the experiments.

The magnet is powered by a 15-kw Amplidyne motor-generator set. The current in the magnet coils is maintained at a desired value by an electronic circuit which maintains a balance between the potential difference across a shunt in the magnet circuit and that across a potentiometer that is connected across a dry cell battery. Drift in the magnetic field is kept below 0.1% by maintaining temperature control at the current regulator. The field coils are cooled by circulating water through copper tubes that are welded to the copper bars of which the coils are constructed. The magnetic field can be maintained at any desired value up to approximately 11,000 gauss. The field is measured by a Varian Associates Nuclear Fluxmeter which utilizes the proton magnetic moment. The accuracy of the measurement is approximately 0.05%.

The vacuum system includes a well-baffled 300-liter/sec oil diffusion pump backed by a 110-liter/min mechanical pump. For most of the measurements made in these studies the diffusion pump was not used during a run but was used to evacuate the system before admitting the desired gas unless air was being used for the run. The vacuum system is capable of maintaining a vacuum of approximately 10^{-5} mm Hg as measured by a triode-type ionization gauge which is used to measure pressures below 0.001 mm Hg. Pressures from 0.001 to 6 mm Hg are measured with a McLeod gauge; higher pressures are measured with a U-tube manometer.

The data for these studies were obtained with various gases in the system. Gases are bled into the system through a needle valve, and the desired pressure is achieved as a dynamic equilibrium between bleed-in and pump-out. In some of the experiments it is desirable to fill only the deflection chamber with gas in order that higher

pressures may be maintained without stopping the fragments. Hereafter this will be referred to as using "gas in the magnet" as opposed to "gas in the system" when the entire vacuum system is filled with gas.

Provision for using gas in the magnet was accomplished by mounting 100-$\mu g/cm^2$ Formvar windows* between the deflection chamber and the entrance and exit arms. A separate pump is provided to establish the dynamic equilibrium with gas bled into the deflection chamber, while the regular pumping system evacuates the entrance and exit arms, which are connected by rubber hose. The pressure in the magnet is measured with U-tube manometers leading to each side of the windows.

Radiation shielding is required for working with the system as it is installed at the reactor. A 1-ton beam catcher is located beyond the magnet in line with the reactor hole. Other shielding includes 700 lb paraffin, 2000 lb lead bricks, 25 ft^2 cadmium sheet and a thirty-gal water tank which surrounds the exit arm. At the focal plane, radiation levels of gamma rays and neutrons are approximately at maximum permissible levels for 40 hr/wk exposure.

---

* The windows were made of Formvar films which were peeled off a glass plate that had been dipped into a solution of Formvar and chloroform. The thickness of individual films was approximately 33 $\mu g/cm^2$ as determined by weighing a large film. To eliminate the problem of pin holes three films were stacked to make a laminated film. This film was dried under a heat lamp and in a vacuum desiccator before it was attached to the window frame with rubber cement. Since the windows were several square inches in area the films were supported by 50% transparent nickel grids. A test before the windows were installed showed that they can support a pressure of 20 cm Hg or more. The windows were built with the cooperative assistance of Dr. B. H. Kettelle of the Chemistry Division of Oak Ridge National Laboratory.

1.2 Mass Identification Studies

Studies of fission fragments of a particular mass are achieved by collecting the fragments arriving at the focal plane on a 0.001-in. aluminum foil for several hours after which the foil is removed and cut into strips, each strip corresponding to a given range of $H\rho$, the product of the magnetic field $\underline{H}$ and the radius of curvature $\underline{\rho}$. The strips are then processed radiochemically for the desired fission product and the resulting activity is measured with end-window geiger counters. The activities are counted for several hours with a separate counter for each of the 10 specimens obtained in a run. Automatic recording of the counts is achieved with an Esterline Angus Operation Recorder making pen marks corresponding to register counts and the chart drive providing the time scale.

Corrections are applied to the measured activities before the $H\rho$ distribution is obtained. Corrections are made for decay while the fragments are being collected on the aluminum foil and for decay while the foils are being radiochemically processed. The strips into which the foils are cut are weighed and corrections for variation in area are made. Chemical yields are weighed and normalized to 100% yield of the carrier that is added after the films are dissolved. The counters used to measure the activities are cross-calibrated with a phosporus-32 beta source at frequent intervals. Background counts of at least three-hr duration are obtained almost daily.

1.3 Studies by Scintillation Detection

While the radiochemical method is extremely accurate the rate of data accumulation is very low. For studies that do not require the extreme accuracy and mass identification, the rate of data accumulation is greatly increased by scintillation detection of the fission fragments.

A CsI(Tl) crystal was selected for scintillation counting of the fission fragments because of its non-deliquescent properties. The 1-in. diameter crystal was cemented to a Lucite light pipe which

passed through a flange that was mounted on the face plate at the focal plane. R-313 cement, a product of the Carl H. Biggs Company of Los Angeles, California, was used. After the crystal was cemented to the light pipe it was machined to a thickness of 0.003 in. This is thick enough to stop all fission fragments except the long range alpha particles and is thin enough to eliminate detection of much of the background of gamma and beta rays.

A Dumont 6292 photomultiplier tube was taped to the outside end of the Lucite light pipe with Dow Corning stopcock grease making contact between the two. The electrical pulses resulting from the arrival of fission fragments at the crystal were amplified by an Oak Ridge National Laboratory Instrument Department DD-2 Linear Amplifier, analyzed by Atomic Instrument Model 510 Single Channel Pulse Height Analyzers, and counted by Atomic Instrument Company Model 162 Glow Transfer Counters. Most of the data were taken with one single channel analyzer in use but other data were taken with three in parallel. Prior to use they were checked for linearity and cross-calibrated with a NaI(Tl) crystal and gamma rays from Zn^{65}, Co^{60}, and Cs^{137}. These calibrations were done during a reactor shutdown to insure against background problems. The pulse height of the Po^{210} alphas was measured frequently to check for counter drift and to normalize the data when changes in the crystal mounting were made. The photomultiplier tube was operated at a positive potential of 920 volts which was supplied by an Atomic Instrument Company Model 312 Super Stable High Voltage Power Supply.

CHAPTER 2

EQUILIBRIUM CHARGES OF FISSION FRAGMENTS IN GASES AS FUNCTIONS OF VELOCITY, GAS PRESSURE, AND TYPE OF GAS

2.1 Introduction

The phenomena associated with the penetration of high speed particles through matter are a most important source of information about atomic processes. Nuclear fission provides a unique source of high speed ions of large charge and mass, the study of which reveals many interesting features, especially regarding the capture and loss of electrons by such ions.

Bohr (1940) estimated the charge of a heavy ion in a medium by assuming it to be stripped of all orbital electrons which have velocities smaller in magnitude than the translational velocity of the ion. This estimate assumes that the charge of the ion is uniquely dependent on its velocity and that the influence of the medium is negligible.

Lassen (1950, 1951[ab]) found that the charges of fission fragments are influenced by the medium in which they are moving. Using the magnetic deflection arrangement referred to in the introduction of this thesis, he showed that the average charge of a fission fragment which passes through a thin metallic foil into the deflection chamber at high vacuum is approximately 50% higher than that measured for a fragment of the same mass and velocity if the deflection chamber contains gas. Lassen also found that as the gas pressure is increased, at low values of pressure, the average fragment charge increases but reaches a maximum and does not change with additional increase of gas pressure.

The measurements of Lassen were made for fragment velocities of 6.48 v_o for the light fragments and 4.42 v_o for the heavy fragments.* Due to the rather short path the fragment velocities were not changed

---

*v_o is the velocity of the electron in a hydrogen atom in the ground state, i.e., $(e^2/\hbar)$ or 2.19×10^8 cm/sec.

appreciably by the gas. Some subsequent measurements of equilibrium charge of fission fragments in gases at a lower velocity for each group of fragments were made by Lassen. The lower velocity was achieved by covering the uranium plating with a thin mica foil of uniform thickness. This reduced the velocities of the light and heavy fragments to about 5.4 v_o and 3.4 v_o, respectively. These are the only measurements of fission fragment equilibrium charge in gases that have been reported.

Bohr (1948) and Bohr and Lindhard (1954) have given theoretical treatments describing electron capture and loss by heavy ions penetrating through matter. Bohr's earlier assumption, that the charges of the ions are uniquely determined by velocity, was modified to account for the experimental observations of Lassen.

2.2 Approximate Description of Heavy Ion Constitution

Encounters between highly charged ions and neutral atoms result in considerable change in electron binding, particularly in the atom, where the more loosely bound atomic electrons at an early stage of the collision are greatly influenced by the strong electric field around the ion. The transfer of energy accompanying excitation and ionization of the atom is the principal mechanism for energy loss by the ion.** During the collisions, processes also take place which may result in excitation of the ion, or a change of ion charge due to electron capture and loss. A rigorous description of the processes involved presents a problem of great complication, but since the binding states in the ion involved in electron capture and loss are specified by high quantum numbers, simple mechanical considerations can be used to survey the essential features of the processes and interpretation of the experimental results reported later in this chapter.

** This holds true until the ion has been slowed to a velocity of the order of v_o, at which time it becomes a neutral atom. Due to its large mass, the energy of the ion is still of the order of several million electron volts. The principal stopping mechanisms during the remainder of the path are nuclear or hard particle collisions.

As heavy ions, such as charged fission fragments, move through matter they will both lose and gain electrons due to collisions with atoms and the charges of the ions will fluctuate about an equilibrium value between the two competing processes. As the charge of the ion is increased, the electric field which it exerts on neutral atoms that it encounters in the medium being penetrated is increased, and thus the electron capture cross section is increased. On the other hand as the charge on the ion is increased there will be increased numbers of unfilled energy states to which electrons in the ion can be raised during the encounter, thus the probability of excitation without ionization is increased. This causes the electron loss cross section to decrease with increasing ion charge. For a particular value of ion charge the electron capture and loss cross sections are equal. Due to the opposite effect, on the respective cross sections, as the charge changes the ion charge will fluctuate about an equilibrium value in penetrating a medium.

Figure 2 illustrates the variation of the respective cross sections as functions of ion charge. These curves were plotted for a light fission fragment of nuclear charge 38, mass 95, and velocity 4 v_o, moving in argon. The cross sections were calculated from theoretical formulae derived by Bohr and Lindhard (1954).

After an encounter one or more electrons in the ion may be in an excited state. In a short time this excitation energy is shared among a number of the electrons in the ion. If the ion is penetrating a medium of low density this excitation energy will be dissipated by radiation between collisions, and the electron loss cross section for the ground state will determine the equilibrium charge. At higher gas pressure the time between collisions is reduced and the residual ion excitation must be considered. An electron in an excited state is more easily removed from the ion and the electron loss cross section is thus increased with the result that the equilibrium charge is increased. If the pressure is increased enough so that almost none of the excitation energy is dissipated by radiation between encounters, the electron loss cross section will have reached a saturation value and the equilibrium charge will not increase with additional increase of pressure.

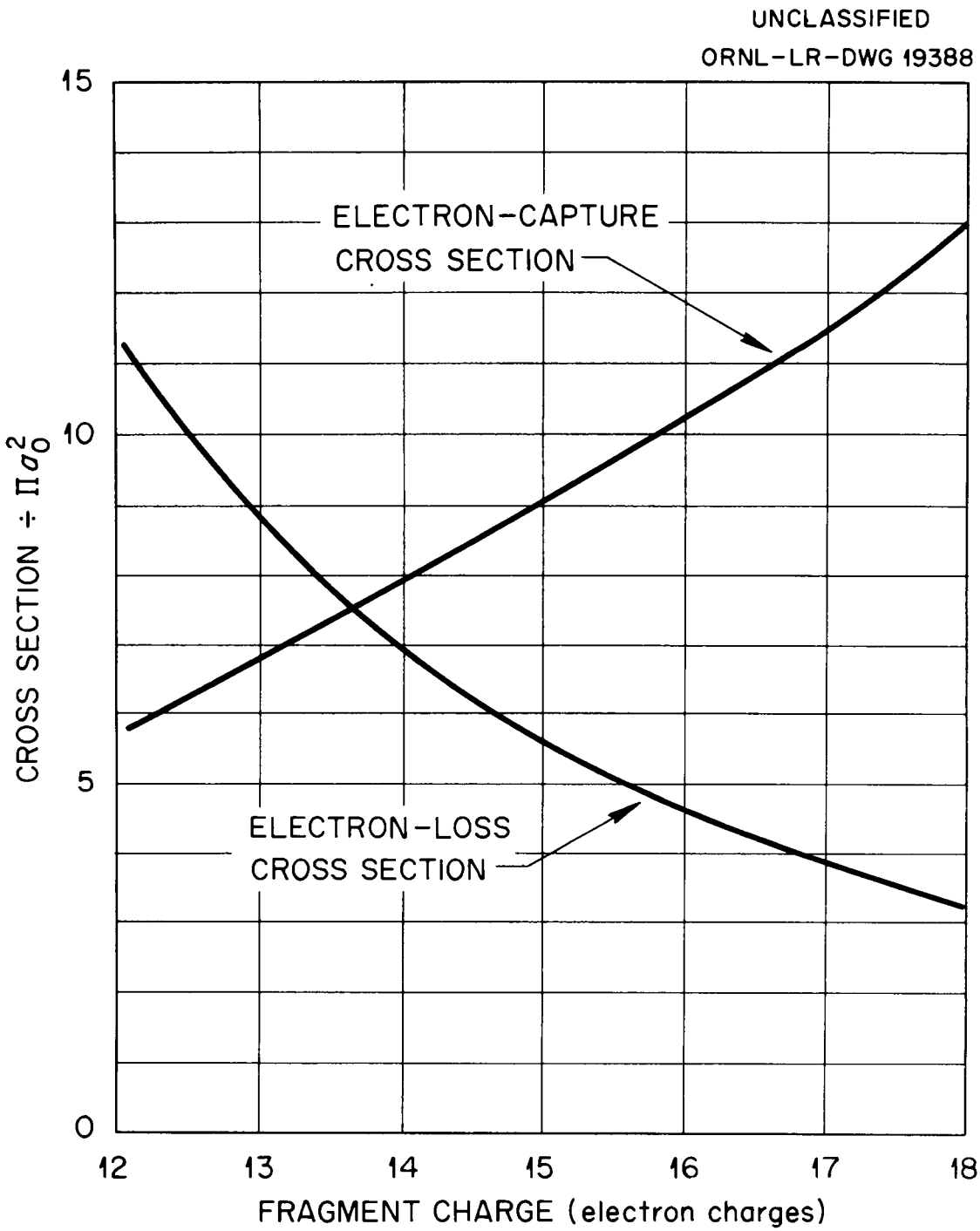

Fig. 2. Theoretical Electrons Capture and Loss Cross Sections for Medium Light Fission Fragments in Argon Gas at Low Pressure.

The time required for distribution of the excitation energy within the ion is of the order of the period of revolution of the excited electron about the nucleus, which is approximately ($2\pi a/v$) or about 10^{-16} second. In solids the time between successive collisions which is ($1/nV\sigma$) may be shorter than the time required for distribution of the excitation energy. Thus the ion may enter a collision with an electron in a higher state of excitation than would be the case if the energy distribution process was complete and the electron loss cross section is further increased. This in a qualitative way accounts for the higher charges of fission fragments in metals that were observed by Lassen.

The loss of electrons from the heavy ion is accomplished by transfer of sufficient energy to its electrons to allow one or more electrons to escape. The more loosely bound electrons of the atom, due to their small mass and charge, are not able individually to transfer sufficient energy to the ion for ionization. The main contribution to the electron loss process arises from the action of the nucleus of the atom on the ion if the gas is composed of light atoms. For heavier atoms the orbital velocities of part of the electrons are larger than the fragment velocity and these electrons screen part of the nuclear charge. The contribution to the electron loss process arises from the atomic core in the case of heavier atoms. Thus some variation of equilibrium charge as a function of atomic number of the stopping gas is expected for light atoms. This variation will decrease with increasing atomic number where the unscreened part of the nuclear charge does not vary appreciably with atomic number.

2.3 Experimental

Equilibrium charges of the light and heavy groups of fission fragments were measured for a large range of velocities in gas. Data were taken at low pressures with gas filling the system and at high pressure with gas in the deflection chamber only. This was done to study the effect of velocity on the $H\rho$ distributions. The complete set of measurements was used to study the pressure effect on equilibrium charge. The gases used were H_2, He, air, and argon.

The fragments were detected at the focal plane by the 0.003-in.

CsI(Tl) crystal and photomultiplier tube. The $H\rho$ distributions were determined with integral pulse counting, with the discrimination level set to eliminate background.

The $H\rho$ distributions of the light and heavy groups of fragments were determined by taking a one-minute count at a given magnetic field setting, changing the field by approximately 2% and repeating. The magnet was passed through a hysteresis cycle between settings to insure against magnetic lag. The counting rates at the peaks of the distributions were approximately 1200 counts per minute, with the windows installed at the entrance and exit of the deflection chamber, and correspondingly higher without the windows so the counting statistics were good. A typical distribution curve of the type obtained is shown in Fig. 3. The distribution on the left is for the light group of fragments and the distribution on the right is for the heavy group. The peaks obviously correspond to the peaks of the well-known fission fragment mass distribution curve.

The magnetic field $\underline{H}$ in gauss, radius of curvature of the fragments in the magnetic field $\underline{\rho}$ in centimeters, energy of the fragments $\underline{E}$ in Mev, mass of the fragments $\underline{M}$ in atomic mass units, and equilibrium charge $\bar{e}$ in electron charges are related by the equation

$$H\rho = 14.35 \times 10^4 (ME)^{1/2}/\bar{e}. \qquad (2,1)$$

The values of $\underline{E}$ were obtained from range $\underline{vs}$ energy curves which are discussed in Chapter 4. Values were computed for masses 95 and 139 which correspond to the peaks of the mass distribution curve.

While the peaks of the $H\rho$ distributions determined by scintillation detection correspond to the median light and heavy fission fragments, there is considerable overlapping of the distributions of neighboring masses. This might be expected to obscure any structure in the equilibrium charge as a function of fragment velocity results obtained. To check this, data were obtained by the mass identification method (see Chapter 1) for mass 97 with He gas in the system. The range of pressures covered by these data are from 0.44 to 10 mm Hg.

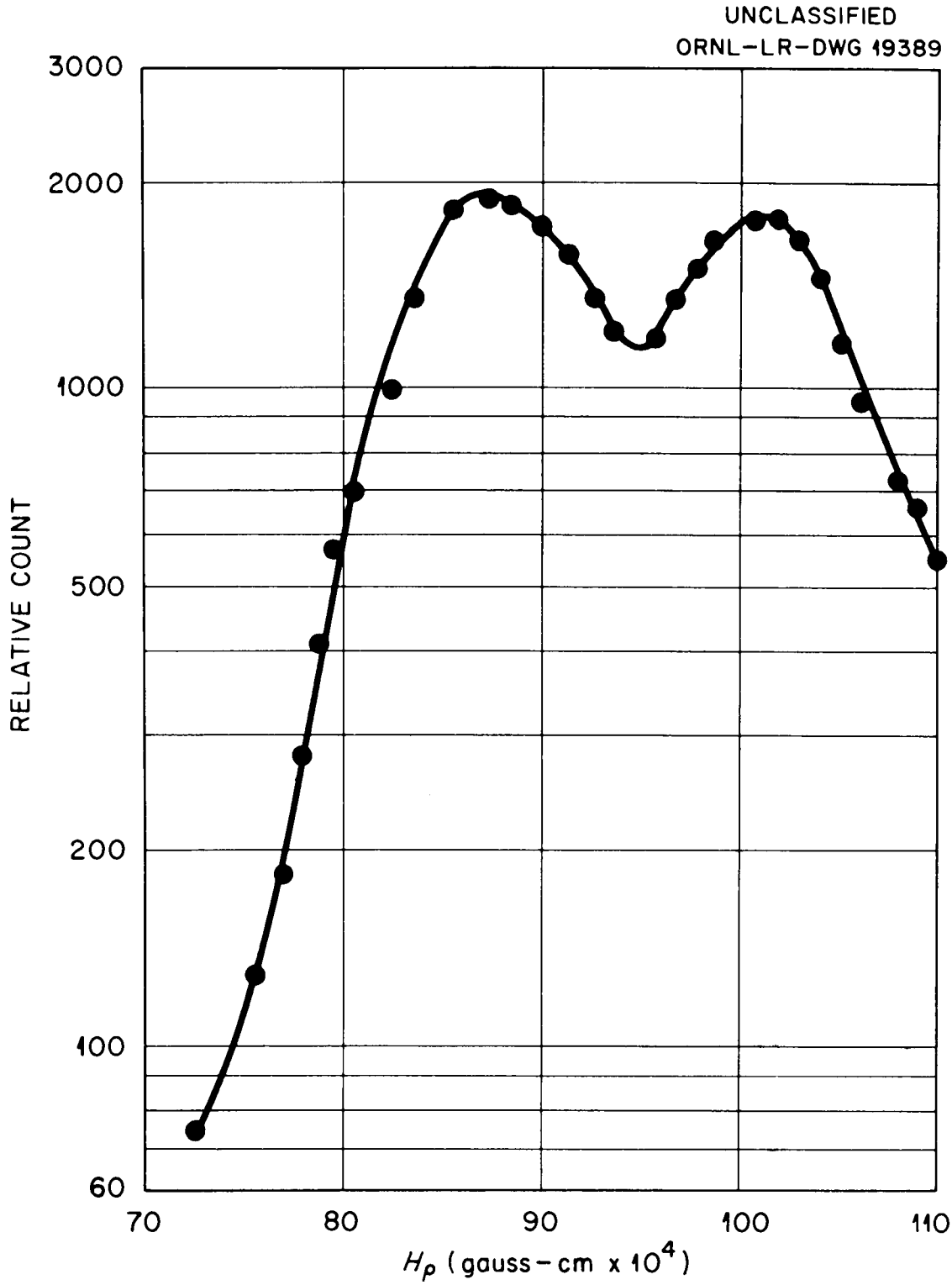

Fig. 3. $H\rho$ Distribution of Fission Fragments in Air at a Pressure of 100 Microns.

2.4 Presentation of Data and Discussion of Results

The $H\rho$ values of the peaks of the $H\rho$ distributions for the light and heavy fragments are plotted as a function of gas pressure and the resulting curves are shown in Fig. 4, 5, 6, 7. The triangles or full circles refer to data obtained with gas filling the system and the open circles refer to data with gas in the deflection chamber only. The ordinate scales are greatly expanded and do not start at zero. The $H\rho$ values are plotted as a function of gas pressure multiplied by fragment velocity and the resulting curves are shown in Fig. 8, 9, 10, 11. The peaks of the $H\rho$ distributions of the heavy fragments, with helium gas filling the system, are beyond the range of the magnet. Part of the distribution is within the range and from this the $H\rho$ values of the peaks are estimated.

The reason for presenting the data with different abscissa scales is as follows. If the abscissa scale is properly chosen it will be inversely proportional to the average time between charge-changing collisions and the resulting curve will show in detail the pressure effect on the equilibrium charge. The time between collisions is determined by the density of the gas and by the cross section for electron capture or loss. The density is directly proportional to the pressure. The exact relationship between the cross section and the fragment velocity is not known. Bohr and Lindhard (1954) derived an expression for equal capture and loss cross sections in which the magnitude of the cross section at equilibrium varies inversely with fragment velocity. If this relation is correct the graphs of $H\rho$ vs (pressure) are the appropriate ones for studying the pressure effect. The graphs of $H\rho$ vs (pressure x velocity) correspond to the assumption that the cross sections are independent of fragment velocity.

The velocity effect on $H\rho$ was studied with the fragments in helium gas. The data for gas in the system and in the deflection chamber overlap for a large range of abscissa values in Fig. 5 and 9. For a given abscissa the fragment velocity, with gas in the deflection chamber only, is about 50% larger than if gas is filling the system. The data show the

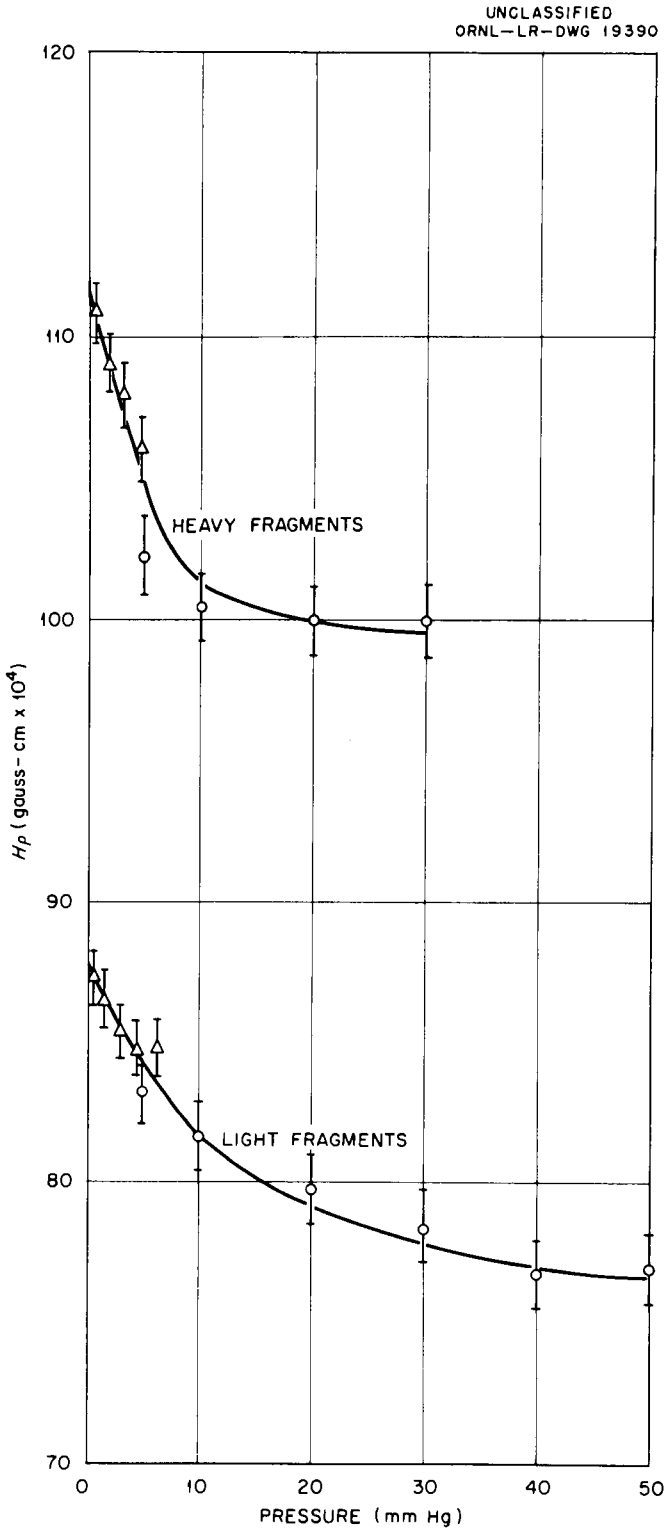

Fig. 4. Hρ Values of Median Light and Heavy Fission Fragments in Hydrogen as Functions of Pressure.

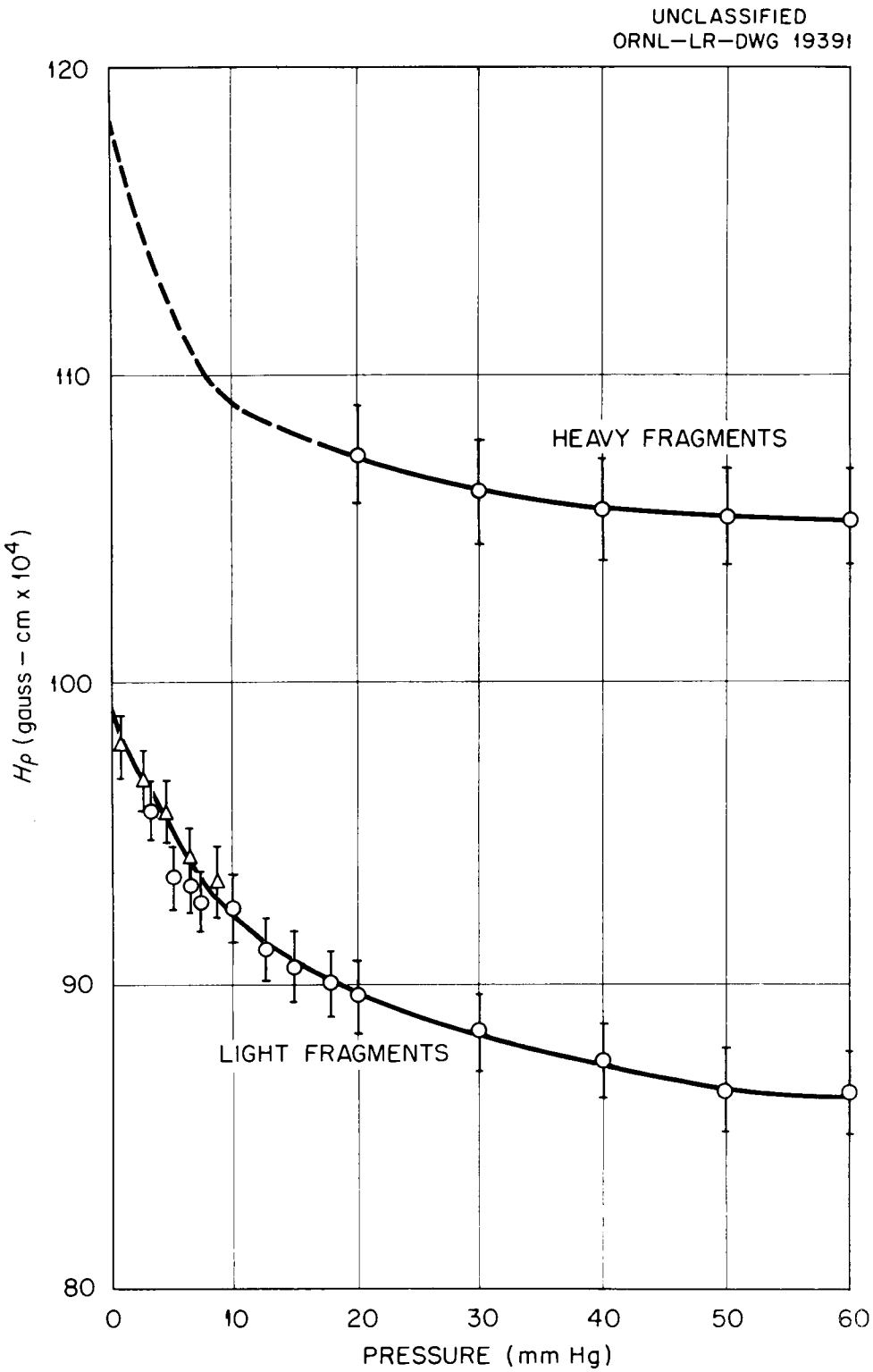

Fig. 5. $H\rho$ Values of Median Light and Heavy Fission Fragments in Helium as Functions of Pressure.

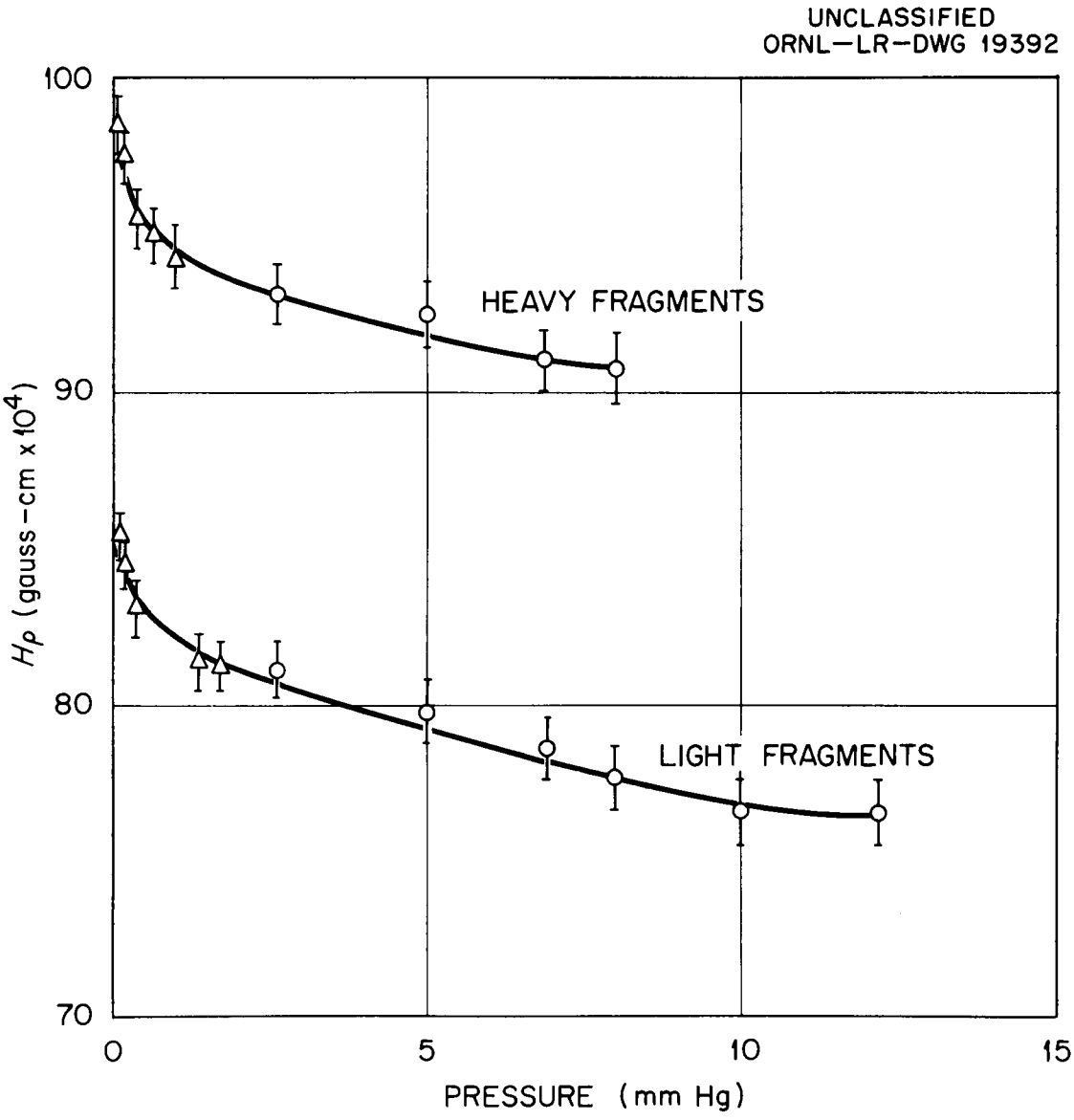

Fig. 6. $H\rho$ Values of Median Light and Heavy Fission Fragments in Air as Functions of Pressure.

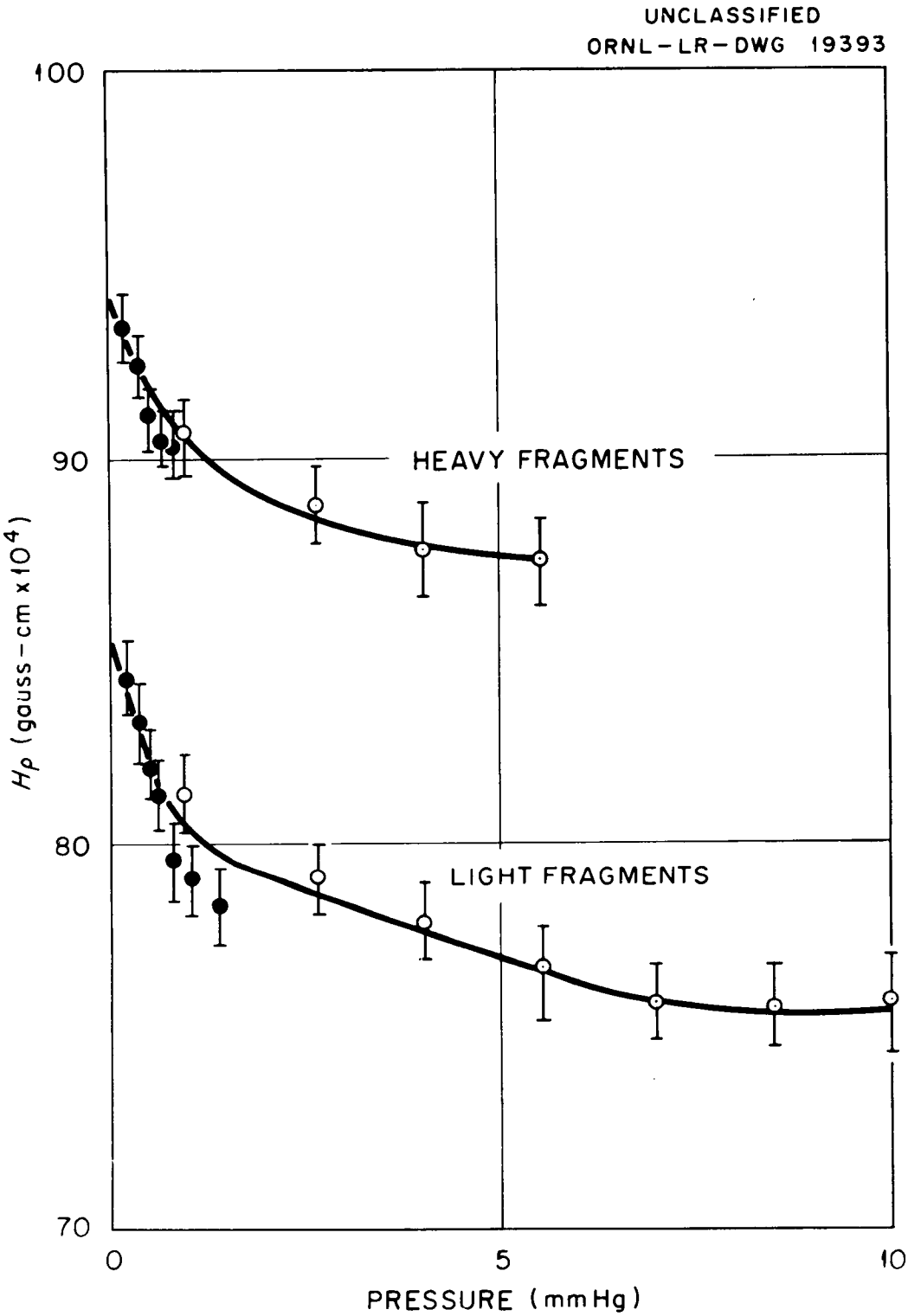

Fig. 7. $H\rho$ Values of Median Light and Heavy Fission Fragments in Argon as Functions of Pressure.

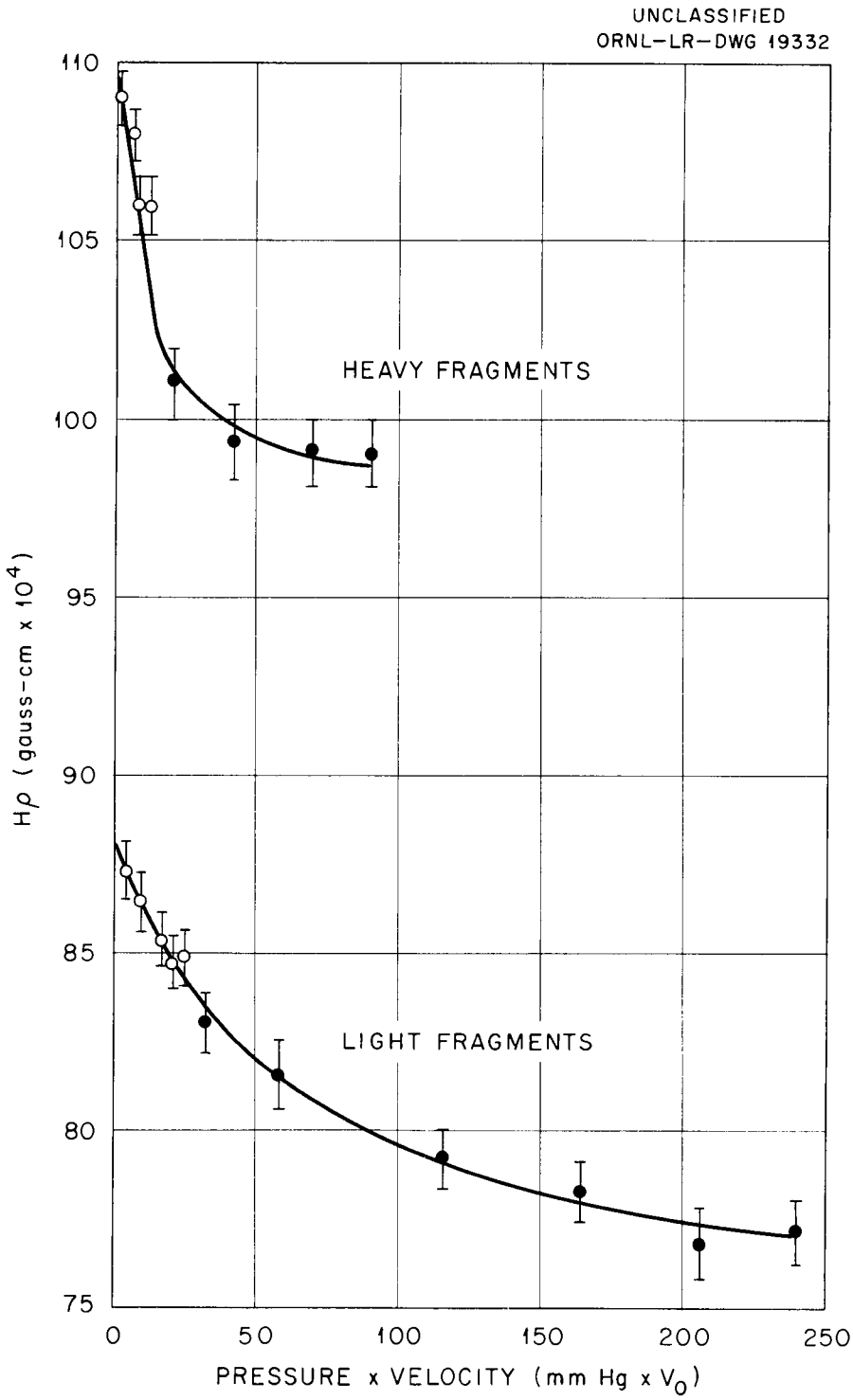

Fig. 8. $H\rho$ Values of Median Light and Heavy Fission Fragments in Hydrogen as Functions of (Pressure x Velocity).

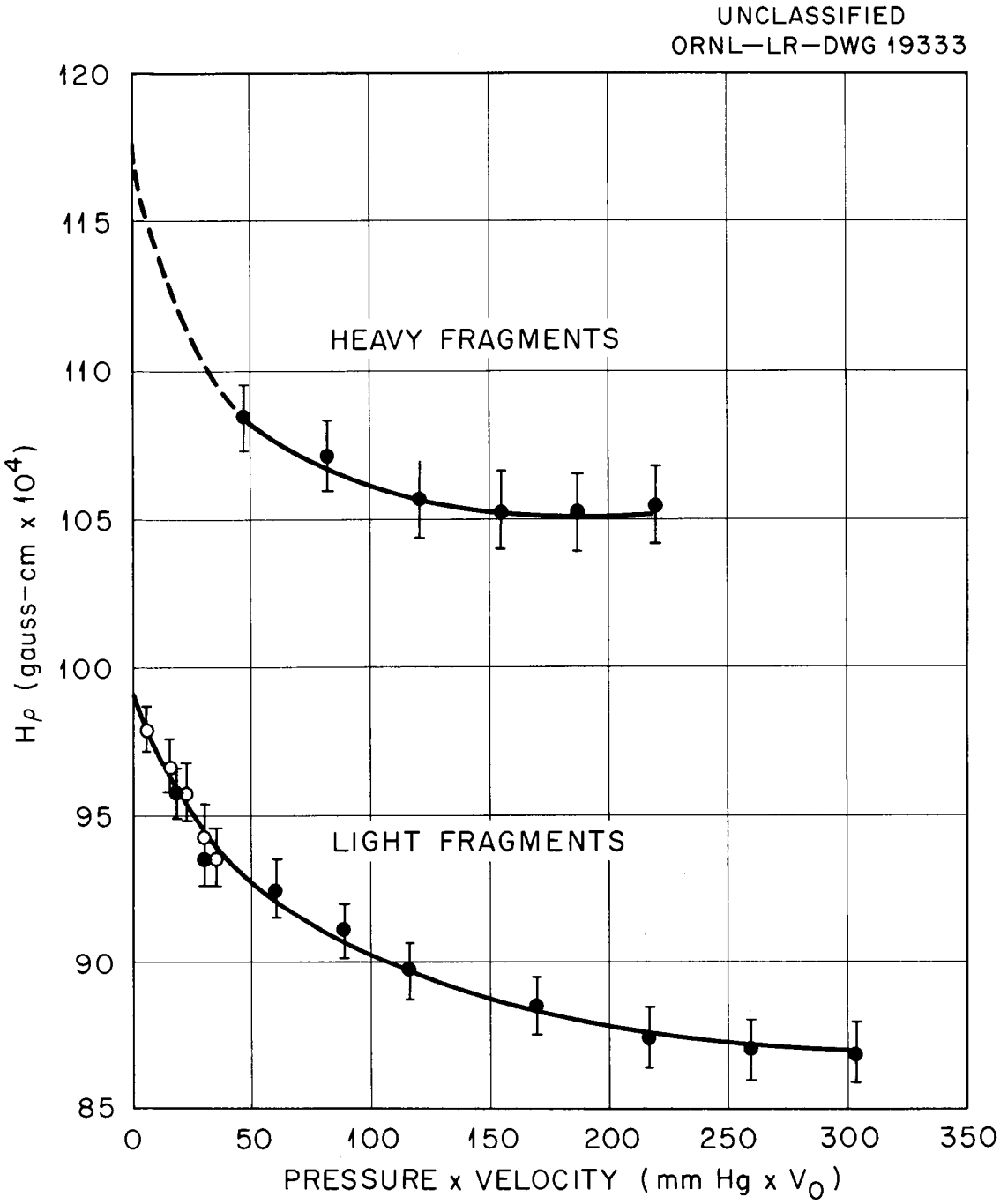

Fig. 9. $H\rho$ Values of Median Light and Heavy Fission Fragments in Helium as Functions of (Pressure x Velocity).

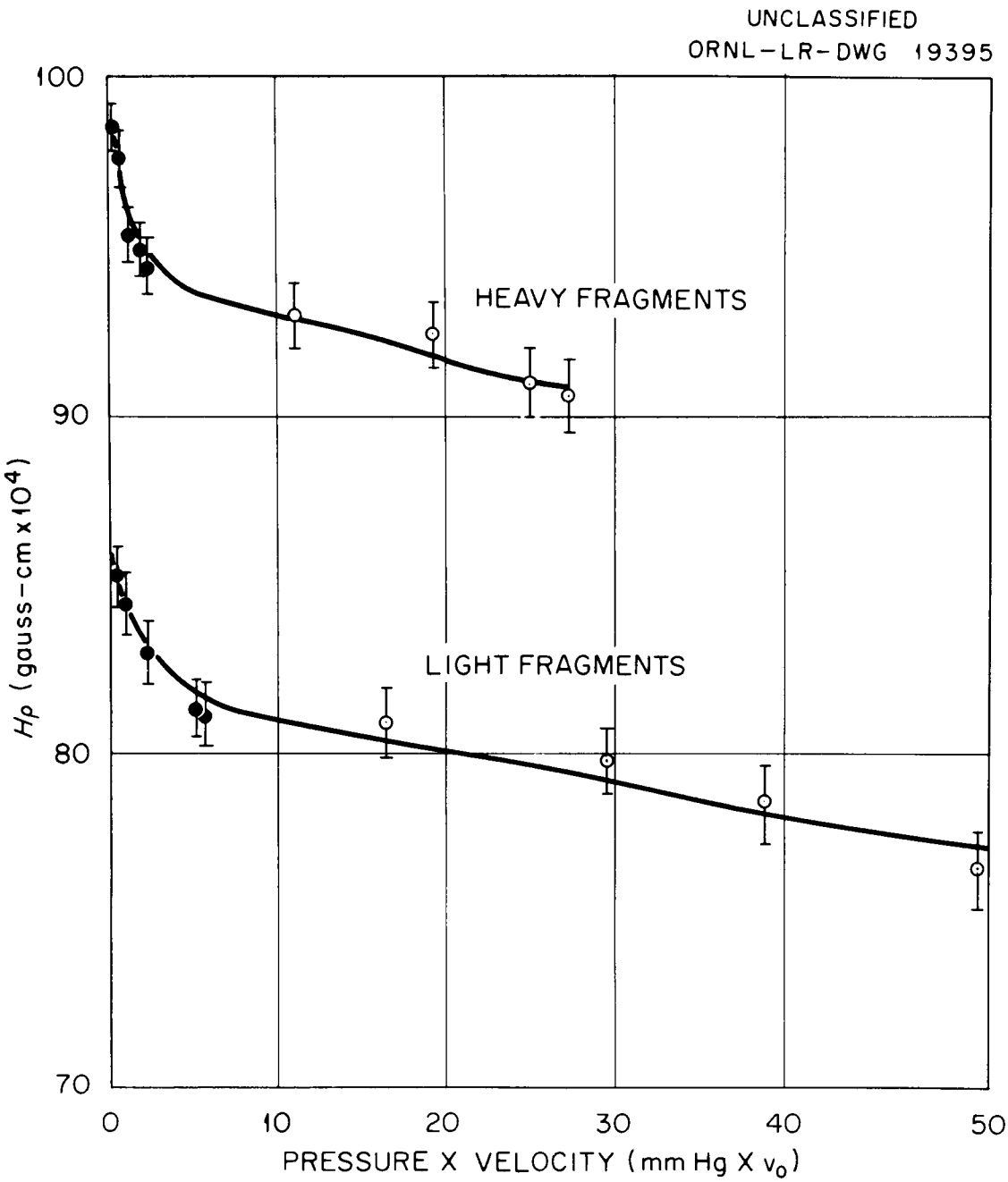

Fig. 10. $H\rho$ Values of Median Light and Heavy Fission Fragments in Air as Functions of (Pressure x Velocity).

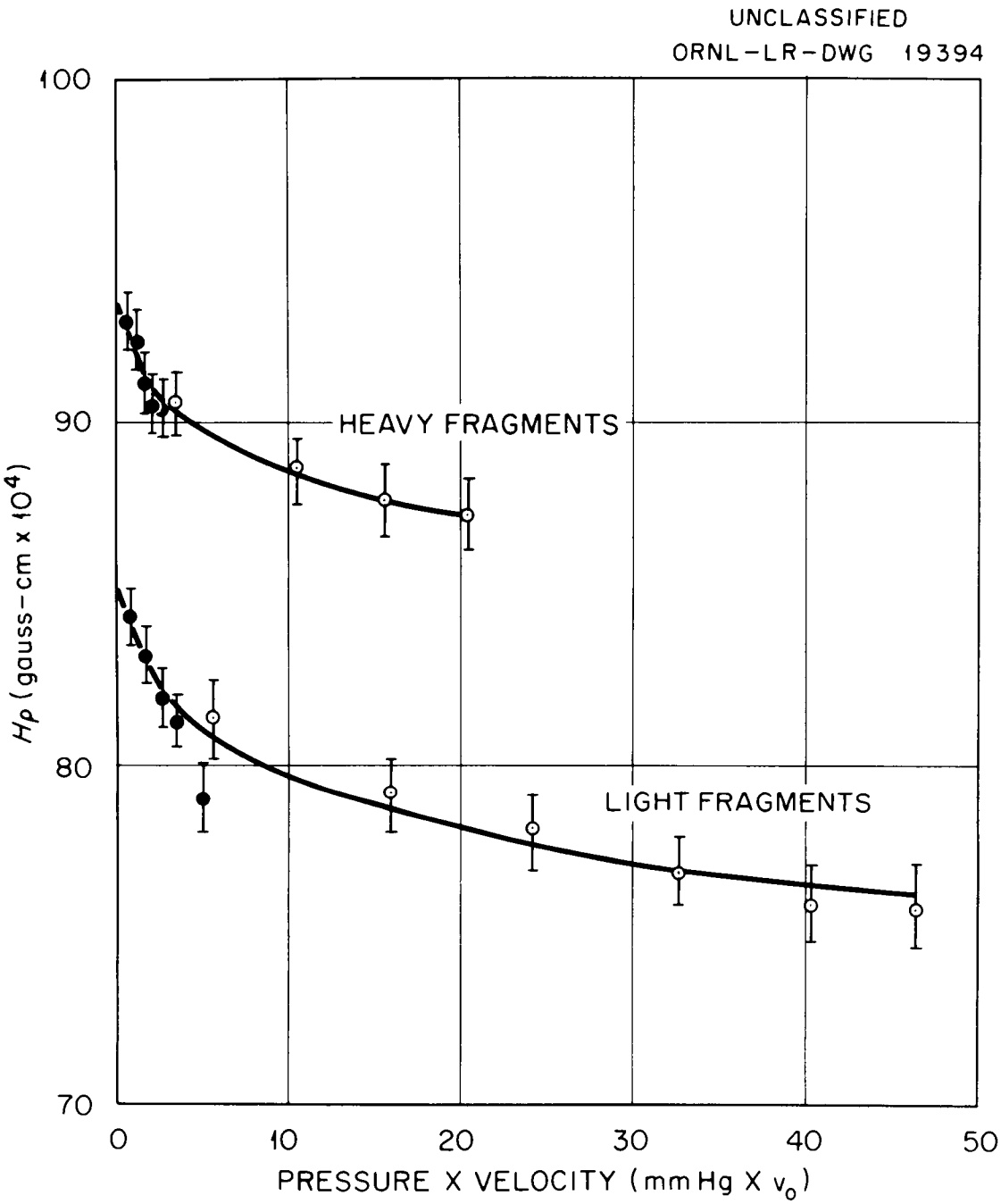

Fig. 11. $H\rho$ Values of Median Light and Heavy Fission Fragments in Argon as Functions of (Pressure x Velocity).

velocity effect on $H\rho$ to be less than 2% for the light fragments in helium. The same results were obtained with less complete data in H_2 and air. The data obtained with argon (Fig. 7 and 11) show velocity effects of almost 5% on $H\rho$.

The ordinate values approached by the curves, as they approach zero abscissa, correspond to the absence of the pressure effect on the equilibrium charge. The flat portions of the curves correspond to saturation of the pressure effect. The range of $H\rho$ values covered by each curve corresponds to the range of the pressure effect on the equilibrium charges of the fragments. The maximum effect on each group of fragments for each gas are tabulated in Table I.

TABLE I

Maximum Pressure Effect on Equilibrium Charges of Light and Heavy Fission Fragments

Type of Gas	Maximum Percentage Increase of $\bar{e}$ for Light Fragments	Maximum Percentage Increase of $\bar{e}$ for Heavy Fragments
Hydrogen	13.6	10.7
Helium	14	11
Air	16	9.1
Argon	17	11

In Fig. 12 values are shown of equilibrium charge of the light and heavy fragments in the various gases as functions of fragment velocity. These curves correspond to the maximum $H\rho$ values, i.e., the pressure effect is removed. The value of equilibrium charge of mass-97 fragments as a function of velocity in helium, is shown in Fig. 13. These data were obtained by the mass identification method.

Fig. 14 shows the equilibrium charges of the light and heavy fragments, corrected for pressure effect, as a function of atomic number of the stopping gas. These curves correspond to velocities of 6.5 v_o and 4.4 v_o for the light and heavy fragments, respectively. The dotted lines show the results obtained by Lassen (1951[b]) for the same

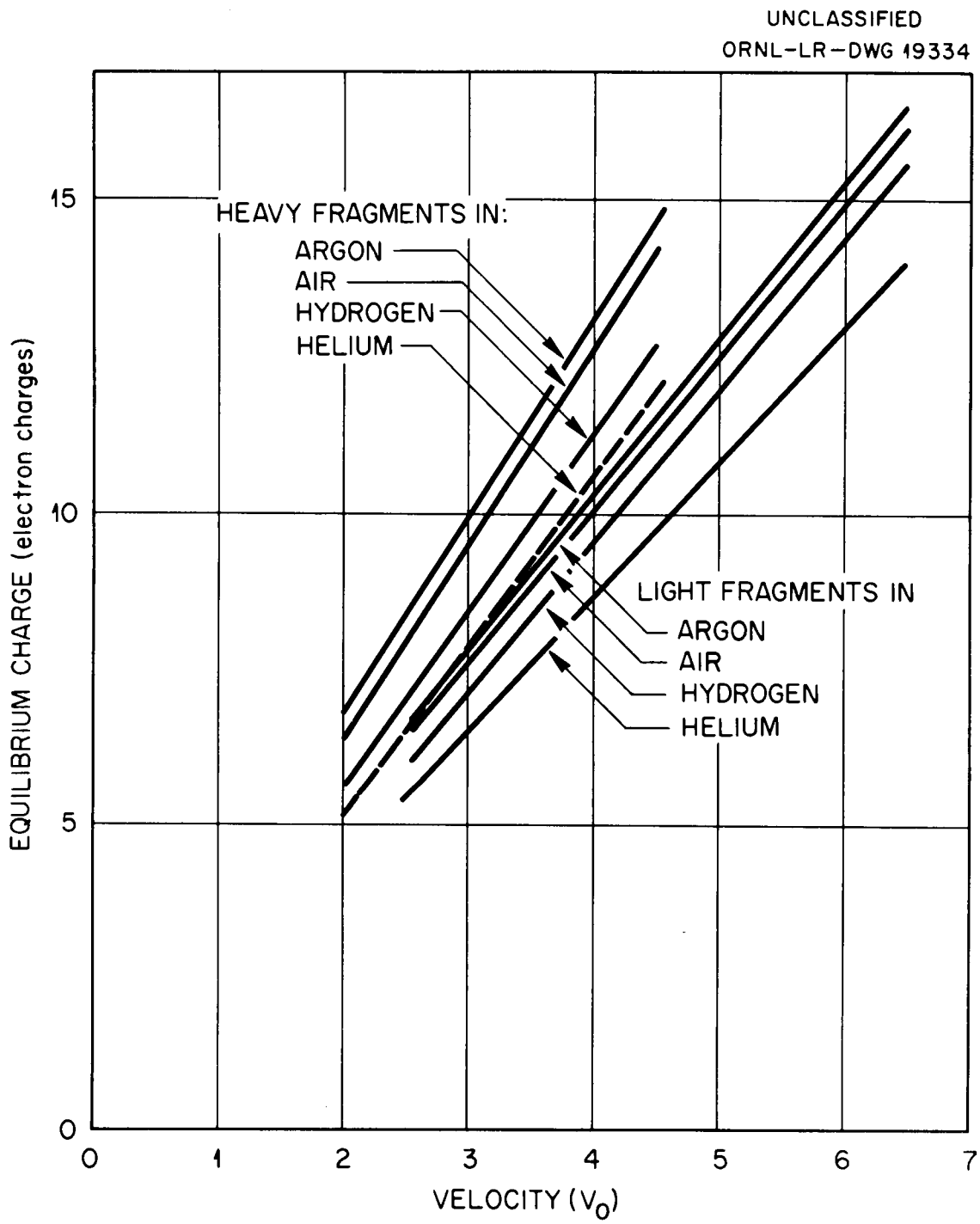

Fig. 12. Equilibrium Charges of Median Light and Heavy Fission Fragments as Functions of Velocity in Various Gases.

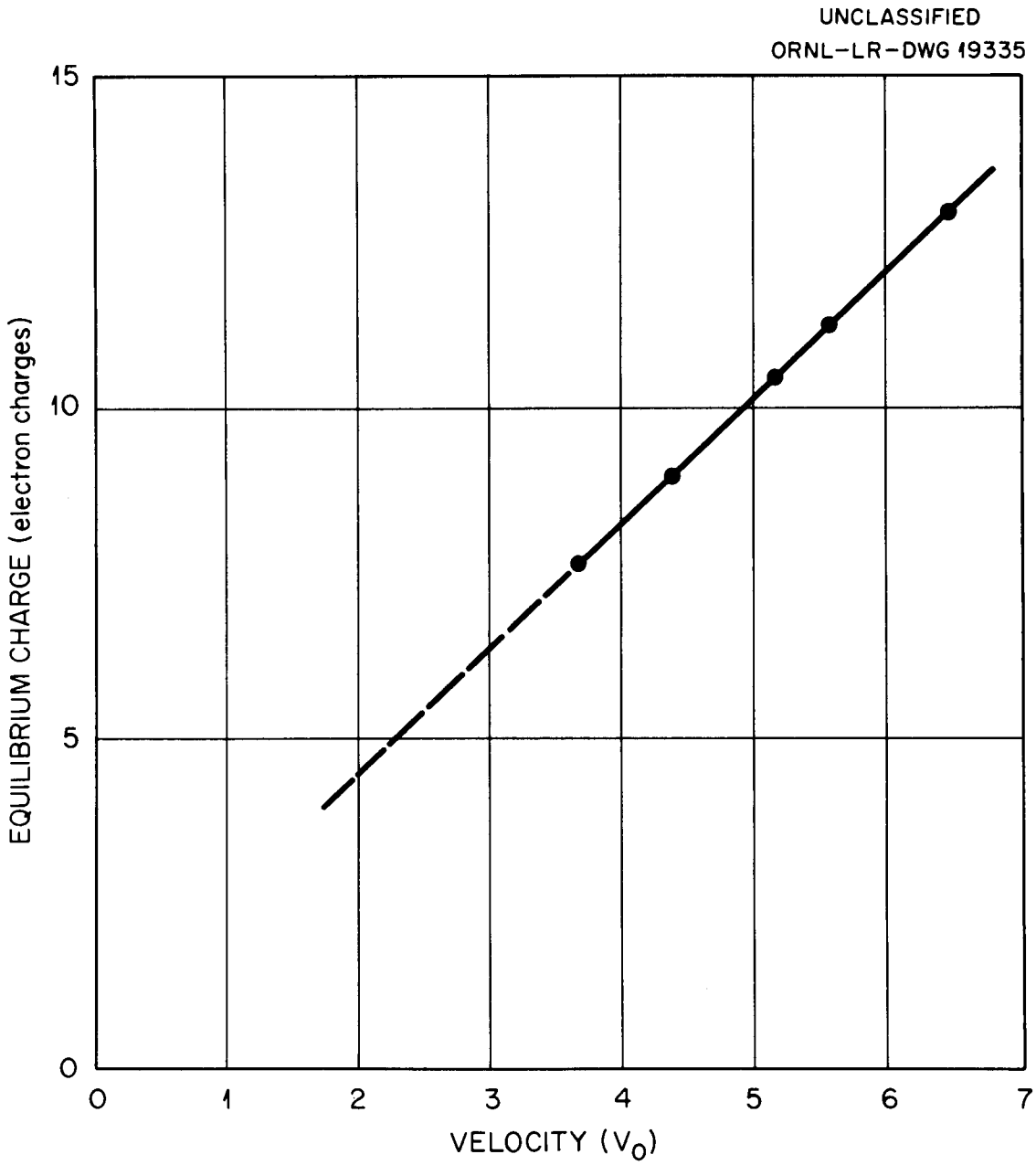

Fig. 13. Equilibrium Charge of Mass-97 Fission Fragments as a Function of Velocity in Helium.

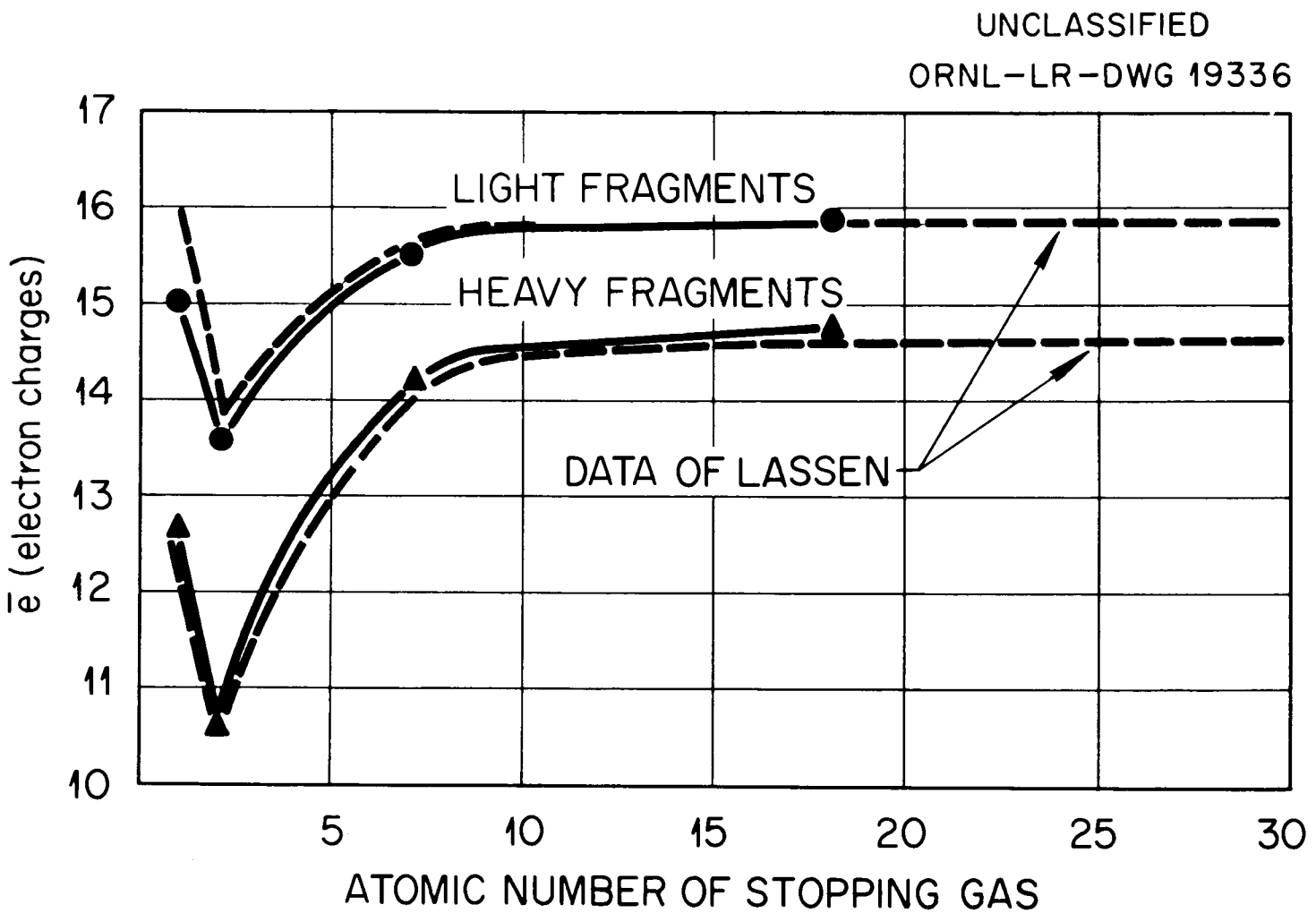

Fig. 14. Equilibrium Charges of Fission Fragments with Initial Energies as Functions of Atomic Number of Stopping Gas.

fragment velocities. There is excellent agreement between the two sets of results except for the light fragments in hydrogen. From the curves in Fig. 12 additional sets of curves of fragment charge as a function of atomic number of the stopping gas are directly obtained for the range of velocities covered by the data. It is seen that the curves of Fig. 14 are repeated for all fragment velocities with only the values of the ordinates changed.

It is interesting to compare the experimental values of equilibrium charge as functions of fragment velocity with some theoretical results. Dr. Jacob Neufeld, of Oak Ridge National Laboratory, is preparing some theoretical curves of ion charge as a function of velocity for ions of various nuclear charge. These curves are based on theoretical estimates of binding energies of the ions which were computed by Lisitzin (1938). Dr. Neufeld has kindly consented to the use of two of these curves, prior to publication, for comparison with the experimental results. These curves are for a light fragment of nuclear charge 38 (Fig. 15) and a heavy fragment of nuclear charge 54 (Fig. 16). The experimental results are shown in the same figures along with the experimental results of Lassen.

The experimental results agree in general but not in detail with the theoretical results for the light fragment. There is less agreement in the case of the heavy fragment. Agreement with the experimental results of Lassen and those of the author is obtained for both the light and heavy fragments.

The most significant disagreement between the experimental and theoretical results is the presence of structure in the theoretical results and the lack of it in the experimental results. The flat portions of the theoretical curves correspond to closed electron shells where there is an appreciable difference between the electron binding for the last electron in the lower shell and that of the first electron in the higher shell.

It is true that the peaks of the $H\rho$ distributions determined by scintillation detection do not correspond to a single mass but rather there is considerable overlapping of nuclear masses. However, the

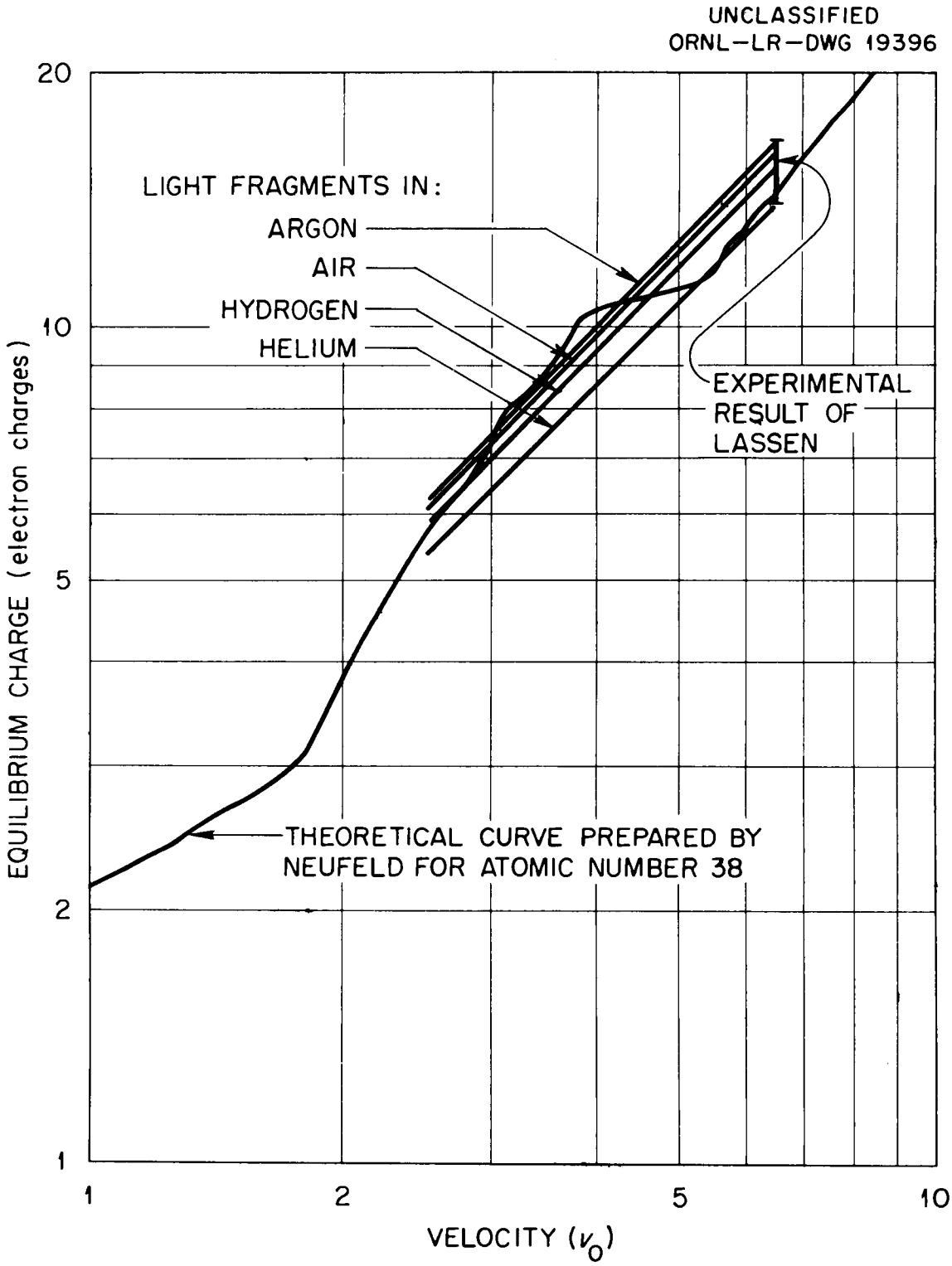

Fig. 15. Comparison of Theoretical and Experimental Values of Equilibrium Charge of Median Light Fission Fragments as a Function of Velocity.

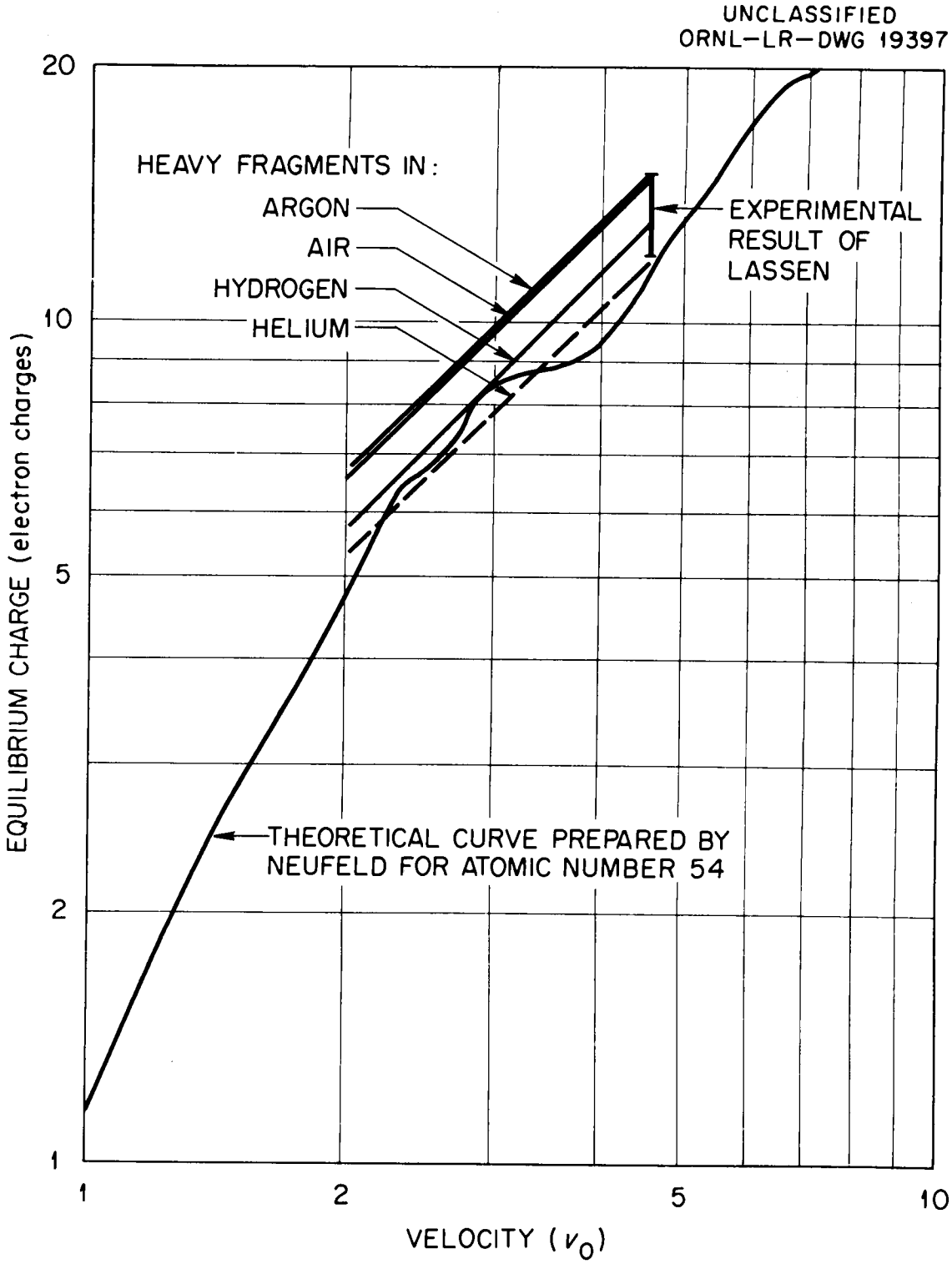

Fig. 16. Comparison of Theoretical and Experimental Values of Equilibrium Charge of Median Heavy Fission Fragments as a Function of Velocity.

equilibrium charge of mass-97 fragments as determined by the mass identification method (Fig. 13) does not reveal any structure either. Thus the lack of structure in the case of the experimental results cannot be attributed to mass distribution.

Assuming that the structure in the theoretical results is valid, the lack of it in the experimental results must be attributed to the masking effect of nuclear charge distribution of fragments of a given mass. An experimental determination of this is discussed in Chapter 6. Dr. Neufeld does not have theoretical curves for fragments of neighboring atomic numbers at present. When they are available it will be of interest to compare the experimental results with the average theoretical curve for ions of atomic numbers 37-39 and 36-40.

2.5 Mean Radiative Lifetime of Fission Fragments

The pressure effect on the equilibrium charge of fission fragments is due to incomplete radiative dissipation of the excitation energy between successive collisions with the gas atoms or molecules. It is easily seen that a given fraction of the maximum pressure effect corresponds to the same fraction of the excitation energy being retained by the fragments between collisions.

Let f represent the fraction of the fragments that are in excited states at the time of collision; $\Delta\bar{e}$ represent the increase in $\bar{e}$ due to ion excitation; $\bar{e}_o$ represent the value of $\bar{e}$ if all collisions occur with the fragments in the ground state. Then

$$\bar{e} = f(\bar{e}_o + \Delta\bar{e}) + (1-f)\bar{e}_o$$

$$f = \frac{\bar{e} - \bar{e}_o}{\Delta\bar{e}} \qquad (2,2)$$

If it is assumed that the radiative dissipation is achieved by simple exponential decay, then

$$f = \epsilon^{-\lambda t} \qquad (2,3)$$

where λ is the fractional dissipation per unit of time.

From equation (2, 1) it is seen that $\bar{e}$ is inversely proportional to $H\rho$, thus the maximum decrease in $H\rho$ corresponds to the maximum increase in $\bar{e}$. Making use of this and equation (2, 3), information about the mean radiative lifetimes of the excited ionized fission fragments is obtained from the curves in Fig. 4-11.

The time t between successive collisions is given by the relation

$$t = \frac{1}{nv\sigma} \qquad (2, 4)$$

where n is the number of molecules per unit volume, v is the fragment velocity, and σ is the combined cross section for electron capture and electron loss, i.e., the cross section for a charge changing collision. n is equal to kP where P is the gas pressure and k is the proper conversion factor. Equation (2, 4) may be written

$$t\left(\frac{\sigma v}{\pi a_o^2 V_o X 10^{-11}}\right) = \frac{1}{kP\pi a_o^2 V_o x 10^{-11}} \qquad (2, 5)$$

or

$$t\left(\frac{\sigma}{\pi a_o^2 x 10^{-11}}\right) = \frac{1}{kPv\pi a_o^2 x 10^{-11}} \qquad (2, 6)$$

The constants are included to reduce the dimensions of the expressions to time. Equation (2, 5) refers to the assumption that σ varies as (1/v) and equation (2, 6) refers to the assumption that σ is independent of fragment velocity. The expressions on the right of equations (2, 5) and (2, 6) correspond to the reciprocals of the abscissae of the $H\rho$ vs (pressure) graphs and of the $H\rho$ vs (pressure x velocity) graphs, respectively.

The graph in Fig. 17 is constructed by plotting the fraction of the maximum change in $\bar{e}$, i.e., f for the light fragments, corresponding to a given value of the abscissa in Fig. 8 vs the reciprocal of the abscissa value. The graph in Fig. 18 is constructed in the same manner from the graph corresponding to the light fragments in Fig. 4. The curves in Fig. 19 and 20 are similarly constructed from the curves corresponding to the light fragments in Fig. 9 and 5, respectively.

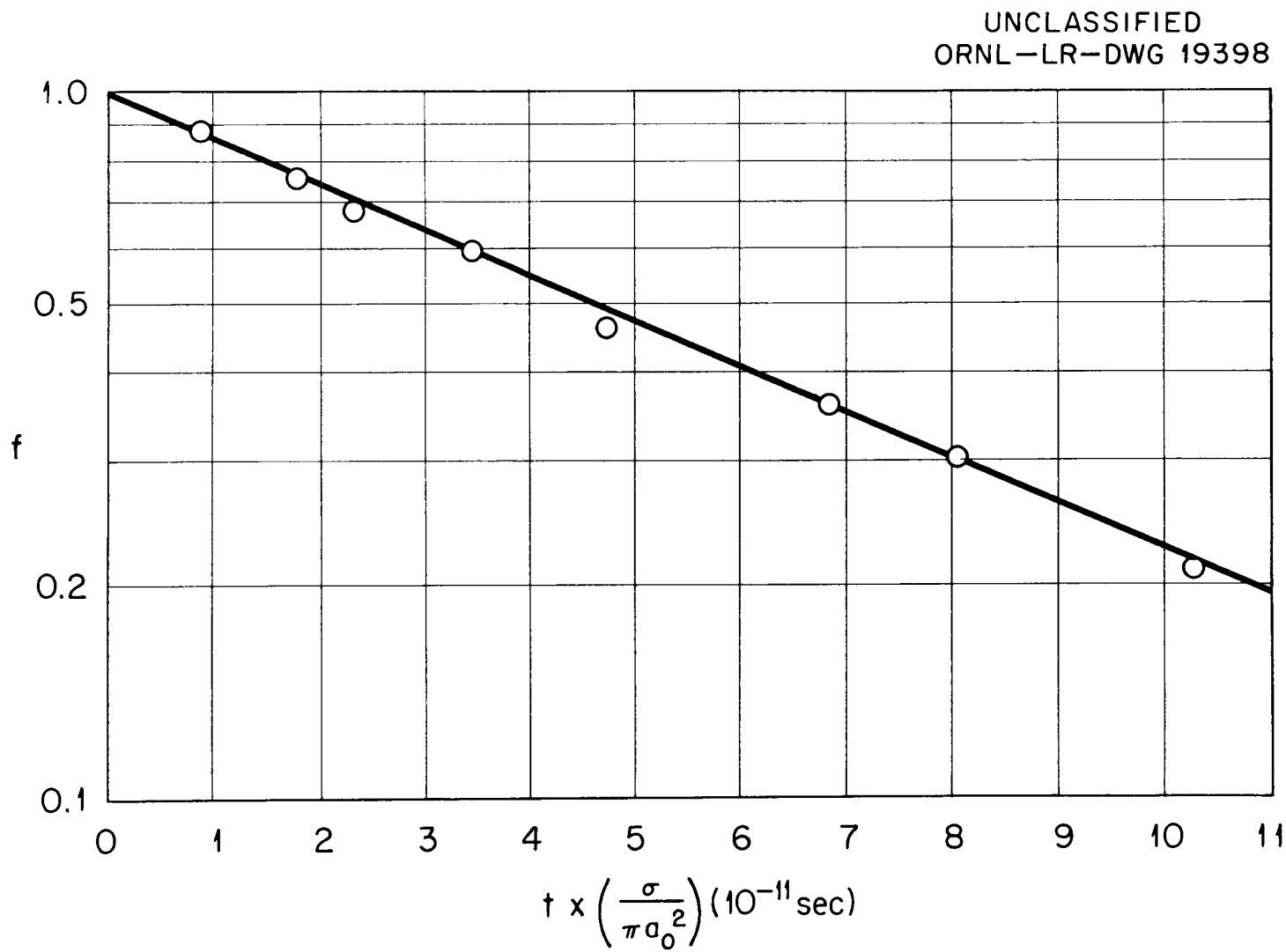

Fig. 17. Fraction of Excitation Energy Retained by Median Light Fragment as a Function of Time Between Collisions for Velocity-Independent Cross Section - Hydrogen Data.

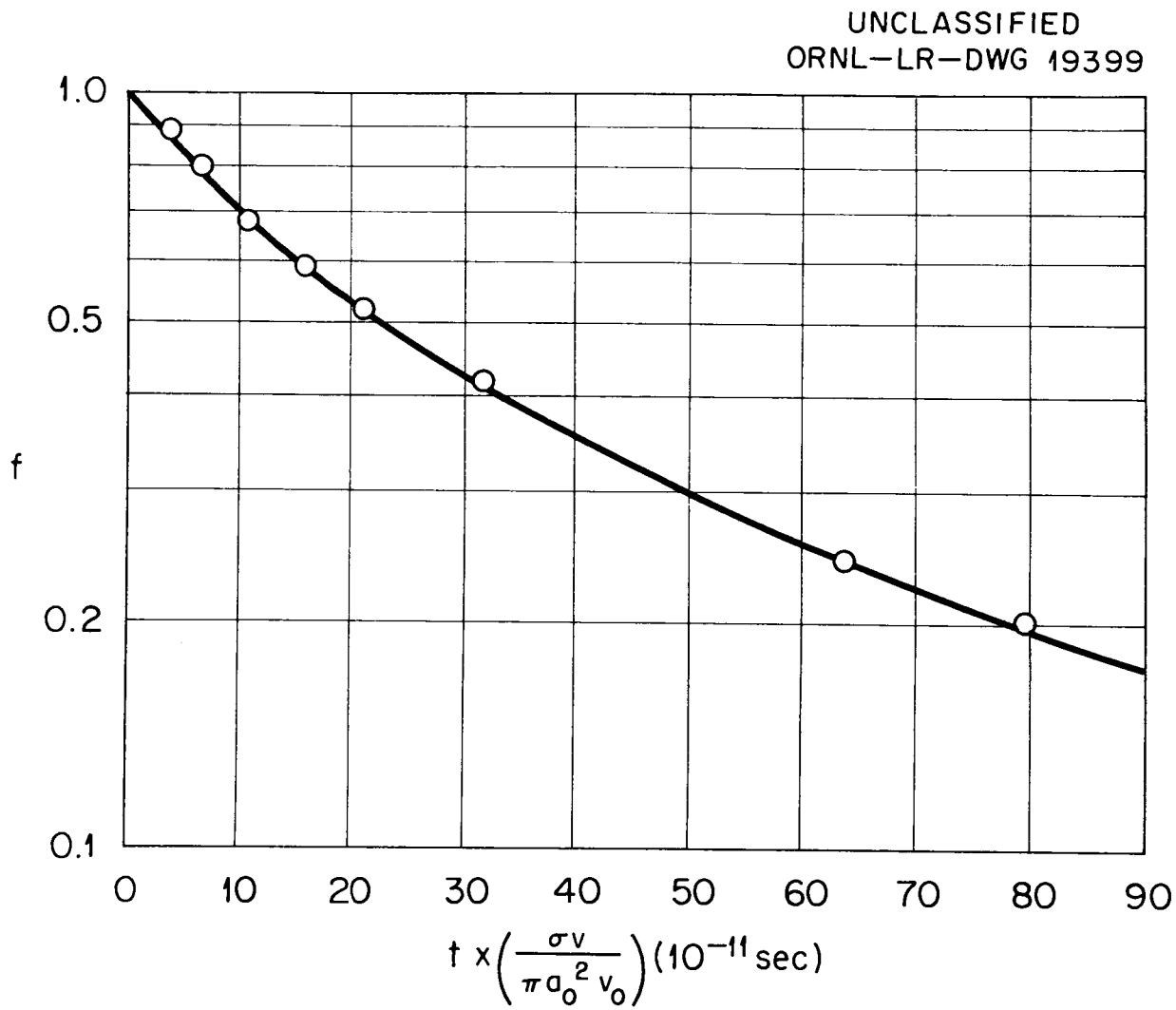

Fig. 18. Fraction of Excitation Energy Retained by Median Light Fragment as a Function of Time Between Collisions for (1/v) Cross Section - Hydrogen Data.

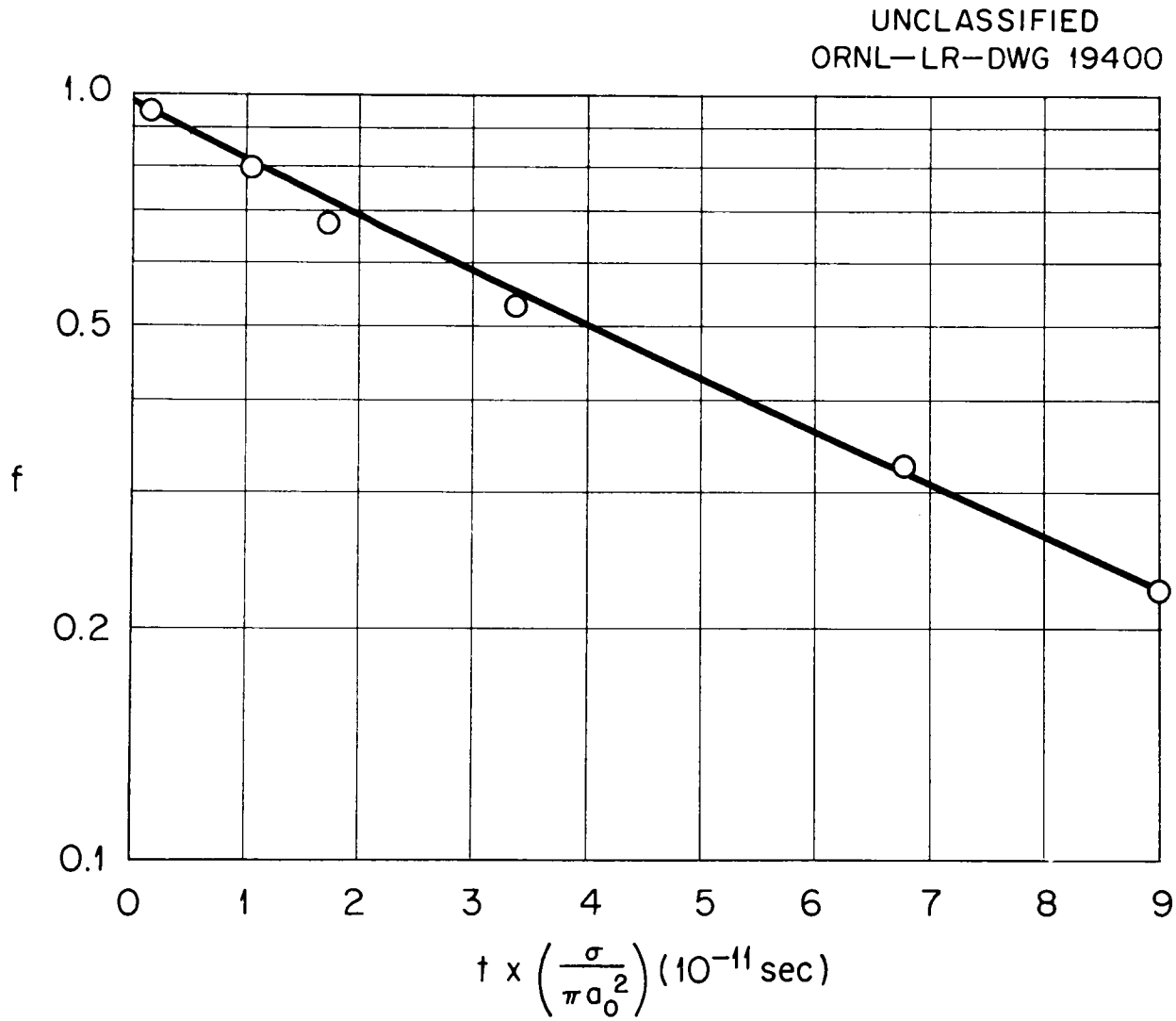

Fig. 19. Fraction of Excitation Energy Retained by Median Light Fragment as a Function of Time Between Collisions for Velocity-Independent Cross Section - Helium Data.

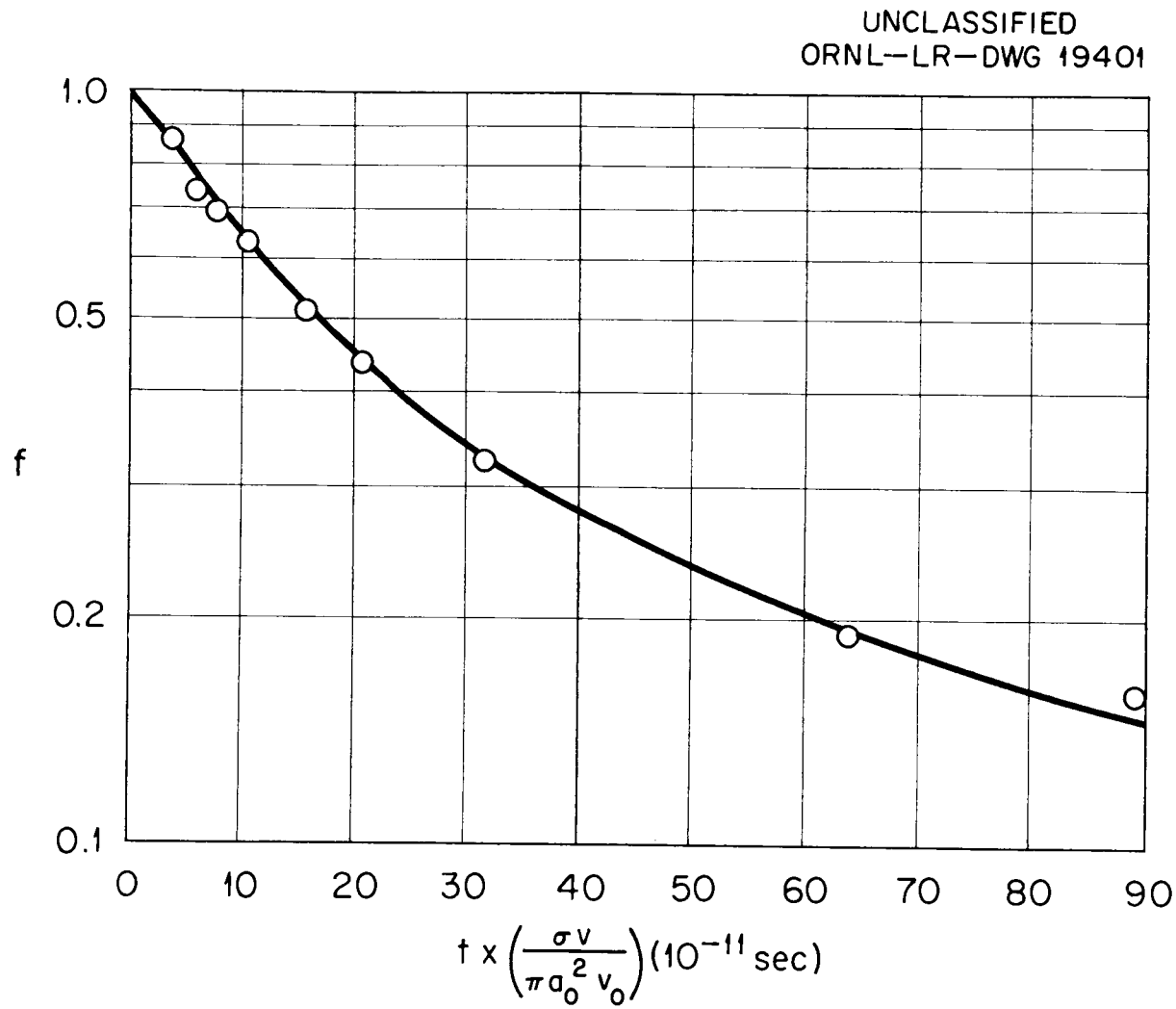

Fig. 20. Fraction of Excitation Energy Retained by Median Light Fragment as a Function of Time Between Collisions for (1/v) Cross Section - Helium Data.

Similar sets of curves are obtained for the light fragments in air and argon. The $H\rho$ data for the heavy fragments are less complete but similar results are obtained.

The curves in Fig. 17 and 19 are decay curves for the excited electron states of the fragments if σ is independent of fragment velocity, and from these curves estimates of the mean radiative lifetimes are obtained. These estimates are given in Table II. The curves are straight lines which imply simple decay of the excitation energy. The curves in Fig. 18 and 20 are decay curves for the excited electron states if σ varies as $(1/v)$. The curves are not straight lines but are convex with respect to the abscissa axis which imply that the excitation energy is not dissipated by simple radiative decay if the assumption of $(1/v)$ dependence of σ is correct. The data do not reveal which assumption about the velocity dependence of the cross section is the correct one.

For the assumption that the cross section is independent of fragment velocity, numerical estimates of the mean radiative lifetimes are obtained. The cross section for a hydrogen atom is of the order of πa_o^2, and for a hydrogen molecule it is twice as large. The width of the $H\rho$ distribution is given by the relation

$$W = \frac{K}{\sqrt{\sigma p}} \qquad (2, 7)$$

In Chapter 6 it is shown that $\underline{K}$ is reasonably independent of energy. If it is assumed that $\underline{K}$ is the same for various gases then relations between the cross sections for other gases compared to hydrogen are obtained from the width $\underline{W}$ of the $H\rho$ distribution for single mass fragments in the gases. Values of $\underline{W}$ were determined for mass-97 fragments by the mass identification method in H_2, He, air, and A at relatively low pressures. From these data and the assumed value of the cross section for H_2, estimates of the charge changing cross sections were obtained. These values together with the estimates of the mean radiative lifetimes are presented in Table II.

TABLE II

Mean Radiative Lifetime as Determined from $H\beta$ Data in Various Gases

Type of Gas	Pressure (mm Hg)	W %	PW^2	$\sigma/\pi a_o^2$	$\frac{\tau\ \sigma}{(\pi a_o^2 \times 10^{-11})}$ second	τ (10^{-11} sec)
Hydrogen	0.97	13.6	180	2.0	4.5	2.3
Helium	1.04	9.3	90	4.1	4.0	1.0
Air	0.50	5.0	12.5	30	47	1.6
Argon	0.30	7.2	15.5	24	50	2.1

CHAPTER 3

RESPONSE OF CESIUM-IODIDE CRYSTALS TO FISSION FRAGMENTS

3.1 Introduction

Although a considerable amount of study has been devoted to the scintillation responses of both inorganic and organic phosphors to light particles (e.g. Taylor et al., 1950) and light nuclei (e.g. Allison and Casson, 1953, and Eby and Jentschke, 1954), the responses of only a few phosphors to heavy, energetic, multiply ionized particles such as fission fragments have been reported. Most phosphors show signs of saturation for alpha particles with energies of a few Mev. The mean range in matter of the more energetic group of fission fragments is about three-fourths that of 5-Mev alpha particles. It might thus be expected that the scintillations due to fission fragments are smaller than those of alpha particles. Milton and Fraser (1954) have studied the responses of NaI(Tl), KI(Tl) and stilbene to fission fragments. In all three cases the fission fragment pulses were larger than the pulses of 4.8-Mev alpha particles from the same crystals.

In addition to its intrinsic interest, knowledge of the scintillation response is important in experiments involving fission fragments and fast coincidence techniques where scintillation counters are desirable.

3.2 Experimental

A CsI(Tl) crystal was selected for scintillation detection of fission fragments in connection with obtaining much of the data reported in this thesis. The selection was made because of the non-deliquescent property and availability in rather thin single crystals. Potassium-iodide also meets these requirements.

A description of the crystal mounting is given in Chapter 1. Used in this manner, the requirement of detecting the fission fragments in a high background of gamma and beta rays was adequately fulfilled. The background as measured with the magnetic field turned off was approximately 1% of the counting rate for full energy fission fragments at the peaks of the $H\rho$ distributions.

Concurrent with the data of Chapters 2 and 4, data were also obtained to determine some characteristics of the response of the crystal to fission fragments. Pulse height distributions were determined for the median light and heavy fragments, i.e., for the peaks of the $H\rho$ distributions, with H_2, He, air, and A filling the system to various pressures.

3.3 Presentation and Discussion of Data

Typical samples of the scintillation pulse height distributions of median light and heavy fission fragments are shown in Figure 21. The pulse height distribution of 5.3-Mev alpha particles from Po^{210} is also shown. Although the light and heavy fragments were separated magnetically and thus the distributions were determined individually, it is seen that the energy resolution is sufficient to distinguish between the two groups of fragments. The fission fragment data shown in these curves were obtained with enough argon in the system to equal a path length of 1.3 mm at standard atmospheric pressure. The energies of the median light and heavy fragments, for this range in argon, are 90 and 63 Mev, respectively. The pulse heights, i.e., the peaks of the distributions plus half the channel width of the pulse height analyzer, are 55 and 39, respectively. The ratio of the energies are approximately equal to the ratio of the pulse heights.

The resolutions of the pulse height distributions, defined as the full width at half maximum, are 31%, 37%, and 14%, respectively, for the light and heavy fragments and the alpha particles. Part of

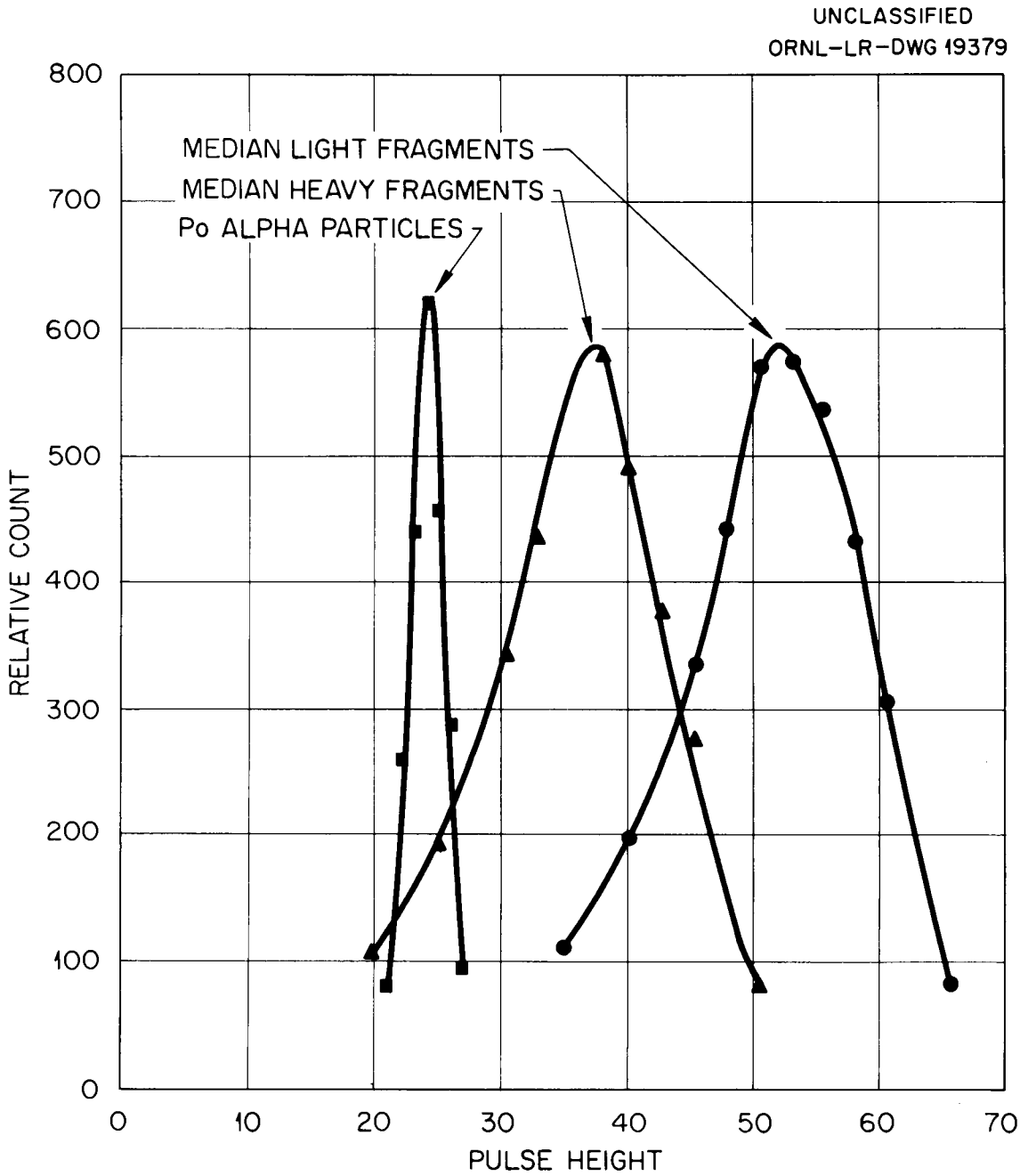

Fig. 21. Scintillation Pulse Height Distributions of 5.3-Mev Alpha Particles and Median Light and Heavy Fission Fragments in Cesium-Iodide (Thallium) Crystals.

the widths for the fission fragments is due to energy distribution widths. The width of the energy distribution of mass-97 fission fragments was determined by Cohen, Cohen, and Coley (1956) to be 11.4%.

The pulse height values that were measured with various pressures of argon in the system are plotted as a function of range in Fig. 22. From these data estimates of pulse height as a function of residual range in argon are obtained and used to plot the curve in Fig. 23. It is seen that, within the accuracy to which the full ranges are estimated from Fig. 22, the pulse heights as a function of residual range for both groups of fragments are in coincidence. Similar results are obtained for H_2, He, and air.

An estimate of specific fluorescence (dL/dx) as a function of specific energy loss (dE/dx) for fission fragments in CsI(Tl) is obtained as follows. The range of the fragments in CsI is assumed to be equal to the range in Ag, which from the data of Suzor (1949) is 7.6 and 6.6 mm/cm^2 for the light and heavy fragments, respectively. It is further assumed that the ratio of the specific energy loss in two materials is equal to the inverted ratio of the ranges of the fragments in the materials.

Values of specific energy loss are obtained by differentiating the range vs energy curves for fission fragments in argon (see Chapter 4) at various points along the range. Correspondent values of specific fluorescence are obtained in the same manner from the curves in Fig. 22. After multiplication by the ratio of the ranges in the two materials and a conversion factor (converting millimeters of gas into milligrams per square centimeter) these values are plotted in Fig. 24. Additional points that were obtained from data with hydrogen in the system are plotted. The reasonable agreement between the points obtained from A and H_2 data indicates that the assumed ranges of fission fragments in CsI are not much in error. Although it is an approximation the graph in Fig. 24 shows that the

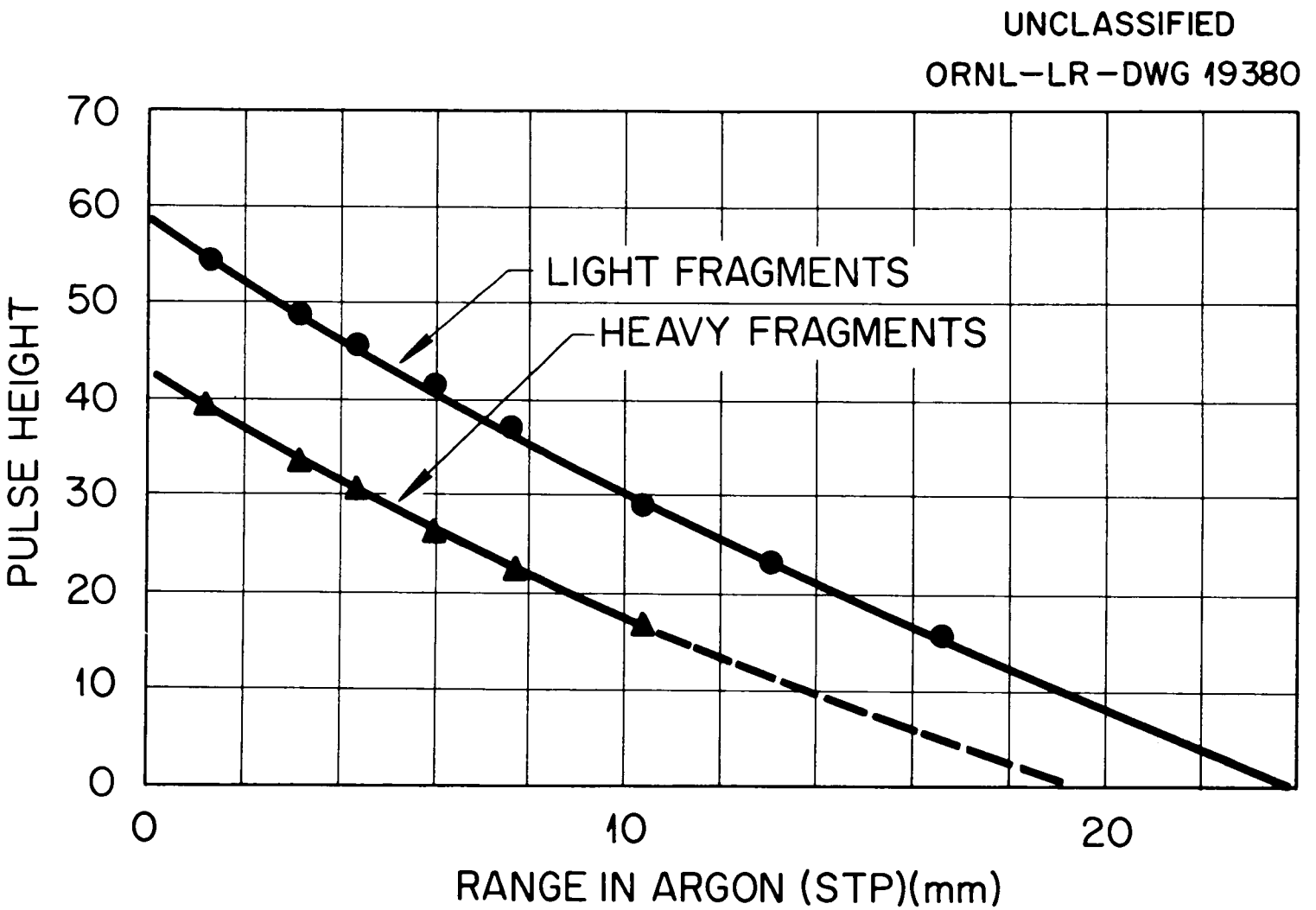

Fig. 22. Scintillation Pulse Heights of Median Light and Heavy Fission Fragments in Cesium-Iodide (Thallium) Crystals as Functions of Range in Argon Gas.

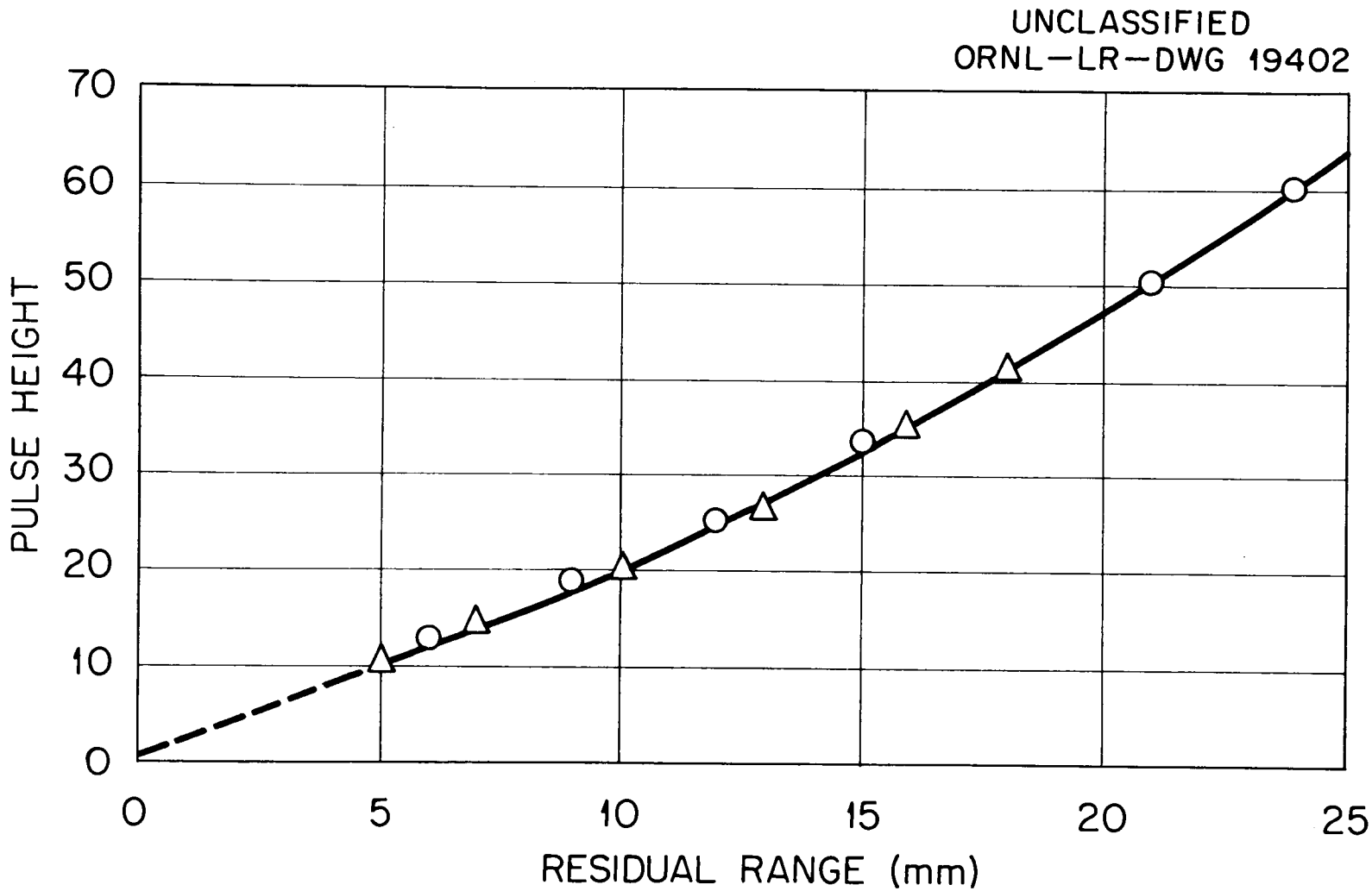

Fig. 23. Scintillation Pulse Height of Fission Fragments in Cesium-Iodide (Thallium) Crystals as a Function of Residual Range in Argon Gas at Standard Pressure.

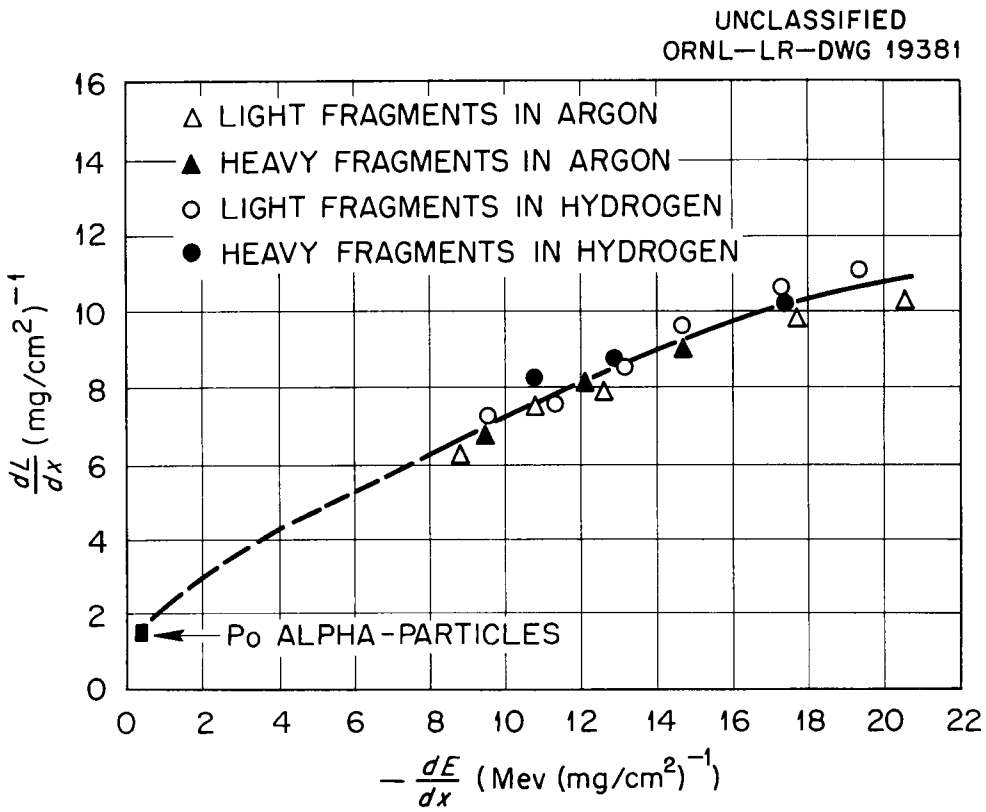

Fig. 24. Specific Fluorescence as a Function of Specific Energy Loss of Fission Fragments in Cesium-Iodide (Thallium).

crystal does not saturate within the range of specific energy loss covered by fission fragments, but rather (dL/dx) increases monotonically with (dE/dx).

Some conclusions can be drawn from this analysis of the response of CsI(Tl) crystals to fission fragments. Most of the light is produced near the beginning of the fragment path where the specific energy loss is high. There is no large contribution to the scintillation response from nuclear recoils as these occur near the end of the fragment track. Since most of the light is produced near the surface of the crystal, surface effects are important. A deliquescent phosphor would be suitable for fission fragment detection only in the absence of humidity.

CHAPTER 4

ENERGY OF FISSION FRAGMENTS AS A FUNCTION OF RANGE IN VARIOUS MATERIALS

4.1 Introduction

The phenomenon of energy loss of heavy ions in penetrating matter differs from that of protons and alpha particles. The effective charge of a light ion remains constant during most of its path, while an energetic heavy ion begins its path with a high positive charge which diminishes as the ion is slowed down.

As developed in a theoretical treatment by Bohr (1948), the range of fission fragments in matter may be divided into two parts over which the stopping mechanisms are different. In the first part, where the fragment velocity is high compared with the orbital velooities of the most loosely bound electrons in the atoms of the stopping material, energy loss takes place primarily through excitation and ionization of the atoms. Since the charge of the fragment decreases as the fragment is slowed down the specific energy loss, i.e., the energy loss per unit of path length, is expected to decrease along the range. When the fragment reaches a velocity of the order of v_o it becomes completely neutralized but due to the large mass it has a residual energy of several Mev and thus may move an appreciable distance before finally being stopped. Over this part of the range the energy loss is supposed to take place mainly by encounters in which kinetic energy is imparted to the stopping atom as a whole.

4.2 Survey of Previous Measurements

Measurements of the specific energy loss of fission fragments along their range in H_2, He, and A were made by Lassen (1949[a, b]). For these measurements an ionization chamber was used. It was located inside the gas chamber in which the fragments were slowed down. From the data obtained, Lassen constructed energy vs range curves for fission fragments in the gases used.

Experimental values of the range of fission fragment in air have been published by Boggild, Minnhagen, and Nielsen (1949) who made measurements by means of a cloud chamber. Boggild, Arroe, and Sigurgeirsson (1947) investigated the ranges of fission fragments in deuterium, H_2, A, and Xe. Campbell, Good, and Strauser (1949) have measured the ranges of two delayed neutron emitters in the same gases.

Katcoff, Miskel, and Stanley (1948) made direct measurements of the ranges in air of Pu^{239} fission fragments of twenty known masses. The collimated fragments passed along a tube containing a known pressure of air and were stopped in a series of thin Zapon films. The films were analyzed radiochemically for individual fission fragments and the activities plotted as functions of the distance traveled.

Segrè and Weigand (1946) and Suzor (1949) have investigated the ranges of fragments from U^{235} in collodion, cellulose acetate, Al, Cu, Ag, and Au. Segrè and Weigand used both ionization chambers and the method of measuring the activity in catcher foils. Suzor used a chemical method in which the activities of Te^{132}, Mo^{99}, and Zr^{97} were measured in a series of thin foils. The measurements of Suzor are considered to be very accurate.

Schmitt and Leachman (1956), using a time-of-flight method, made very accurate determinations of the energies of median heavy and light fission fragments at the beginning of their paths and after the fragments had been passed through three different thicknesses of aluminum foil.

While there has been a large number of measurements of total ranges of fission fragments in various materials, very few determinations of energy as a function of range have been made.

4.3 Experimental

Scintillation pulse height distributions of the median light and heavy fragments in the CsI(Tl) crystal were determined after the fragments passed through various thicknesses of absorbing material. The absorbers used include H_2, He, air, A, Al, Ni, and Au. The desired thicknesses of the gas absorbers were achieved by filling the system to the proper pressures. For the metallic absorbers, thin foils of known thicknesses were placed in the path of the fragments a short distance from the crystal.

In order to obtain energy vs range graphs from the pulse height vs range data, a calibration of the scintillation detector was required. For this the pulse height vs range data for the fragments in aluminum were used with the accurate energy vs range data of Schmitt and Leachmann (1956) to plot a curve of pulse height as a function of fragment energy. The resulting curve is shown in Fig. 25. The circles and triangles refer to data obtained with the median light and heavy fragments, respectively. It is noted that the data for the light and heavy fragments agree reasonably well and that the curve is linear.

4.4 Presentation and Discussion of Results

The pulse height as a function of range in aluminum is shown in Fig. 26. The dotted lines are extended to the full ranges as determined by Suzor (1949). The curves probably should deviate from the dotted lines due to nuclear stopping near the end of the range. The data obtained here does not give information about this part of the range.

The energy vs range relations obtained for the various materials are shown in Fig. 27, 28, 29, 30, 31, 32, and 33. A check on the validity of the energy vs range curves obtained here is provided at one point for each group of fragments by an accurate determination, by a time-of-flight method, of the energies of median light and heavy fragments after they pass through 1.1 mg/cm^2 Ni (Schmitt and Leachman, 1956). These measurements agree within

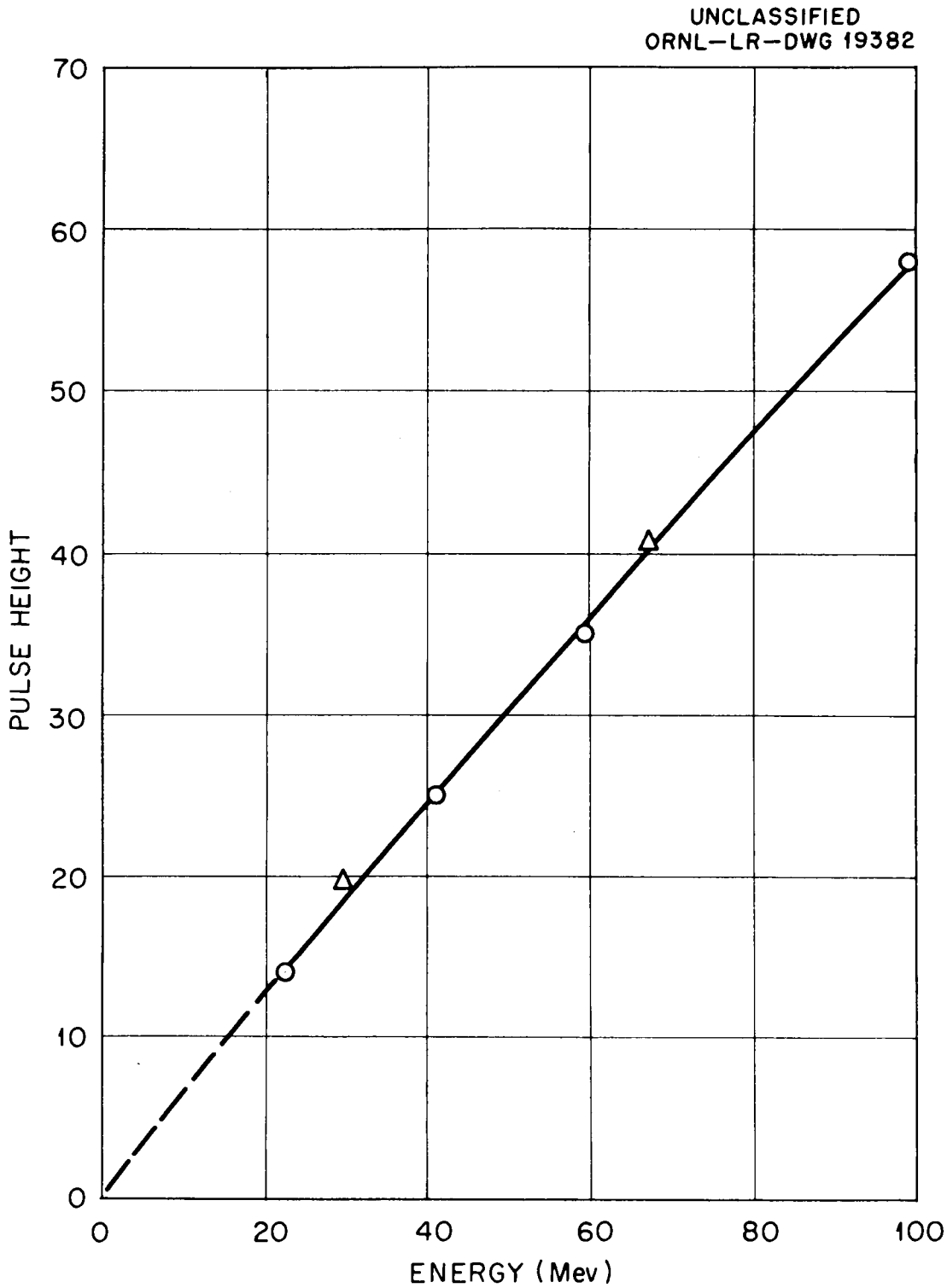

Fig. 25. Energy Calibration of Scintillation Detector for Fission Fragments.

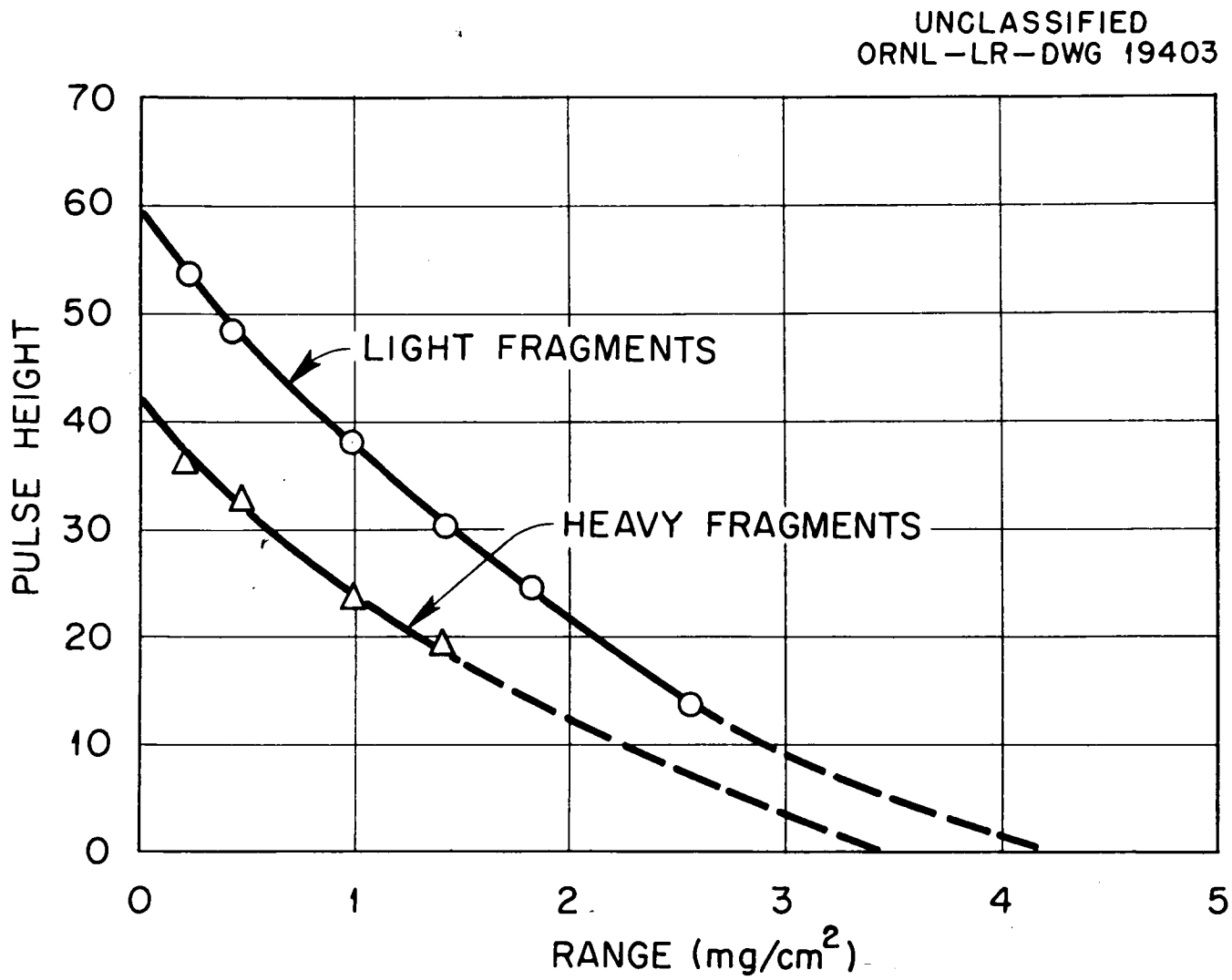

Fig. 26. Scintillation Pulse Heights of Median Light and Heavy Fission Fragments as Functions of Range in Aluminum.

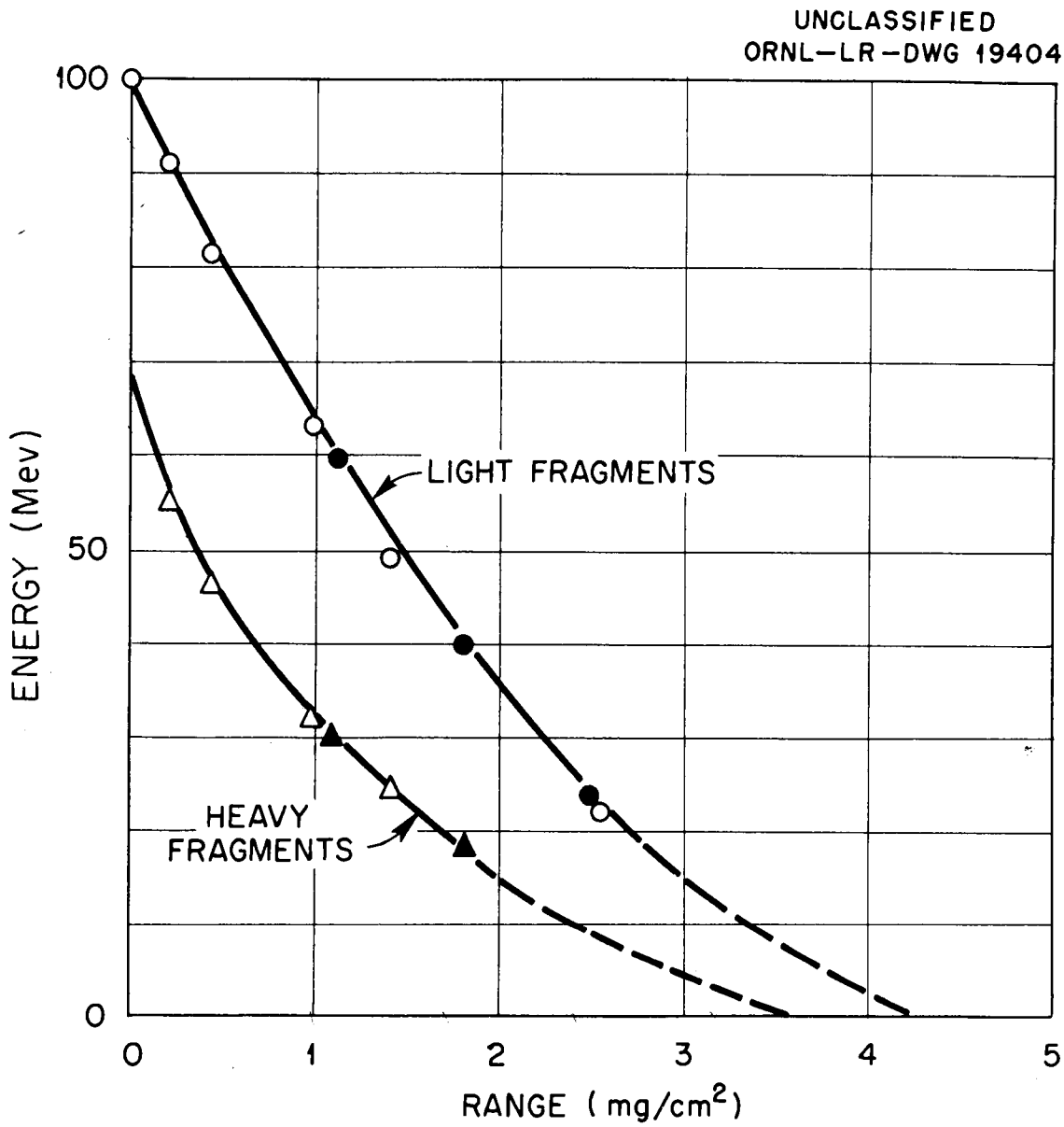

Fig. 27. Energy of Median Light and Heavy Fission Fragments as Functions of Range in Aluminum.

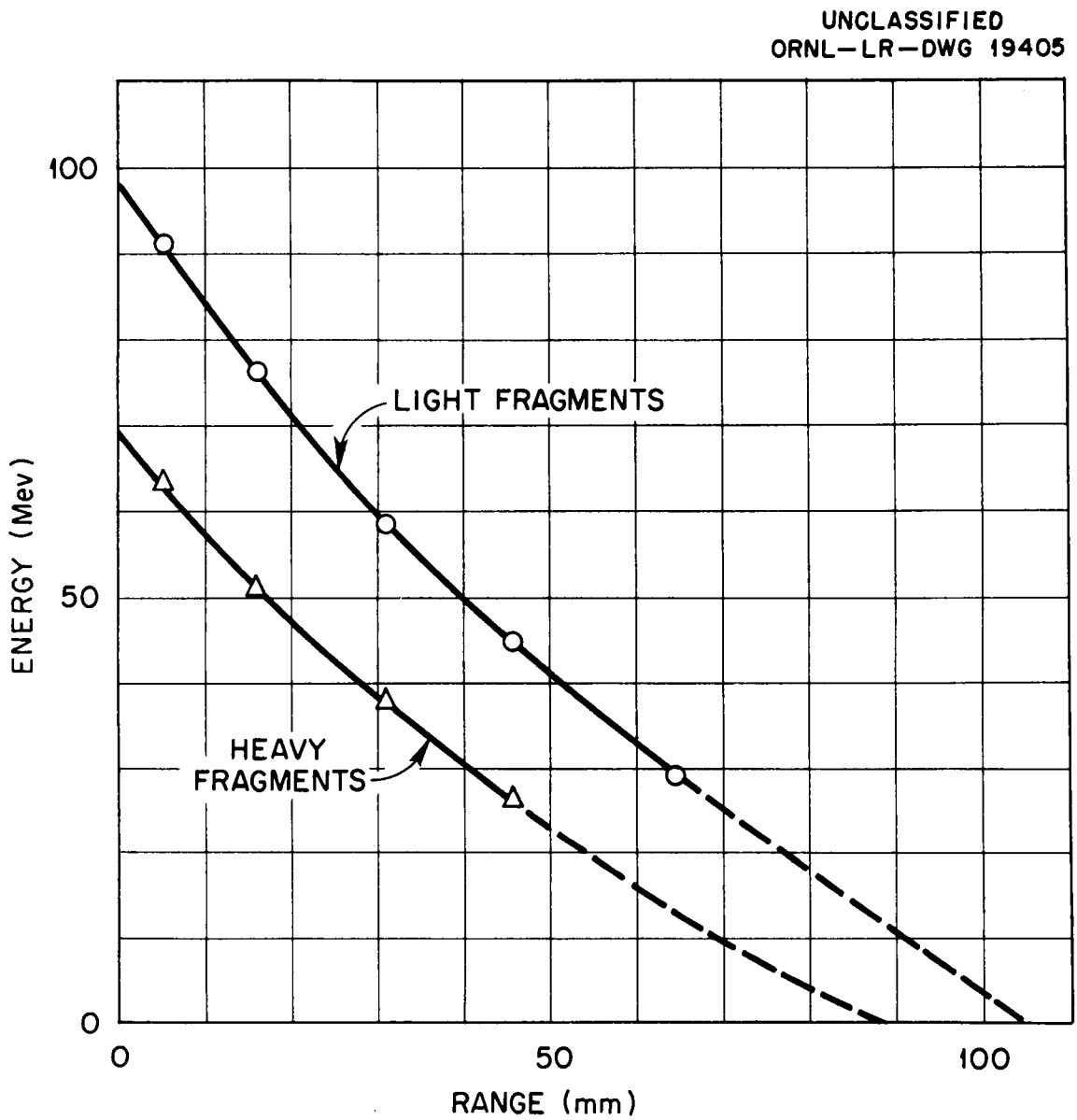

Fig. 28. Energy of Median Light and Heavy Fission Fragments as Functions of Range in Hydrogen Gas at Standard Pressure.

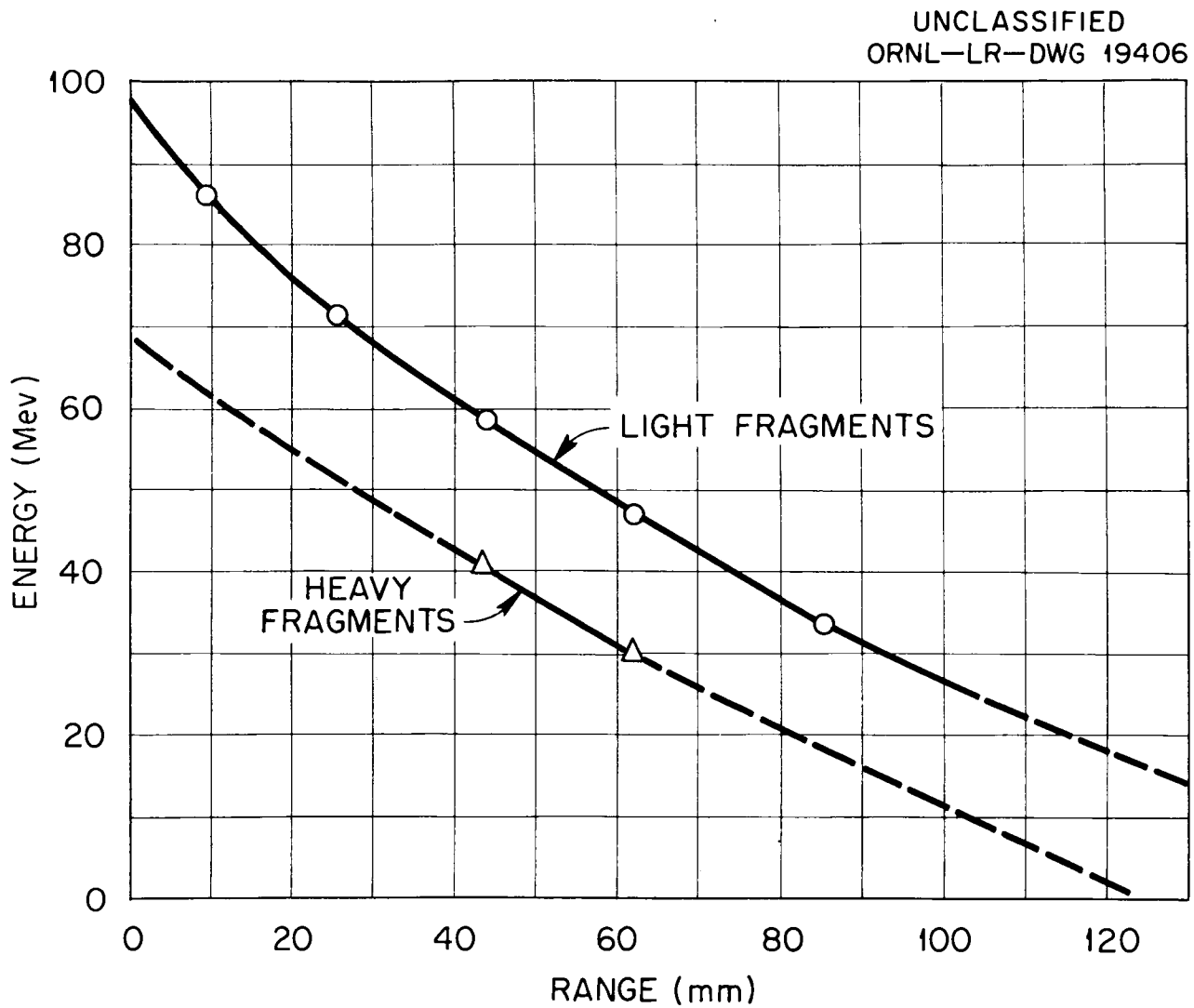

Fig. 29. Energy of Median Light and Heavy Fission Fragments as Functions of Range in Helium at Standard Pressure.

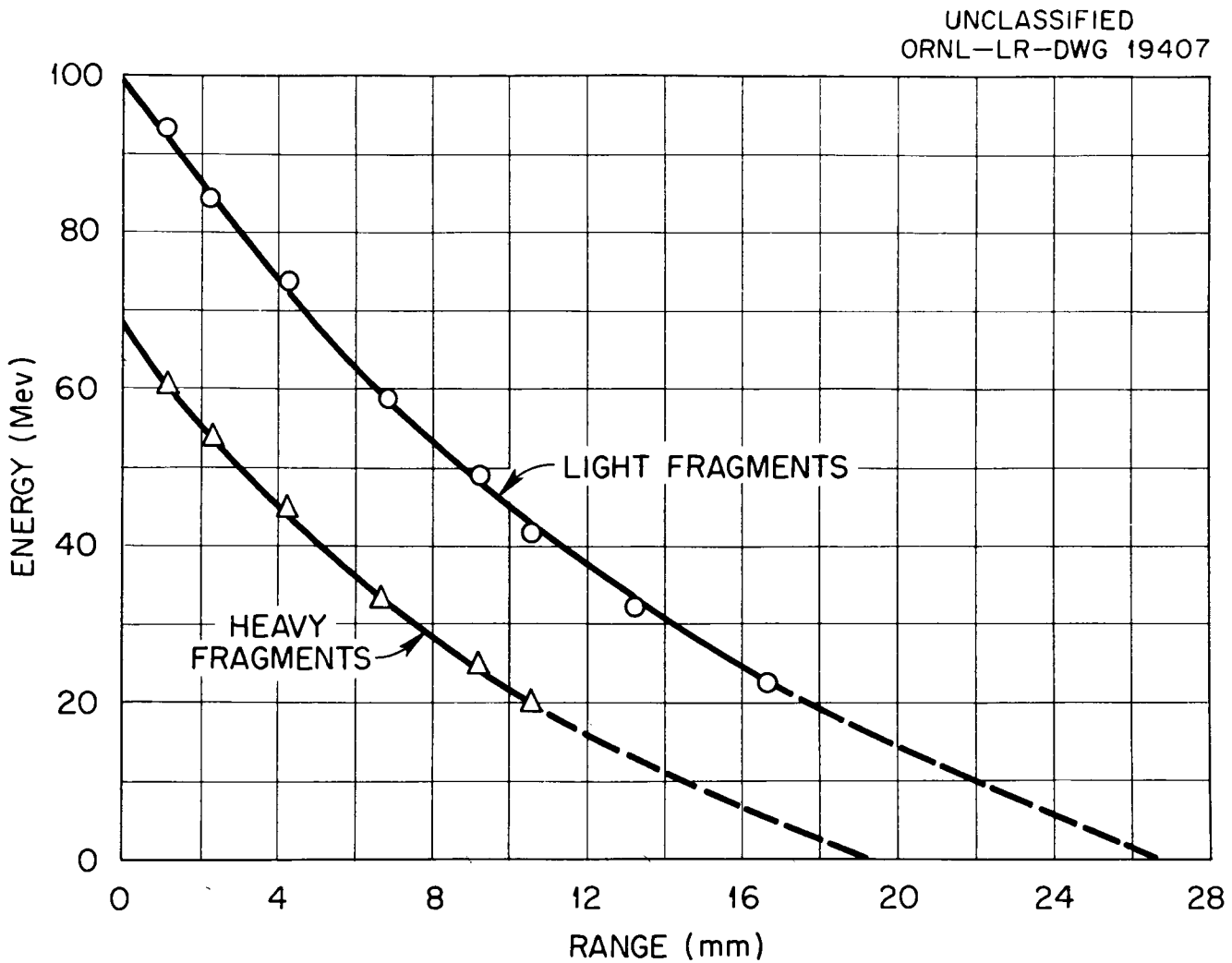

Fig. 30. Energy of Median Light and Heavy Fission Fragments as Functions of Range in Air at Standard Pressure.

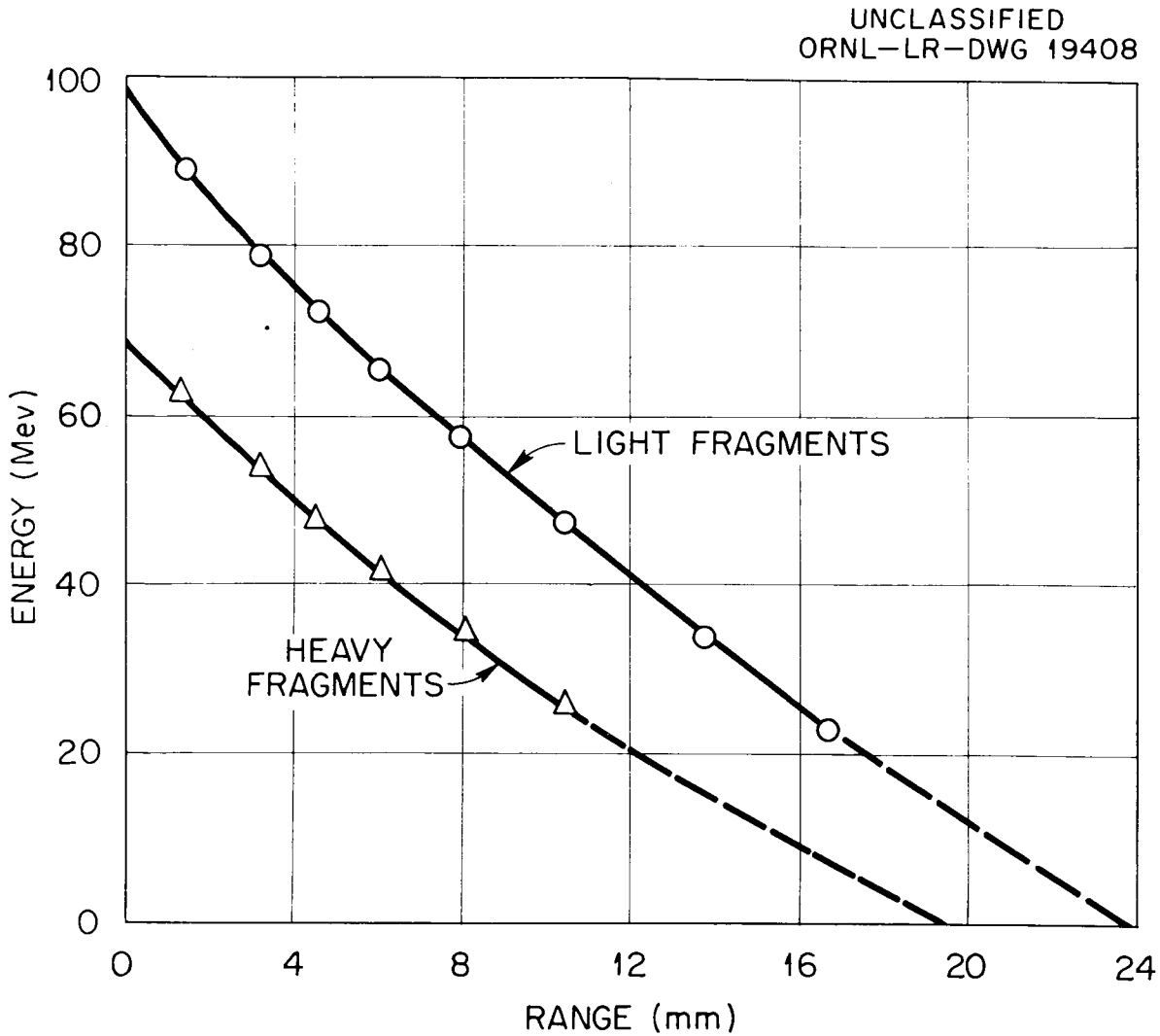

Fig. 31. Energy of Median Light and Heavy Fission Fragments as Functions of Range in Argon at Standard Pressure.

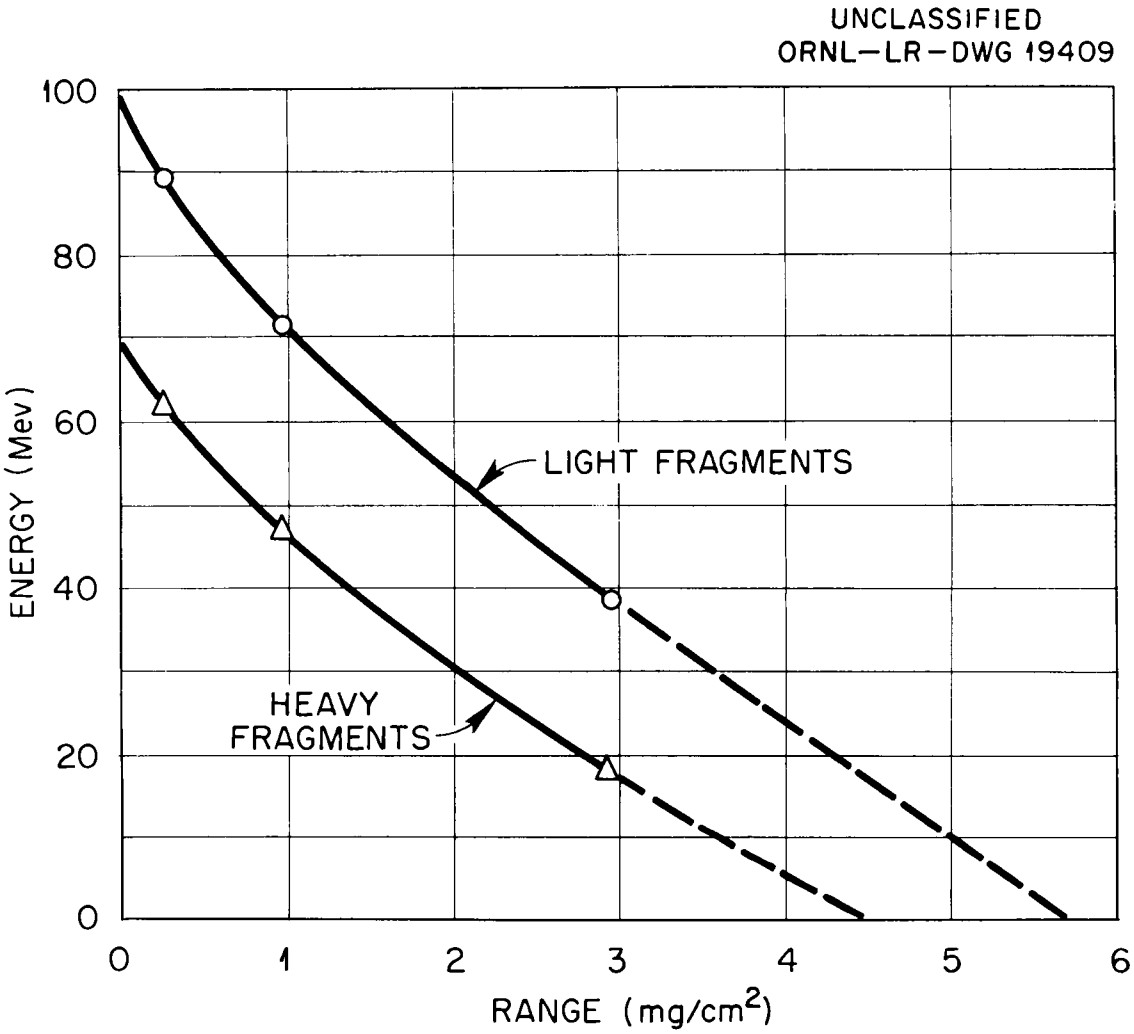

Fig. 32. Energy of Median Light and Heavy Fission Fragments as Functions of Range in Nickel.

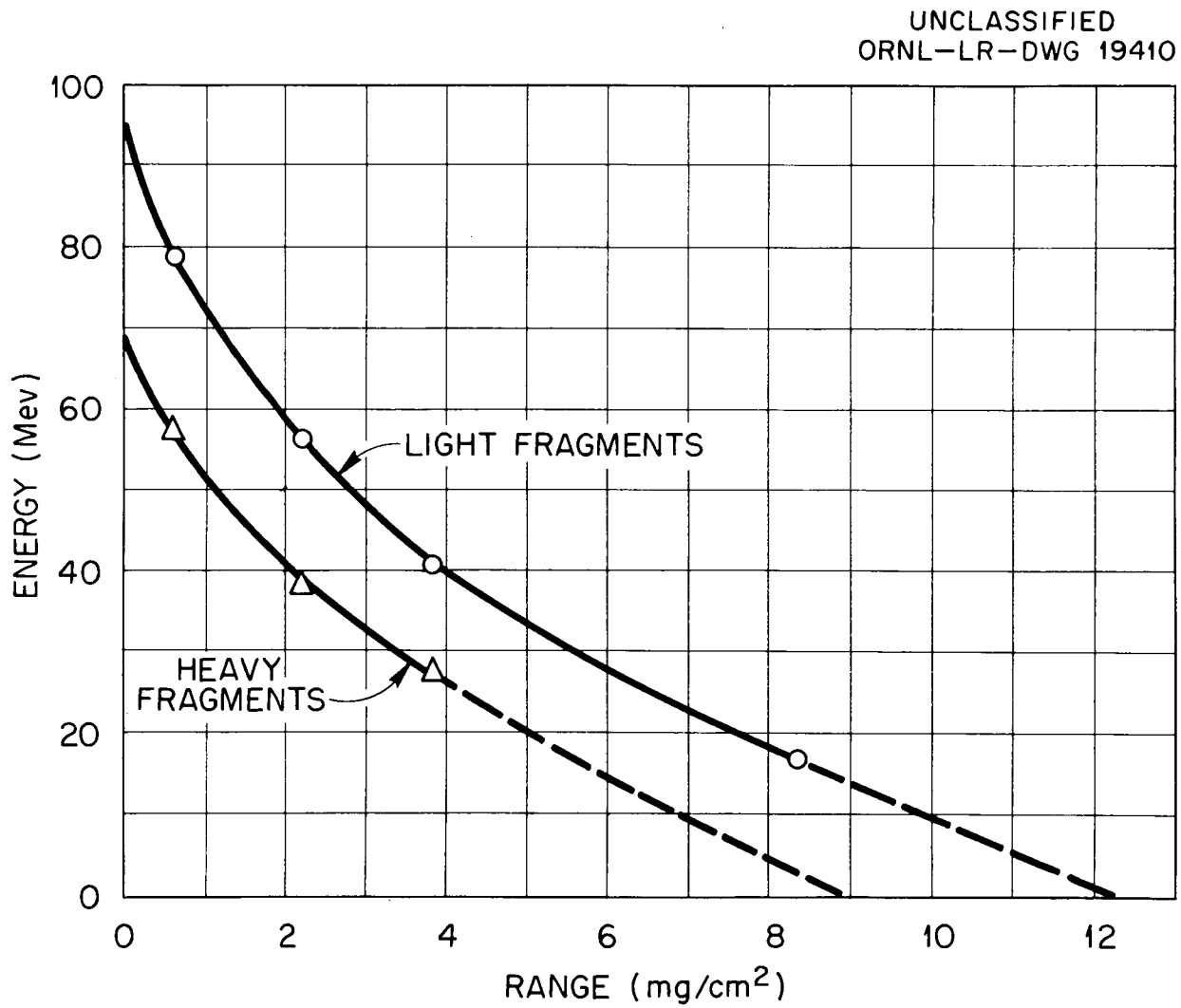

Fig. 33. Energy of Median Light and Heavy Fission Fragments as Functions of Range in Gold.

3% with the curves of Fig. 32. It is noted that the data for the light and heavy fragments agree reasonably well and that the curve is linear.

For comparison, curves of energy as a function of range for the light fragments in all the materials studied are shown in Fig. 34. A similar set of curves for the heavy fragments is shown in Fig. 35. It is noted from these sets of curves that the ranges of the fragments increase monotonically with atomic number of the stopping material.

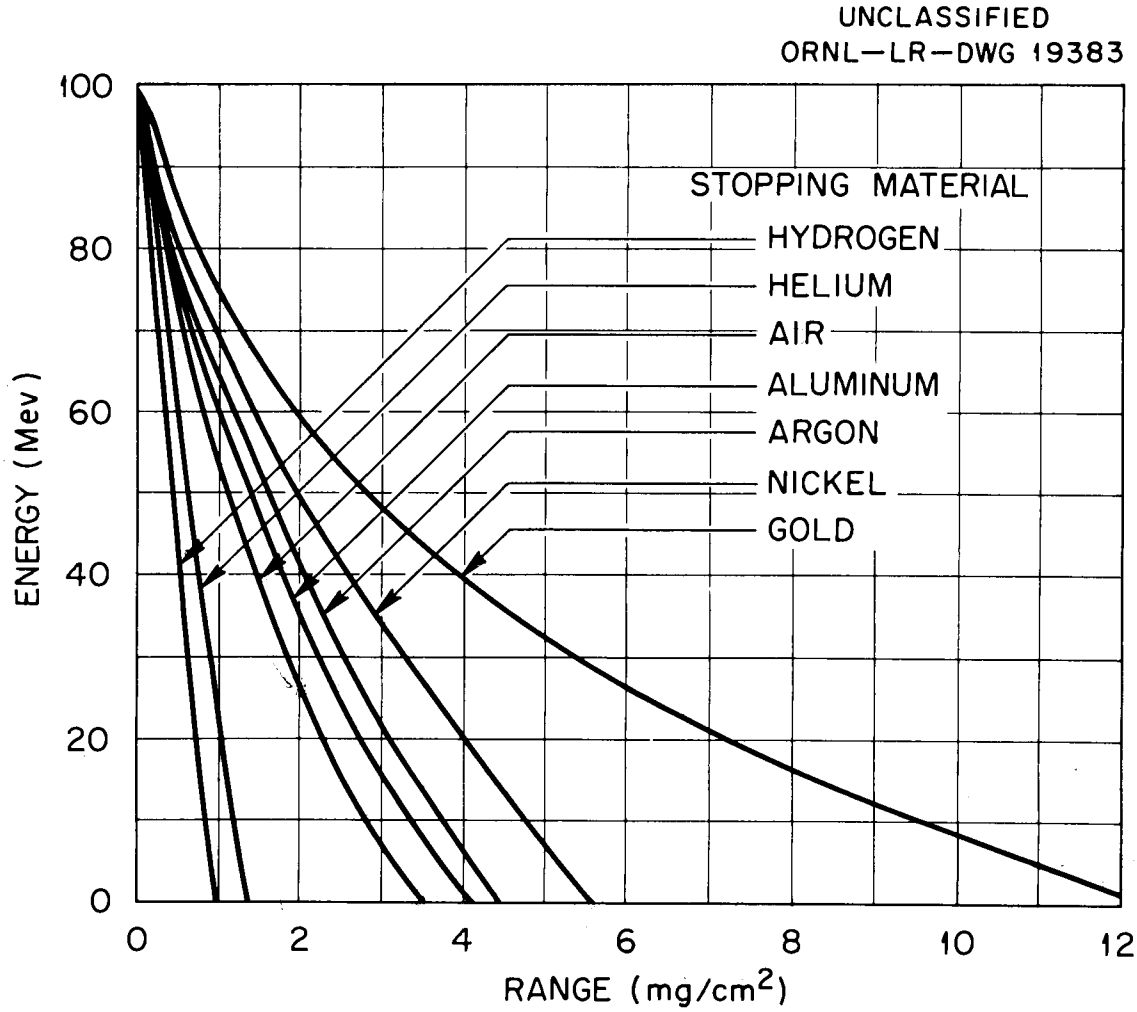

Fig. 34. Energy of Median Light Fission Fragments as a Function of Range in Various Materials.

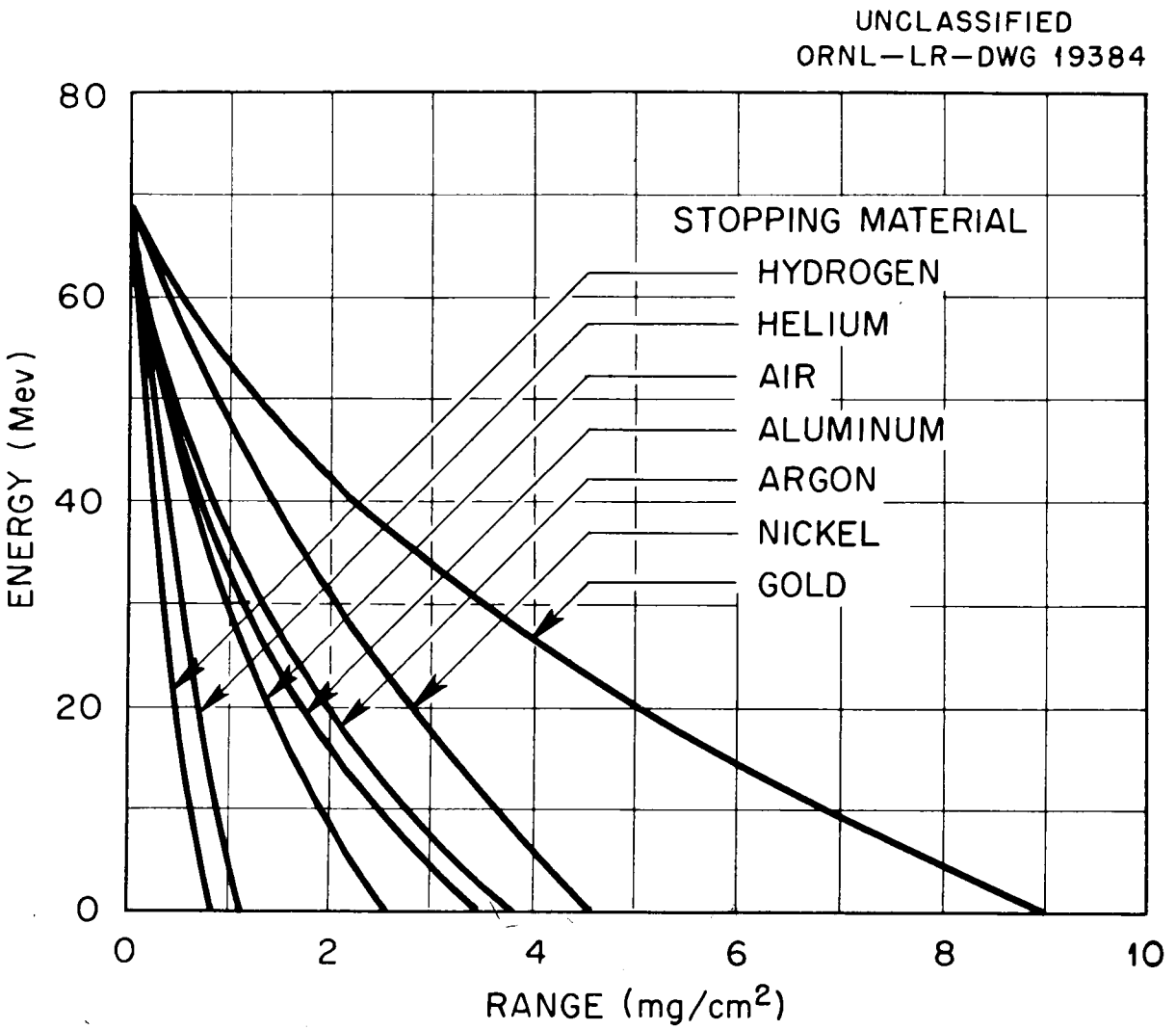

Fig. 35. Energy of Median Heavy Fission Fragments as a Function of Range in Various Materials.

CHAPTER 5

MAGNETIC ANALYSIS OF THE LONG RANGE PARTICLES FROM NUCLEAR FISSION

5.1 Existence of Long Range Particles from Nuclear Fission

The liquid drop model of the nucleus was used by Present (1941) to predict that fission of a heavy nucleus into three charged fragments is dynamically possible. Emission of light nuclei of long range from slow neutron fission of U^{235} was observed by Alvarez in 1943.* Since these first observations there has been considerable work devoted to the study of the light nuclei from fission.

5.2 Survey of Previous Studies of Long Range Particles from Fission

Farwell, Segré, and Weigand (1947), using a double ionization coincidence arrangement, found light particles from fission with ranges up to 23 cm of air. The resolving time of the apparatus used showed that the particles are emitted within 5×10^{-6} sec of the fissions from which they originate. The ionizing power of the particles indicated that they are alpha particles. From these observations the particles were estimated to occur in one of each 250 slow neutron fissions of uranium-235.

Demers (1946) in observing 1500 pairs of fission fragment tracks in photographic emulsion found six alpha tracks originating within 0.2 micron of the fission fragment tracks. Since the velocity of fission fragments is of the order of 10^9 cm/sec, the emission of the alphas must occur within 2×10^{-14} sec of the fission events.

---

*These observations were reported by Farwell, Segré, and Weigand (1947).

Wollan, Moak, and Sawyer (1947) observed alpha particle tracks from fission in photographic emulsion. The maximum range of the particles in the emulsion corresponded to about forty cm of air. The observations indicated that the alpha particles are released within 10^{-13} sec of the fission events from which they originate.

Marshall (1949) observed 18,500 pairs of fission fragment tracks in photographic emulsions and found 80 long range alpha tracks associated with fission of uranium-235. The maximum energy of the alphas, as indicated by the length of the tracks in the emulsion, is 26.4 Mev.

Allen and Dewan (1950) made a careful study of long range particles emitted in slow neutron fission of U^{233}, U^{235}, and Pu^{239}. They used coincidence counting methods employing two different arrangements of proportional counters. They studied the range distribution of the particles in air, and found it to be continuous with a broad maximum near 20 cm and extending to 50 cm. The resolving power of the apparatus used was 4.0 cm of air. Comparison of energies and ranges in air showed that all the long range particles are alphas. The frequency of emission of the particles from thermal neutron fission of U^{235} was estimated to be 1 in 550 ± 50.

Titterton (1951) reported the results from the study of over 500,000 fission events that were recorded in photographic emulsions. Ilford C-2 and D-1 emulsions, impregnated with a saturated solution of uranyl acetate, were irradiated in slow neutron fluxes in the reactors GLEEP and BEPO. The studies indicated that the frequency of emission of the long range particles is 1 in 422 ± 50. Angular distribution of the particles relative to the main fission fragments showed the preferred direction to be at a slightly acute angle with respect to the lighter of the fragments. The energy distribution was determined from the observations.

5.3 Advantages of Studying the Long Range Particles by Magnetic Analysis

None of the studies of the long range particles from fission, that have been reported, employed magnetic analysis. There are some obvious advantages to this method. The $H\rho$ distribution corresponds directly to the energy distribution of the particles, thus the energy resolution is much better than either the proportional counter or the nuclear emulsion techniques. If there were fine structure in the energy distribution it would be revealed by the higher resolution study. If a few microns of gas pressure is maintained in the system the $H\rho$ distribution of the particles does not overlap that of the fission fragments thus separation is achieved without absorbers.

5.4 Experimental

Scintillation counting methods were employed for these studies. A preliminary search for the long range particles was made with air filling the system to a pressure of 3 mm Hg. This is enough air to stop all the primary fission fragments. This search revealed particles with $H\rho$ values ranging from 3.7×10^5 gauss cm to 7.4×10^5 gauss cm. For alpha particles this range of $H\rho$ corresponds to an energy range of 6.6 Mev to 26.5 Mev.

The 0.003-in. CsI(Tl) crystal was replaced by another of the same material 0.007 in. thick so that the range of the particles, in the crystal, would not exceed the thickness.

Measurements were made to determine whether the particles observed in the preliminary search are indeed alpha particles. Scintillation pulse heights of the particles were determined at several points of the $H\rho$ distribution, and these were plotted as a function of energy as determined from the $H\rho$ values. The pulse height of the Po^{210} alpha was determined and included in the resulting graph shown in Fig. 36. Because of the very low counting rates pulse height data were not obtained at the high energy end of the $H\rho$ distribution.

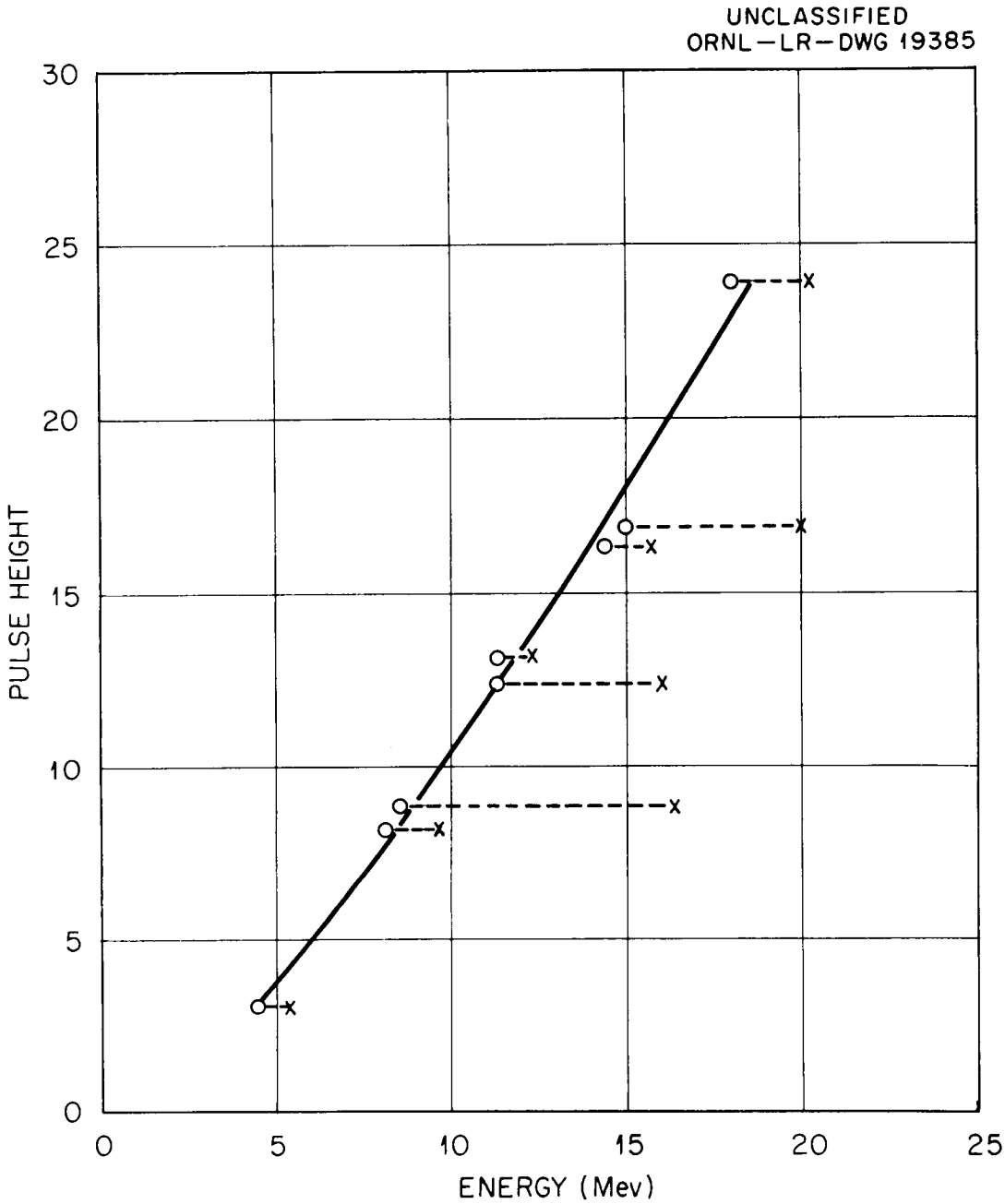

Fig. 36. Scintillation Pulse Heights of Long Range Alpha Particles from Fission of Uranium-235 as a Function of Energy. (Dotted lines show the reduction in energy due to aluminum absorbers in the path of particles.)

Aluminum foils of known thicknesses were placed in the path of the particles near the crystal. From the energy vs range in aluminum data of Aron, Hoffman, and Williams (1951), the change in energy of alpha particles due to the absorbers was known. The scintillation pulse heights of the particles of reduced energies were determined and the results included in the graph shown in Fig. 36. The dotted lines show the shifts in energies due to the aluminum absorbers. Since these measurements show that the particles being studied have both the same momentum to charge ratio and range in aluminum to energy ratio as alpha particles, they demonstrate conclusively that they are alpha particles.

Much of the data were obtained during nights and week-ends through the cooperative assistance of the reactor operation personnel under the supervision of Mr. J. A. Cox, Superintendent, and Mr. W. R. Casto, Supervisor of the Reactor Operations Department of Oak Ridge National Laboratory. At the end of each two-hour counting period one of the men would record the accumulated count, reset the counters, and change the setting of the instruments according to instructions that were prepared for each run.

Detailed data were obtained to determine the energy distribution of the long range alpha particles. Integral pulse counts of two hours duration were taken at intervals of approximately 1 Mev between 5 and 30 Mev. The counting rate at the peak of the energy distribution was about 700 counts in two hours. Proper discrimination level settings, which were determined from the pulse height distributions obtained earlier, eliminated background over most of the distribution. For the lower part of the energy distribution it was necessary to integrate the area under the pulse height distribution curves to obtain the integral counting rate.

A background of tritons prevented the study of the long range alphas of energies less than 6.6 Mev. The tritons were presumably formed from Li_3^6 (n, α)H_1^3 reactions from a concentration of a few parts per million of lithium in the aluminum entrance arm.

An extensive search for fine structure in the energy distribution was made by taking 30-minute integral pulse counts at intervals of 1/4 Mev over the entire energy distribution. No fine structure was found.

5.5 Presentation of Data and Discussion of Results

The energy distribution as determined by these experiments is shown in Fig. 37. The distributions determined by Allen and Dewan (B) and by Titterton (C) are also shown.

Allen and Dewan determined the distribution by a proportional counting method which had an energy resolution of four cm of air. Titterton determined the distribution from the lengths of less than a thousand long range particle tracks in photographic emulsions. There is excellent agreement between the results of the three methods for the high energy half of the distribution. The location of the peak, as determined by the three methods, is also in agreement. There is some difference in the determinations of the low energy part of the distribution. The resolution of the magnetic analysis method is more accurate than either of the other methods. This probably accounts for the lack of agreement for the lower energy part of the the distribution.

There is no detailed and generally accepted explanation for the formation of the long range particles. Feather (1947) has suggested that the alpha particle is emitted from a highly excited fragment which is in one of the regions of alpha instability, i.e., atomic number near 40 or 60. The very high state of excitation of the fragment is used to explain the emission of the particle within such a short time. An alternate view is that the alpha particle is formed during the actual fission process. It is compared to the plateau droplet which is often seen to form in the division of an ordinary

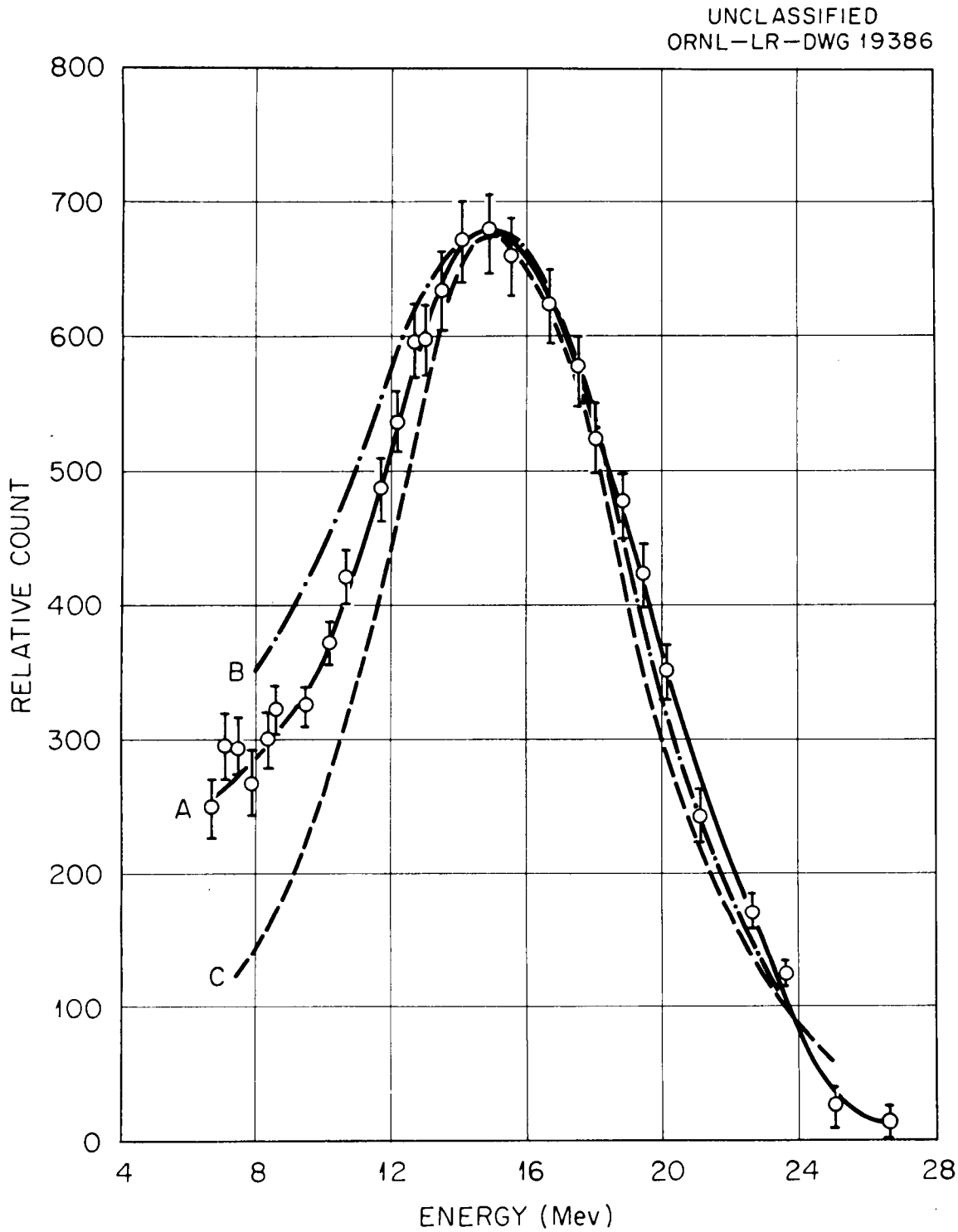

Fig. 37. Energy Distribution of Long Range Alpha Particles from Pile Neutron Fission of Uranium-235. (B and C are the distributions determined by Allen and Dewan and by Titterton, respectively.)

liquid drop. The angular distribution of the alpha particles with respect to the primary fission particle tracks, reported by Titterton (1951), favors the hypothesis that the three particles are formed simultaneously and fly apart under the influence of their mutual electrostatic repulsions.

The shape of the energy distribution demonstrates that the alpha particles are formed at the instant of fission. From the reciprocity theorem for nuclear reactions, such as is presented by Blatt and Weiskopf (1952), the Coulomb barrier penetration factors for escape of an alpha particle from a compound nucleus are approximately the same as the cross sections for the formation of a compound nucleus. These factors are plotted in Fig. 38 from tables in Theoretical Nuclear Physics by Blatt and Weiskopf, page 353. The curves shown cover the range of possible nuclei that might emit an alpha particle either before or after fission.

The solid curve in Fig. 38 corresponds to the variation of the barrier penetration factor as a function of particle energy that would apply to the energy distribution that was determined. This curve is plotted as follows. The assumption is made that the part of the energy distribution with the greatest negative slope corresponds to a Maxwell distribution of alpha particles for a temperature of 1.4 Mev. A straight line is drawn tangent to this part of the energy distribution. The ratios of the intensity obtained for lower energy and the corresponding intensity indicated by the straight line are used to plot the curve. It is seen that the rates of decrease of the penetration factors as functions of particle energy for all available nuclei are too great to satisfy the energy distribution of the long range particles.

The frequency of emission of the long range alpha particles was estimated. Numerical integration of the counting rate of the alpha particles as a function of $H\rho$ and of the counting rate of the fission fragments, after correcting for variation in counting geometry as $H\rho$ changed, and normalizing the counting rates to the same counting periods, indicated that a long range alpha occurs in one of each 310 ± 40 fissions. The large error that is assigned reflects the range

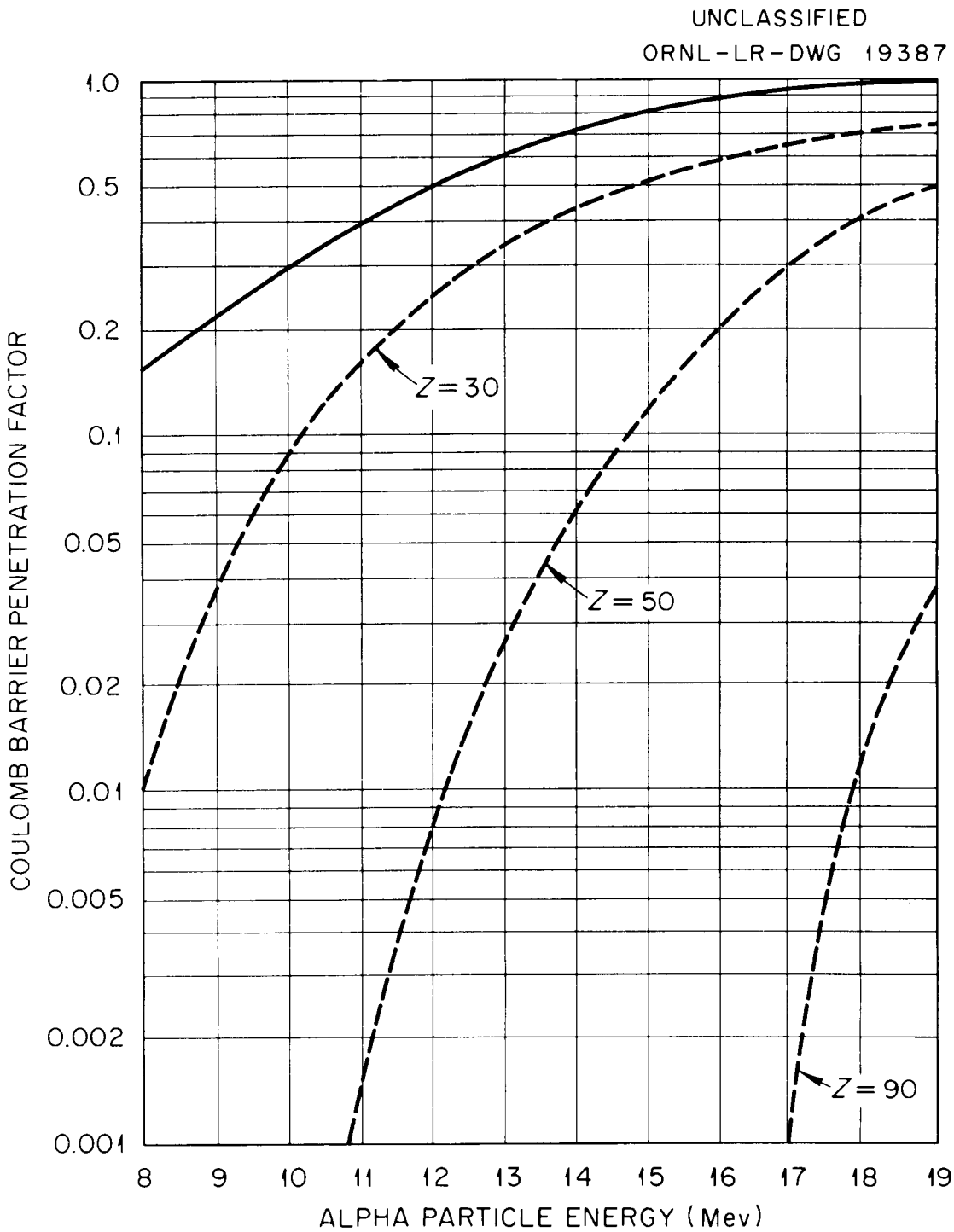

Fig. 38. Coulomb Barrier Penetration Factors for Emission of Alpha Particles from a Compound Nucleus as Functions of Particle Energy. (The slopes rather than the amplitudes of the theoretical curves are to be compared with the experimental curve.)

of results obtained from numerical integration of $H\rho$ distribution curves obtained in various gases. This result is compared in Table III with the estimates obtained by other investigators for U^{235}. The reason for the large variation of the estimates obtained is not clear, but as suggested by Allen and Dewan, it may be due to different energy distributions of the neutrons causing the fissions.

TABLE III

Rate of Occurrence of Long Range Alpha Particles in Fission of U^{235}

Observers	Rate	Type of Neutrons
Allen and Dewan	1 in 550 ± 30	thermal
Allen and Dewan	1 in 515 ± 50	pile
Titterton	1 in 422 ± 50	pile
Green and Livesey	1 in 300	cyclotron produced and slowed down
Farwell, Segré and Weigand	1 in 250	cyclotron produced and slowed down
Demers	1 in 250	Ra-α-Be slowed down
Marshall	1 in 230	thermal from pile
This author	1 in 310 ± 40	pile

CHAPTER 6

A FISSION FRAGMENT MASS SEPARATOR AND THE NUCLEAR CHARGE DISTRIBUTION OF SINGLE MASS FISSION FRAGMENTS

6.1 Introduction and Operating Principles

The properties of a wedge magnet spectrograph (Bainbridge, 1953) are such that energetic ions originating at the source are focused to a position on the focal plane which is a function only of their radius of curvature, ρ, in the magnetic field H. ρ is determined by the well known relation

$$H\rho = m\,v\,c/e \qquad (6,1)$$

where m, v, and e are the mass, velocity, and charge of the ions, respectively. If e is much larger than one electron charge and if the system contains an appreciable quantity of gas, the charges of the ions may frequently change due to electron capture and loss collisions with the gas molecules. In this case, the focal position is still determined by (6,1) but with e replaced by $\bar{e}$, the time-average of the charge while the particle is in the magnetic field. In general, $\bar{e}$ is a function of the velocity, the nuclear charge of the ion Z, the type of gas in the system, and the pressure. It has been predicted theoretically (Bohrand Lindhard, 1954) and demonstrated experimentally (see Chapter 2) that for a wide variety of conditions $\bar{e}$ is proportional to ion velocity. Bohr (1948) has shown to some approximation that $\bar{e}$ is proportional to $Z^{1/3}$. Thus, for given conditions of gas filling,

$$e \propto Z^{1/3} V \qquad (6,2)$$

Inserting (6,2) in (6,1) then gives

$$H\rho \propto \frac{M}{Z^{1/3}} \qquad (6,3)$$

Ignoring for the moment the relatively small spread in nuclear charge of fission fragments of a given mass (Whitehouse, 1952), and taking $\underline{m}$ proportional to $\underline{Z}$, (6,3) gives

$$H\rho \propto m^{2/3} \qquad (6,4)$$

Thus, by simply passing fission fragments through a magnetic spectrograph which is filled with gas, mass separation of the fragments is achieved, independent of their energy and direction of motion (within the acceptance angle of the spectrograph), and with a reasonably good dispersion; i.e., 0.7% and 0.4% per mass unit for the light and heavy fragments, respectively. This separation, which ideally would be at least equivalent to, and usually superior to the results achieved by chemical procedures, is accomplished in a time of the order of one microsecond. It therefore allows the fragments to be separated and studied before any beta decay or delayed neutron emission has occurred.

The principal difficulty with the instrument is its lack of resolution. This arises from several sources. In the first place it is noted that the process of charge changing by electron capture and loss collisions with gas molecules is a statistical one. Thus the average charge, $\bar{e}$, for different fragments of the same mass, velocity, and initial charge* is subject to a statistical fluctuation, $\Delta \bar{e}$. From usual statistical considerations $\Delta \bar{e}$ varies inversely as the square root of the number of charge changing collisions. Since the latter is just proportional to the density of gas molecules, and hence the gas pressure, $\underline{P}$, the width of the $\underline{H}\rho$ distribution is given by

---

* Actually the initial charge is of negligible importance if the total number of charge changing collisions is much larger than the number of charge states that can be reached by charge changing collisions with reasonable probability. This condition is fulfilled for all cases of interest here. For example, at the most favorable pressures, the number of charge changing collisions in the deflection chamber is about 10^5.

$$W = K/\sqrt{P} \qquad (6,5)$$

where W is defined as $\Delta(H\rho)/H\rho$, and K is a constant. In principle, then, this spreading of the resolution can be reduced indefinitely by increasing the pressure. However, this also causes the fragments to lose energy and thus suffer multiple scattering, so that a resolution limit is set by the ratio of the electron capture and loss cross sections to the energy loss cross section. Shortly before this limit is reached, however, another factor, the nuclear charge distribution of fission fragments of a given mass, comes into predominance. By noting the manner in which this factor limits the resolution, it is possible to determine the width of this charge distribution. Since this is a very important quantity in the theory of nuclear fission, the measurement of this width is one of the most important results of these studies.

6.2 Experimental

A description of the fission fragment spectrograph has been given in Chapter 1. The data used to determine the resolution of the instrument as a function of gas pressure were obtained by the catcher foil and radiochemistry method so that $H\rho$ distributions of single mass fission fragments were obtained. Data were obtained at low gas pressures with gas filling the system and at higher pressures with gas in the magnetic deflection chamber only. The beta activities of Zr^{97}, Sr^{91}, and I^{133} were used to determine the $H\rho$ distributions for fission fragments of those three masses.

Several $H\rho$ distributions obtained for mass-97 fragments with He gas filling the system are shown in Fig. 39. The principal information obtained from these data is the width of the distribution, defined here as the full width at half maximum. The widths of mass-97 fission fragments as a function of pressure are plotted in Fig. 40 for He gas in the system, and in Fig. 41 for He gas in the deflection chamber. The energies shown in Fig. 40 are the energies at the center of the deflection chamber as calculated from the range vs energy data of Chapter 4. Less complete data were also obtained with H_2, air, and A.

UNCLASSIFIED
ORNL-LR-DWG 11569

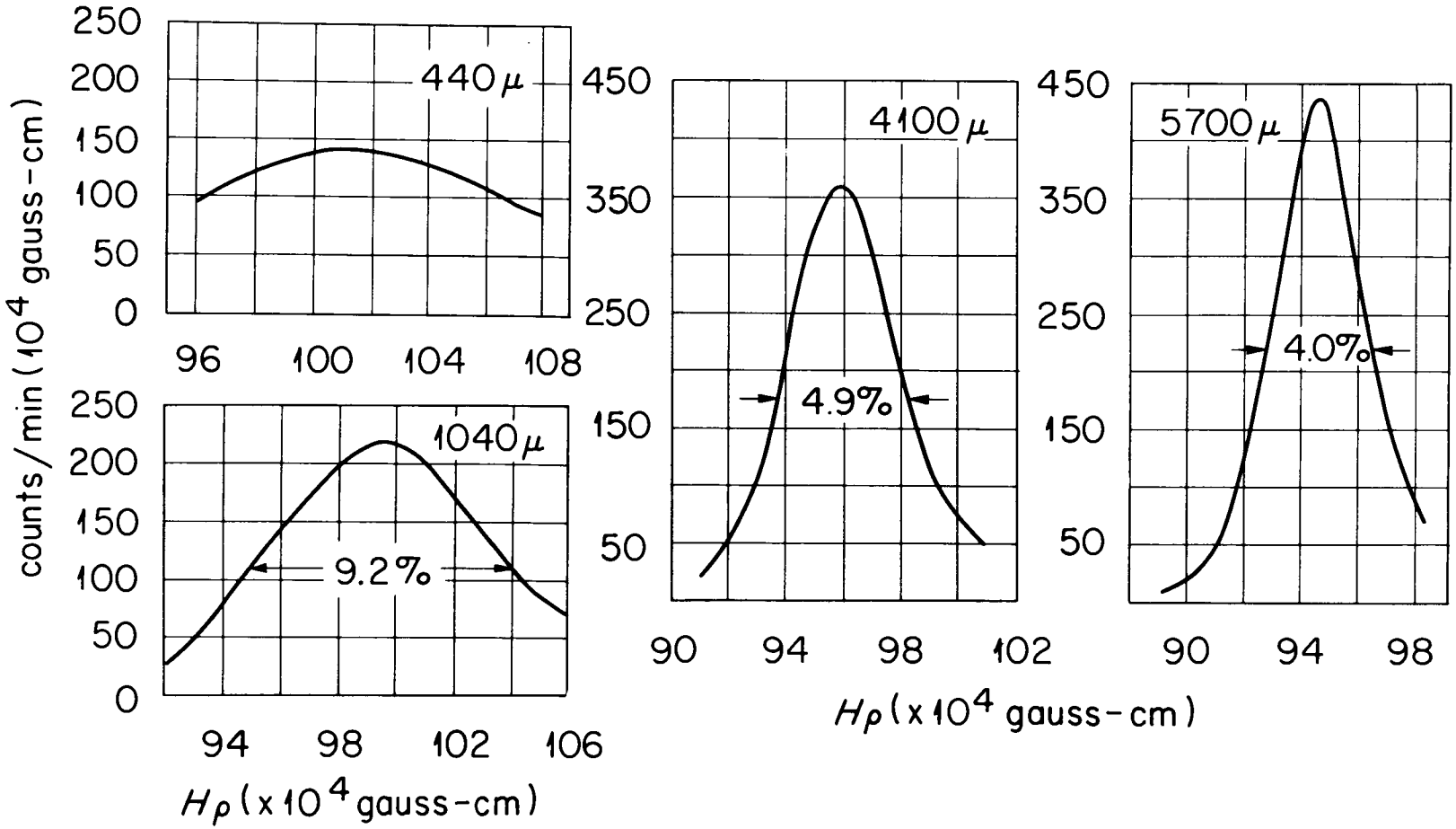

Fig. 39. $H\rho$ Distributions of Mass-97 Fission Fragments in Helium at Various Pressures.

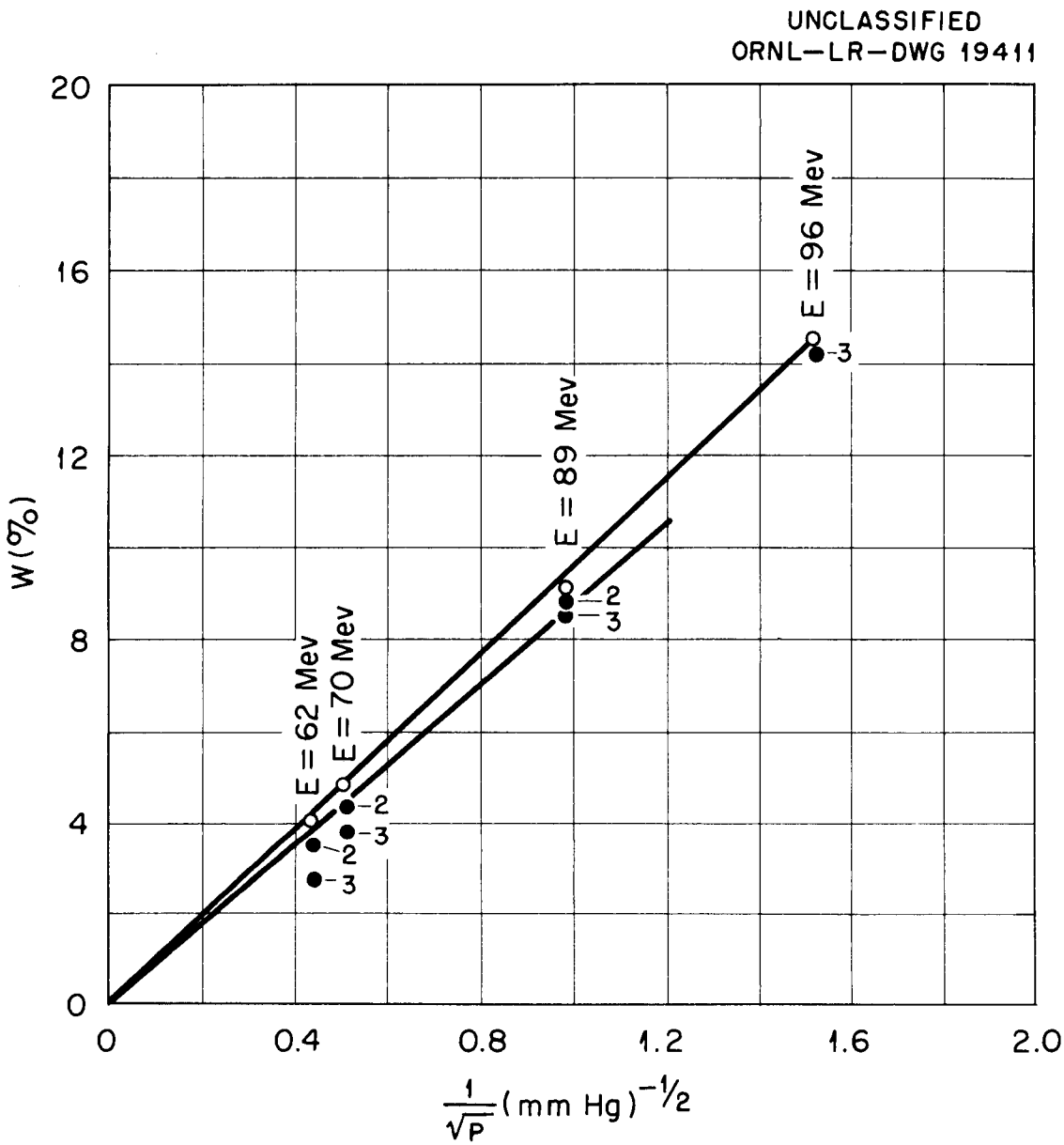

Fig. 40. Width of $H\rho$ Distribution of Mass-97 Fission Fragments as a Function of $(1/P)^{1/2}$.

UNCLASSIFIED
ORNL-LR-DWG 19412

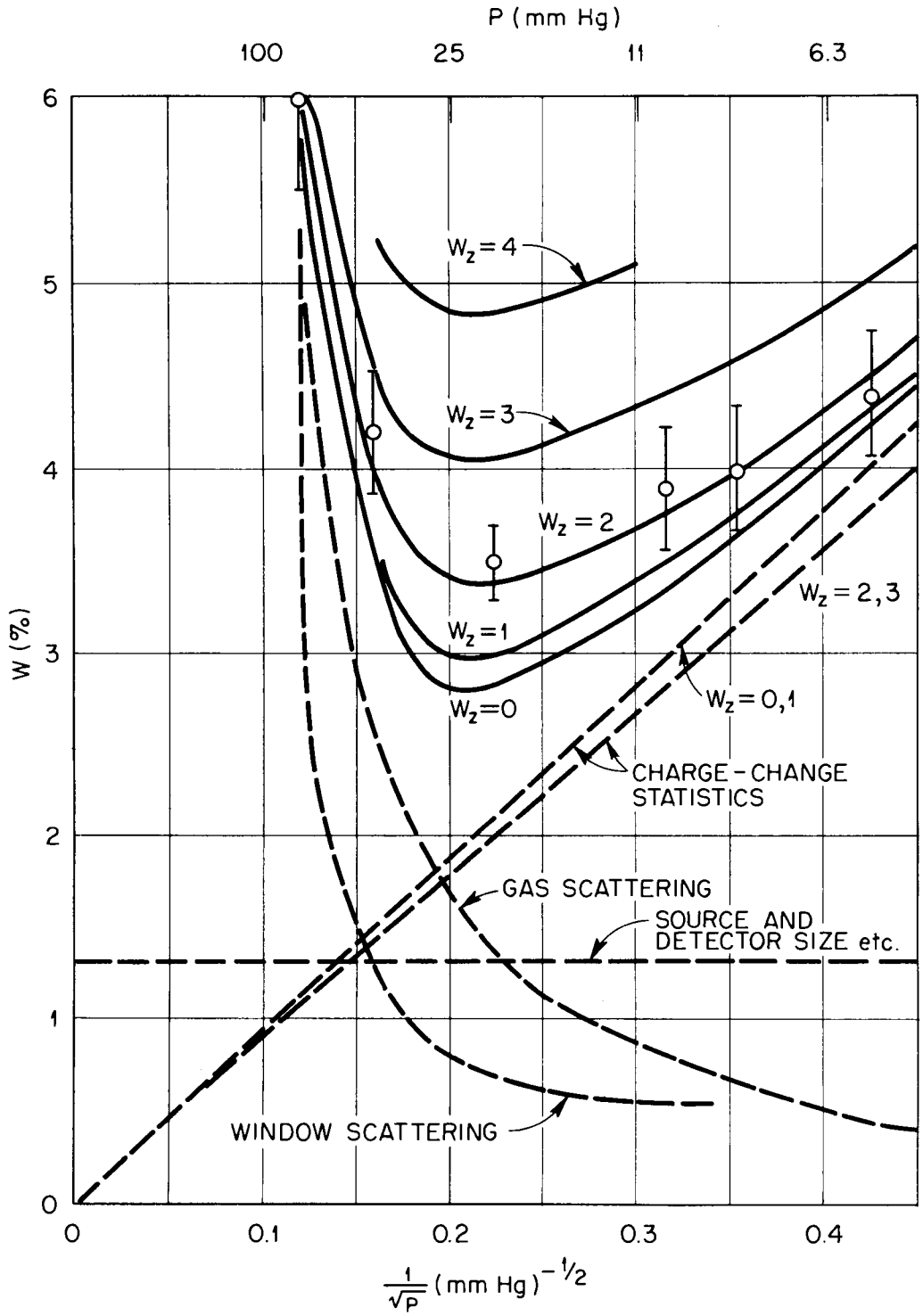

Fig. 41. Width of $H\rho$ Distributions of Mass-97 Fission Fragments Due to Various Contributions and Graph of Experimentally Determined Widths.

6.3 Factors Affecting Resolution

A. Charge Changing Statistics:

The contribution to the resolution width from the statistics of the charge changing process is governed by equation (6, 5). The only problem is to determine K. Since K may in principle be energy dependent, it is desirable to determine it from data obtained at low pressures so that the energy is not changed significantly between points. The determination of K for He is shown in Fig. 40. The upper line is drawn through the two low pressure points assuming that no other factors affect the resolution. The principal other factor that may contribute is the width of the nuclear charge distribution, W_Z. To take this into account the observed points must be corrected. The points labeled "2" and "3" show these corrections for W_Z equal to 2% and 3%, respectively, and the lower line gives the value of K for the average of these. It may be noted from Fig. 40 that the two high pressure points lie on the straight lines reasonably well if W_Z = 2%. This indicates that K is reasonably energy independent, at least down to about 50 Mev if W_Z is found to be sufficiently small. The lines from Fig. 40 are reproduced in Fig. 41.

B. Multiple Scattering:

The width due to multiple scattering in the gas and in the windows was calculated using standard multiple scattering theory, such as is presented by Mott and Massey (1949), and the results are shown in Fig. 41. The dependence of the window scattering on pressure arises from the fact that the latter determines the fragment energy which strongly affects the former. The energy also has a strong effect on the gas scattering.

C. Velocity Dependence of the Quantity $\bar{e}/v$:

Since fission fragments have a relatively wide velocity distribution (Cohen, Cohen, and Coley, 1956) the resolution would be adversely affected if $\bar{e}$ were not strictly proportional to v. This effect was investigated using the data of Chapter 2 and found to contribute no more than 1/2% to the width.

D. Source and Detector Size:

The width of the uranium source contributes a width of 0.8% to the resolution, and the width of the strips into which the detector foil was cut contributes a width of 0.9%. These widths could easily be reduced at the cost of intensity. Their combined contribution, plus that discussed in the preceding paragraph is shown by the horizontal line at W = 1/3% in Fig. 41.

E. Nuclear Charge Distribution:

The contribution to the width from the nuclear charge distribution is not known. The measured resolutions can therefore be used to obtain it. The combined contributions to the width from all other sources are shown by the line labeled $W_Z = 0$ in Fig. 41. The other lines show the total resolution expected for $W_Z = 1$, 2, 3, and 4%. Comparing the observed resolution with these curves indicates $W_Z = 2.1 \pm 0.3\%$.

The error assigned assumes no uncertainty in the other factors affecting resolution. The only one of these factors which is somewhat uncertain is the multiple scattering. The calculation of that quantity assumed that the full nuclear charge of the fission fragments is effective, whereas electron screening might somewhat reduce this. Such a reduction in multiple scattering would destroy the agreement with the high pressure points in Fig. 42, but these are also quite sensitive to the range-energy relations points. In the most extreme case where the multiple scattering is assumed to be negligible, W_Z is increased to 2.8. To take this uncertainty into account the earlier result is revised and the error increased to give

$$W_Z = 2.2 \pm 0.6\% \qquad (6,6)$$

6.4 Nuclear Charge Distribution of Single Mass Fission Fragments

In order to interpret the result for W_Z, it is necessary to determine the dependence of $H\rho$, or equivalently, of $\bar{e}$ on Z. If it is assumed that

$$\bar{e} \propto Z^n \tag{6,7}$$

differentiation gives

$$W_Z = \frac{\Delta \bar{e}}{\bar{e}} = \frac{n \Delta Z}{Z} \tag{6,8}$$

For mass-97 fragments, which were used for the data in Fig. 41, the value of Z is about 38.

An approach to the determination of n is to obtain it empirically. Assuming the dependence of $\bar{e}$ on v and Z to be strictly separable and independent of m, and assuming the dependence of $\bar{e}$ on v to be strictly linear, (6,7) and (6,1) give

$$H\rho \, Z^n/m = \text{constant} \tag{6,9}$$

where the constant is independent of mass, nuclear charge, and velocity. Table IV shows the measured most probable values of $H\rho$ for mass 91, 97, and 133 fragments in He at two different pressures. Using this data the product in (6,9) is computed for various values of n. Satisfying (6,9) for mass-91 and -97 fragments requires n = 0.35 and n = 0.22 in the two cases. Satisfying (6,9) for the average of the two light fragments and the heavy fragment frequires n = 0.50 in each case.

Weighing these results together with the theoretical value of Bohr, a value of n is selected as 0.42 ± 0.08. Inserting this in (6,8) with Z = 38 gives

$$W_Z = \frac{(1.1 \pm 0.2)}{100} \Delta Z \tag{6,10}$$

Inserting the experimental values of W_Z from (6,6) gives

$$\Delta Z = 2.0 \pm 0.6 \qquad (6,11)$$

as the width of the nuclear charge distribution for mass-97 fission fragments. Although the data is somewhat less complete, approximately the same result is obtained for mass-91 fragments. Since the sum of the charges of complementary fragments must be equal to 92, the result (6,11) must also be valid for heavy fragments. This result is in general agreement with determinations from shielded isotope yields and gas sweeping experiments (Whitehouse, 1952). Those results require the application of a rather tenuous theoretical analysis, so that it is gratifying that the method described here, although based on a completely different approach, gives approximately the same result.

The result (6,11) is in strong disagreement with the theory of Brunton (1949) which predicts very wide nuclear charge distributions. In spite of the many assumptions, it is extremely difficult to see how the data presented here can be reconciled with a width larger than about $\Delta Z = 3.5$.

6.5 Performance of the Fission Fragment Mass Separator

In addition to the data discussed above with He gas, measurements were made with H_2, air, and A. Hydrogen appeared to be slightly less favorable than He, and air and A are considerably worse. It thus seems that the performance with He at about 20 mm Hg pressure is about optimum. With source and detector size, and windows optimized, this should give a resolution near mass-97 of about 3.3%, which corresponds to about 4.5 mass units. While this falls somewhat short of what might be desired, it is still very useful for a wide variety of experiments.

TABLE IV

Empirical Determination of n

p = 5 mm - Hg

M	H $(x10^{-3})$	H Z^n/M $(x10^{-3})$ n = 0.3	n = 0.4	n = 0.5	Best n
91	904	28.9	41.3	59.1	
97	939	28.8	41.4	59.8	0.35
133	1112	27.0	40.1	59.3	0.50

p = 20 mm - Hg

M	H $(x10^{-3})$	H Z^n/M $(x10^{-3})$ n = 0.3	n = 0.4	n = 0.5	Best n
91	858	27.5	39.3	65.2	
97	904	27.8	39.9	57.5	0.22
133	1065	25.9	38.3	56.7	0.50

CONCLUSIONS

The studies discussed in this report may be divided into three categories. These are the interaction of fission fragments with matter, analysis of long range light nuclei from fission, and capabilities of a magnetic fission fragment mass separator. The principal results and conclusions may be summarized as follows.

The equilibrium charge studies of median light and heavy fission fragments cover a wide range of fragment velocity in contrast to previous studies (Lassen, 1950[a,b], 1951) which were made at approximately initial velocities of each group of fragments. The equilibrium charge data of Fig. 13 are the first that have been reported for single mass fission fragments. The absence of structure in the results obtained, especially for single mass fragments, demonstrates the influence of nuclear charge distribution on the measurements.

The suitability of CsI(Tl) crystals for scintillation detection of fission fragments has been demonstrated by the monotonic increase of specific fluorescence as a function of specific energy loss. The feasibility of scintillation detection of fission fragments in a high background of gamma and beta radiation has been demonstrated by the data obtained with the very thin crystal used for these studies.

The energy vs range data obtained for fission fragments includes a much larger number of stopping materials than have been previously reported.

It has been demonstrated that the long range particles from fission have the same momentum to charge ratio and range in aluminum to energy ratio as alpha particles. This supports the evidence of previous investigations in which either ionization chambers or photographic emulsions were used. No fine structure was found in the energy distribution of the long range particles as determined by the magnetic analysis method which provides much better energy resolution than the previously used techniques for studying the particles.

Studies of the capabilities of a fission fragment mass separator have shown a resolution limit of 3.2% for mass-91 or -97 fragments of which

2.2% is the result of nuclear charge distribution of single mass fragments. From the study of the dependence of equilibrium charge on the nuclear charge, the full width at half-maximum of the nuclear charge distribution of single mass fragments was found to be 2.0 ± 0.6 units.

These are but a few of the experiments for which the magnetic fussion fragment spectrograph is well suited. With optimum conditions, sufficient resolution is achieved to determine the lengths of the various fission fragment decay chains. This in turn gives the average nuclear charge division between the two fragments in fission. This quantity, which is very important in fission theory, is only poorly known.

Mass identification problems may be resolved in a very simple matter with this separator. As a particular example, the masses of the strontium isotopes between atomic weight 91 and 97 are not well established. The masses of delayed neutron emitters could also be determined, and for the first time the various emitters could be separated and studied individually. By use of time-of-flight techniques, the neutron energies could be accurately determined.

This technique should open up many new possibilities in the study of decay chains. Prominent beta and gamma rays can be detected with greatly reduced background and their grow-in and decay can be followed. Short lived isomers can be detected, identified, and studied. It would seem quite interesting to investigate some of these possibilities.

ACKNOWLEDGEMENTS

The author is greatly indebted to B. L. Cohen, A. Foner Cohen, J. J. Pinajian, B. H. Ketelle, C. D. Coley, L. R. Hall and S. S. Hale for help in various phases of the experimental work, to F. T. Howard for assistance in preparing the report, and to R. S. Livingston and A. M. Weinberg for support and encouragement. The cooperation of the reactor operating personnel was most helpful.

BIBLIOGRAPHY

Allen, K. W. and Dewan, J. T. 1950. The emission of long-range charged particles in the slow neutron fission of heavy nuclei. Phys. Rev. 80:181-188

Allison, S. K. and Casson, H. 1953. The scintillation response from NaI(Tl) crystals under bombardment with positive ions of energies 60-600 kev. Phys. Rev. 90:808-885

Aron, W. A., Hoffman, B. G., and Williams, F. C. 1951. AECU report 663

Bainbridge, K. T. 1953. Experimental Nuclear Physics 1:559-681. John Wiley and Sons, Inc., New York.

Blatt, J. M. and Weisskopf, V. F. 1952. Theoretical Nuclear Physics. John Wiley and Sons, Inc., New York.

Boggild, J. K., Arroe, O. E., and Sigurgeisson, T. 1947. Cloud-chamber studies of electronic and nuclear stopping of fission fragments in gases. Phys. Rev. 71:281-287

Boggild, J. K., Minnhagen, L., and Nielsen, O. B. 1949. Cloud-chamber study of fission fragment ranges in air. Phys. Rev. 76:988-989

Bohr, N. 1940. Scattering and stopping of fission fragments. Phys. Rev. 58:654-655

Bohr, N. 1948. The penetration of atomic particles through matter. Kgl. Danske Videnskabs, Selskab, Mat-fys. Medd. 18, no. 8

Bohr, N. and Lindhard, J. 1954. Electron capture and loss by heavy ions penetrating through matter. Kgl. Danske Videnskabs, Selskab, Mat-fys. Medd. 28, no. 7.

Campbell, E. C., Good, W. A., and Strauser, W. A. 1949. Stopping of fission fragments in gases. Phys. Rev. 75:1292-1293

Cohen, B. L., Cohen, A. F., and Coley, C. D. 1956. Energy distribution of mass-97 fission fragments from thermal-neutron fission of uranium-235. Phys. Rev. 104:1046-1053

Demers, P. 1946. Pairs of fission fragments from U^{235}. Phys. Rev. 70:974-975

Eby, F. S. and Jentschke, W. K. 1954. Fluorescent response of NaI(Tl) to nuclear radiations. Phys. Rev. 96:911-920

Farwell, G., Segrè, E., and Weigand, C. 1947. Long range alpha-particles emitted in connection with fission preliminary report. Phys. Rev. 71:327-330

Feather, N. 1947. Emission of secondary charged particles in fission. Nature 159:607-608

Katcoff, S., Miskel, J. A., and Stanley, C. W. 1948. Ranges in aid and mass identification of plutonium fission fragments. Phys. Rev. 74:631-639

Lassen, N. O. 1945[a]. On the effective charge of fission fragments. Kgl. Danske Videnskabs, Selskab, Mat-fys. Medd. 23, No. 2

Lassen, N. O. 1945[b]. $H\rho$ -distribution of fission fragments. Phys. Rev. 68:142-143

Lassen, N. O. 1945[c]. Ionization by fission fragments in nitrogen, argon, and xenon. Phys. Rev. 68:230-231

Lassen, N. O. 1946[a]. On the variation along range of the $H\rho$ -distribution and the charge of the fission fragments of the light group. Phys. Rev. 69:137-139

Lassen, N. O. 1946[b]. Specific ionization by fission fragments. Phys. Rev. 70:577-579

Lassen, N. O. 1949[a]. On the energy loss by fission fragments along their path. Phys. Rev. 75:1762-1763

Lassen, N. O. 1949[b]. On the energy loss by fission fragments along their range. Kgl. Danske Videnskabs, Selskab, Mat-fys. Medd. 25, no. 11

Lassen, N. O. 1950. Total charges of fission fragments in gaseous and solid media. Phys. Rev. 79:1016-1017

Lassen, N. O. 1951[a]. The total charges of fission fragments in gaseous and solid stopping media. Kgl. Danske Videnskabs, Selskab, Mat-fys. Medd. 26, no. 5

Lassen, N. O. 1951[b]. Total charges of fission fragments as functions of the pressure of the stopping gas. Kgl. Danske Videnskabs, Selskab, Mat-fys. Medd. 26, no. 12

Lisitzin, E. 1938. Uber die Ionigierungsspannungen der elemente. Comm. Phys. Math. Soc. Fenn. 10, no. 4

Marshall, L. 1949. Alpha-particles from fission as recorded by photographic emulsions. Phys. Rev. 75:1339-1344

Milton, J. C. D. and Fraser, J. S. 1954. Response of NaI(Tl), and stilbene to fission fragments. Phys. Rev. 96:1508-1511

Mott, N. F, and Massey, H. S. W. 1949. The theory of atomic collisions. Oxford University Press, London

Present, R. D. 1941. Possibility of ternary fission. Phys. Rev. 59:466

Schmitt, H. W. and Leachmann, R. B. 1956. Ionization vs range relation for fission fragments. Phys. Rev. 102:183-185

Segre, E. and Weigand, C. 1946. Stopping power of various substances for fission fragments. Phys. Rev. 70:808-814

Suzor, P. F. 1949. Parcocus dans divers materiaux de fragments determines de fission de l'uranium. Ann. de Phys. 4:269-309

Taylor, C. J., Jentschke, W. K., Remley, M. E., Eby, F. S. and Kruger, P. G. 1951. Response of some scintillation crystals to charged particles. Phys. Rev. 84:1034-1043

Titterton, E. W. 1951. Slow-neutron ternary fission of U^{235}. Nature, London 168:590-591

Turner, L. A. 1940. Nuclear fission. Rev. Mod. Phys. 12:1-29

Whitehouse, W. J. 1952. Nuclear ission. Progr. Nuclear Phys. 2:120-173

Wollan, E. O., Moak, C. D. and Sawyer, R. B. 1947. Alpha-particles associated with fission. Phys. Rev. 72:447-451